Lateral Stability Analysis and MPC Tracking Control for Articulated Heavy Vehicles

by

Tarun Sharma

A thesis submitted to the
School of Graduate and Postdoctoral Studies in partial
fulfillment of the requirements for the degree of

Master of Applied Science in Automotive Engineering

Faculty of Engineering and Applied Science

University of Ontario Institute of Technology (Ontario tech University)

Oshawa, Ontario, Canada

October 2022

THESIS EXAMINATION INFORMATION

Submitted by: **Tarun Sharma**

Master of Applied Science in **Automotive Engineering**

Thesis title: Lateral Stability Analysis and MPC Tracking Control for Articulated Heavy Vehicles

An oral defense of this thesis took place on October 26, 2022 in front of the following examining committee:

Examining Committee:

Chair of Examining Committee	Dr Martin Agelin-Chaab
Research Supervisor	Dr Yuping He
Examining Committee Member	Dr Moustafa El-Gindy
Thesis Examiner	Dr Jaho Seo

The above committee determined that the thesis is acceptable in form and content and that a satisfactory knowledge of the field covered by the thesis was demonstrated by the candidate during an oral examination. A signed copy of the Certificate of Approval is available from the School of Graduate and Postdoctoral Studies.

ABSTRACT

Articulated heavy vehicles (AHVs) exhibit poor maneuverability during curved-path negotiations and low lateral stability under high-speed evasive maneuvers, which may lead to unstable motion modes, e.g., trailer-sway and jackknifing, causing severe accidents. However, vehicle parameters that can improve the static stability may degrade the dynamic stability. Therefore, to design controllers for improving the stability of AHVs, the trade-off between the static and dynamic instabilities is a necessary research topic. To analyze this trade-off, three different trailer payload schemes and two different tractor rear axle arrangements are considered. This trade-off is quantified using numerical simulations. Building upon the above trade-off analysis, this study designs an active safety technique in terms of a tracking-controller based on nonlinear model predictive control (NLMPC) for autonomous AHVs. With the proposed tracking-controller, the AHV tracks the predefined reference path and follows a planned forward speed scheme. Numerical simulation demonstrates the effectiveness of the proposed NLMPC tracking-controller.

Keywords: articulated heavy vehicles; static stability; dynamic stability; trade-off analysis; autonomous vehicles; tracking-controller

AUTHOR'S DECLARATION

I hereby declare that this thesis consists of original work of which I have authored. This is a true copy of the thesis, including any required final revisions, as accepted by my examiners.

I authorize the University of Ontario Institute of Technology (Ontario Tech University) to lend this thesis to other institutions or individuals for the purpose of scholarly research. I further authorize University of Ontario Institute of Technology (Ontario Tech University) to reproduce this thesis by photocopying or by other means, in total or in part, at the request of other institutions or individuals for the purpose of scholarly research. I understand that my thesis will be made electronically available to the public.

Tarun Sharma

YOUR NAME

STATEMENT OF CONTRIBUTIONS

Part of the work described in Chapters 4 and 5 has been submitted as:

1. Sharma, T., and He, Y., "Design of a Tracking-Controller for Autonomous Articulated Heavy Vehicles Using Non-Linear Model Predictive Control Technique", under review, Vehicle System Dynamics (Manuscript ID: NVSD-2022-0410).

I performed all the co-simulation testing and some part of manuscript writing.

2. Sharma, T., Huang, W., and He, Y., "An Autonomous Steering Control Scheme for Articulated Heavy Vehicles Using - Model Predictive Control Technique'', under review, Society of Automotive Engineers (Paper Offer Number: 23SS-0308).

I performed all the co-simulation testing and some part of manuscript writing.

Publications

1. Yu, J., Sharma, T., and He, Y., "Design Optimization of Autonomous Steering Control Schemes for Articulated Vehicles," *Proceedings of the Canadian Society for Mechanical Engineering International Congress 2021*, June 27-30, 2021, Charlottetown, PE, Canada, 10 pages.

2. Rahimi, A., Huang, W., Sharma, T., and He, Y., "An Autonomous Driving Control Strategy for Multi-Trailer Articulated Heavy Vehicles with Enhanced Active Trailer Safety," *The 27th IAVSD Symposium on Dynamics of Vehicles on Roads and Tracks*, Saint-Petersburg, Russia, 2021, 12 pages.

ACKNOWLEDGEMENTS

I am thankful to my supervisor and inspiration Dr Yuping He for his guidance, support and encouragement throughout my thesis work and giving me the opportunity to do research under him. Motivation provided by Dr He is the major driving force behind this thesis work. I feel blessed to have him as my guide.

I am also thankful to my fellow researcher and a very good friend, Mr. Amir Rahimi, for his help and support. Funding support provided by National Research Council Canada is also highly appreciated.

Finally, I would like to thank my family members Mr. T.R Sharma, Mrs. Rajni Sharma and Miss Tania Sharma for their unconditional love and affection in my life and special thanks to my roommate Mr. Nitish Kumar for taking care of me and supporting me during my studies.

TABLE OF CONTENTS

LIST OF FIGURES

LIST OF TABLES

LIST OF ABBREVIATIONS AND SYMBOLS

AVSSs	Active vehicle safety systems
RSSs	Reactive safety systems
PSSs	Predictive safety systems
AAVS	Autonomous articulated heavy vehicles
NLMPC	Non-linear model predictive control
AHV	Articulated heavy vehicle
RA	Rearward amplification
DOF	Degrees of freedom
LPTO	Last point to overtake
PFOT	Path-following off-tracking
RMS	Root of mean square
SUV	Single unit vehicle
CT	Car trailer
CG	Center of gravity
SLC	Single lane-change
HIL	Hardware in loop
AV	Articulated vehicle
CT-AT	Conventional tractor - active trailer
AT-AT	Active tractor - active trailer
ISO	International organization of standardization
4WS	Four-wheel steering

Chapter 1

Introduction

1.1. Application of articulated heavy vehicles and associated issues

Articulated heavy vehicles (AHVs) have a huge impact on the economy of Canada and other countries. An AHVs is a combination of a tractor and trailer(s) that is widely used to transport goods all over the world. The wide application of AHVs is attributed to the positive factors, such as less greenhouse gas emission, low overall cost in terms of fuel and workmen, etc. Despite the above benefits, AHVs exhibit poor directional performance. Almost 1.25 million lives are lost per year on roads which involve accidents mostly due to driver error [1]. A huge number of accidents are witnessed in which heavy duty vehicles are involved. Their long size and high center of gravity (CG) makes them more prone to unstable and various accidents happen because of their poor directional performance. The geography of some north American places makes it very challenging for the drivers to drive specially during cold weather. So, it is necessary to improve the directional performance and increase the safety of AHVs.

1.2. Motivation

AHVs display low high-speed lateral stability and poor low-speed maneuverability due to their multiple vehicle unit configurations, long sizes, and high CGs [2, 3]. AHVs represent 7.5 times higher risk than passenger cars in highway operations [4]. AHVs are featured with unique dynamic characteristics when compared with single unit vehicles, e.g., passenger cars or rigid trucks. Their barely predictable handling character is a big challenge for drivers with less expertise and severe road accidents are often witnessed on highways specially during bad

weather conditions. Compared with a single-unit vehicle, the directional performance of a multi-unit vehicle (e.g., CT) generally deteriorates due to the adverse influence from the trailer in dynamics and kinematics [5]. Unlike single-unit vehicles, for which static or divergent instability associated with oversteer is the main concern, AHVs may also exhibit dynamic or oscillatory instability mainly due to reduced system yaw damping at high forward speeds. The low lateral stability at high speeds may lead to unstable motion modes, e.g., trailer-sway and jackknifing, causing severe accidents [6]. Due to the additional payload on the tractor via the fifth-wheel from the trailing unit, the AHV's static stability (i.e., steady-state handling characteristics) may change from the original understeer to oversteer. Therefore, in designing controllers for improving the stability of articulated vehicles, the trade-off between the static and dynamic instabilities (i.e., sway/snaking) is a critical issue to be addressed. Trailers during harsh maneuvers such as high-speed obstacle avoidance generally experiences higher lateral acceleration with respect to the tractor. Such Scenarios can easily make the rearmost trailer rolled over and it is almost impossible for the driver to handle such situation because the perceived motion cues from trailing vehicle units are very weak due to the filtering function of the suspension of tractor cabin, articulation joints, etc., and driver is not able to predict the failure on time [16]. Figure 1.1 shows the simulation result using TruckSim software, representing a rollover scenario of a tractor/semi-trailer combination over a high-speed obstacle avoidance maneuver.

Figure 1.1 Roll over of an AHV during High Speed Lane Change

Roll and yaw stability are necessary to be discussed in brief to understand the stability issues of articulated vehicles. Roll stability is a performance measure, which represents the capability of a vehicle (or a vehicle combination) to avoid a tip over due to a large lateral acceleration. The rollover typically occurs while turning or lane changing. Several factors influence a vehicle's sensitivity to lateral forces including the payload height, payload offset, road adhesion, suspension stiffness, frame stiffness, and track width of the vehicle. Yaw stability refers to directional stability, which is the ability of the vehicle to follow driver steering input. Much of the focus on directional (yaw) stability is on over-steer situations, which typically lead to jackknives. Figure 1.2 illustrates a simulated jackknifing motion mode based on TruckSim software.

Figure 1.2 Static Instability Mode (Jack-Knifing).

To increase vehicle safety, active vehicle safety systems (AVSSs), e.g., vehicle stability control, have been commercialized, such as active trailer steering and differential braking [7-12]. These AVSSs can be classified as 'reactive safety systems' (RSSs), designed to react to the current vehicle state [13]. Although RSSs are effective in increasing vehicle safety, they do not consider the effect of driver mistakes. Human errors cause the vast majority (about 94%) of traffic collisions [14]. A potential resolution to the human error problem is autonomous driving, removing human factors from the control loop. Since the late 1990s, advanced driver assistance systems, e.g., lane departure prevention, have been developed. These systems are classified as 'predictive safety systems' (PSSs) [15], considering not only current vehicle state, but also predicted vehicle state and hazards. The last two decades have witnessed extensive research of autonomous vehicles. AHVs makes it challenging for the drivers to control the lateral stability during high speed lane change operations due to their multiple vehicle unit configurations, long sizes, and high CGs. Low visibility during winters sometimes makes it necessary for the drivers to do a sudden lane change during high speed highway operations to avoid a collision and it is one of the main reasons of highway accidents. To date, most research

activities carried out in autonomous driving have been dedicated to single-unit vehicles. Little attention has been paid to investigating these PSSs for AHVs [16, 17].

1.3. Thesis contribution

The main contributions of this research are

1) A detailed trade off analysis between the static and dynamic instability of articulated vehicles considering three different values of trailer payload and two different rear axle arrangements of tractor.
2) Design of a novel tracking-controller for articulated vehicles using model predictive control strategy.

To increase the safety of AHVs and facilitate the design of active safety system for these large vehicles, the trade-off relationship between the static and dynamic stabilities is explored. In this study, a detailed trade-off analysis between the static stability and dynamic stability of articulated vehicles is conducted considering different tractor rear axle arrangements and different trailer payloads. In order to understand the effect of adding trailer payload and tractor rear axles on the steady state handling behavior of a tractor/semi-trailer combination, a constant speed test is simulated using a linear yaw plane tractor/semitrailer model developed in MATLAB/Simulink environment. The equivalent understeer gradient values of the tractor/semitrailer are calculated for different payload schemes and various tractor rear axle arrangements. Eigenvalue analysis along with simulated single lane-change maneuver using TruckSim is performed to understand the effect of adding trailer payloads and tractor rear axles on the dynamic behavior of the tractor/semitrailer. This analysis can be very useful for the development of safety systems for AHVs.

To enhance the safety of autonomous AHVs (AAHVs), a tracking-controller is designed in this study. Among various tracking-control techniques for autonomous vehicles, model predictive control (MPC) gains significant popularity due to its abilities of handling model uncertainties, as well as state and control constraints, thereby permitting tracking-control to operate at the limits of attainable performance [18]. An MPC-based tracking-controller design is generally formulated as an online real-time quadratic optimization problem, in which the current control action is obtained by solving a finite horizon open-loop optimal control problem. The key of MPC is 'prediction', that is, predicting the future evolution of the system and the future action effects over a finite time horizon. Based on the prediction, MPC determines the control actions while minimizing predicted errors subject to operating constraints at each sampling time [19].

A novel tracking controller based on nonlinear MPC for AAHVs is developed and discussed in this research. To this end, a 7 degrees of freedom (DOF) nonlinear model is generated to represent the lateral and longitudinal dynamics of a tractor/semi-trailer combination. The 7-DOF model is developed for the tracking-controller design, and the vehicle model considers the following seven motions: the longitudinal, lateral, and yaw motions of the tractor, as well as the yaw motion of the trailer and the spinning motions of tractor and trailer wheels. Given the 7-DOF nonlinear tractor/semi-trailer model, in the proposed tracking-controller design, the vehicle forward speed may be treated as a state variable. Thus, the resulting tracking-controller is able to handle the operating scenarios when the AAHV negotiates curved paths and conducts evasive maneuvers with variable forward speeds. In addition, the tracking-controller design will directly consider both the leading and trailing vehicle units' output variables in order to improve path-following performance and lateral stability of the AAHV under severe high-speed evasive maneuvers. In this study, we adopt a non-linear MPC (NLMPC) technique for the tracking-controller design. To

demonstrate the effectiveness of the NLMPC-based tracking-controller, co-simulations are conducted in a simulation environment, in which the NLMPC controller designed using MATLAB/Simulink is integrated with the virtual tractor/semi-trailer developed in TruckSim [20].

1.4. Thesis organization

The remainder of the thesis is organized as follows. Chapter 2 reviews the previous research on the stability related issues and the safety systems developed for AHVs. Chapter 3 presents a detailed trade-off analysis between the static and dynamic stability of articulated vehicles considering two different tractor rear axle arrangements and three different trailer payload schemes. Chapter 4 describes vehicle modeling and validation of a 7 DOF tractor/semitrailer model, introduces the concept of local motion-planning, defines the reference motion trajectory, and establishes the kinematics for tractor/semi-trailer path-tracking. Chapter 5 presents the design of NLMPC-based tracking control strategy for AAHVs. Chapter 6 provides the conclusions and future work.

Chapter 2

Literature Review

2.1. Introduction

High-speed lateral stability of AHVs is critical and directly associated safe operation of these large vehicles. This chapter is to provide a comprehensive literature review on the previous work in stability related issues and various active safety techniques for increasing the safety of AHVs.

2.2. Lateral stability issues of AHVs

Lateral stability of articulated vehicles includes both yaw and roll stability. Roll over is mainly dependent upon the center gravity (CG) height and the lateral acceleration of trailers [21]. On the other hand, yaw instability is related to factors, such as forward speed, directional (steering) and speed control inputs, path curvature, tire/road interactions, trailer payload arrangement, etc. Below are the three lateral instability modes explained one by one.

Tractor swing is probably one of yaw instability modes [22-24], which is responsible for a lot of accidents. Tractor swing is a situation when the rear tires of the leading unit attain peak tire saturation forces and the driver is left with no control over the yaw motion of the tractor/semitrailer. It normally happens either accelerating/braking hard while negotiating a turn or hard braking on a low friction surface. Tractor is no more aligned with the trailer and the articulation angle between the tractor and trailer varies abnormally. It is considered as divergent instability. According to the reports given by the National Highway Traffic Safety Administration, 3.1% of accidents happened in 2003 were due to jackknifing [25].

Trailer swing is a scenario when the trailer tires reaches the saturation point and no more able to produce lateral force as a function of slip angle. In this case, the trailer shows an aperiodic behavior and starts swinging abnormally in one particular direction [26, 27]. It is also a divergent type of instability. It mostly happens with empty trailers or less vertical forces on the trailer tires at low coefficient of friction surfaces. Sometimes high-speed side winds may also make an empty trailer to behave abnormally which leads to trailer swing. Appropriate amount of the payload is one of the ways to avoid trailer swing.

Snaking/Swaying is considered as an oscillatory type instability mode in which either the leading unit or the trailing unit starts to oscillate in a periodic manner and increases over time until the tractor/semitrailer gets unstable [28]. Shifting the trailer payload towards the front improves the dynamic stability of articulated vehicles.

Roll over instability is another type of instability which is responsible for a lot of accidents over the years. Rollover happens because of high CG of trailers and high lateral acceleration of the trailer(s) [29]. Articulated vehicles possess low roll stability as compared to single unit vehicles due to their complex geometry specially on inclined surfaces or up hilling [30]. Due to high centrifugal forces while negotiating a curved path at high speeds, roll moment acts along the CG of the trailer which is countered by the lateral tire forces acting on the tires. Roll over takes place when the roll over moment is dominated and lateral force is not produced enough to counter the roll moment. Roll inertia, height of CG and suspension damping are some of the factors affecting the roll over stability of articulated vehicles.

In order to address lateral stability issues, many surveys have been conducted. A review done by Vlk [31] which was based on the lateral stability of articulated vehicles discussed the three lateral instability modes. A vehicle model was designed by Fratila based on the dynamics of car van

system [32]. A 24-DOF model was generated to analyze the parameters that affects the lateral stability of a car van system. Mass, yaw moment of inertia, mass of trailer, distance of axle from trailer center of gravity and tire cornering stiffness are the most important parameters affecting the lateral dynamics of a car van system shown in the analysis. Smitha has conducted a state-of-the-art review on the parameters affecting the directional performance and control methods to improve the directional performance for car-trailer systems [33]. She has discussed five different steady state behaviors of a car trailer combination based up on the understeering gradient values of tractor alone and trailer alone. According to her survey, a car-trailer system is always directionally stable if the understeer gradient of tractor is positive. Hac [34] has discussed the dynamics and stability of an articulated vehicle through analysis, simulations, and vehicle testing. He has shown that the dynamic stability of the articulated vehicle increases with keeping the CG of the trailer towards the front. He has shown how the dynamic response of an articulated vehicle is affected by forward speed and loading condition by conducting simulations and collecting data from the road tests.

Darling [35] has also investigated the impact of trailer geometry on the dynamic stability by using an adjustable trailer in his investigation. It was found that the dominant factors affecting stability were the trailer yaw inertia, nose mass (load distribution), and trailer axle position. The tire pressure also affected the stability, although the effect was less significant. A study was conducted to understand the effect of adding trailer axles on the rearward amplification [36]. It is concluded that a tractor/semi-trailer combination generally possess a stable dynamic performance because of the long wheelbase of trailers. However, adding more articulation can reduce the dynamic performance of articulated vehicle. It is also found in the study that central axle trailers and full trailers generally reduce the rearward amplification (RA) of articulated vehicle.

2.3. Safety systems for articulated vehicles

In order to address lateral stability issues, various solutions have been sought to increase the safety of articulated vehicles, including active and passive safety systems [37]. Passive trailer steering is an example of passive safety technique, which may improve the maneuverability at low speeds. Various active safety systems have been proposed and studied, which include active trailer steering [38], trailer differential braking [39], and anti-roll control [40]. The effective operating conditions and the corresponding variation range of lateral acceleration for each of the aforementioned three active safety systems have been discussed and analyzed [21]. Simulation results show that active trailer steering can improve both lateral stability and maneuverability of an AHV with minimal path-following off tracking and rearward amplification [41].

2.4. Passive trailer steering

Attempts have been made on the passive trailer steering systems to improve low-speed maneuverability of AHVs. The effect of self-steering axle location of trailer on the dynamic stability of AHVs was assessed by Aurell [42]. A comparative study of three different passive steering systems, including self-steering, command- or forced-steering, and pivotal bogie, was conducted by Jujnovich and Cebon [43]. It was reported that optimal values of vehicle parameters, such as vertical force distribution, dimensions of trailing unit, axle placement, can improve directional performance. Sanker et al. [44] have examined the direct relation between articulation angle and rear axle steering angle to decide the steering input for the trailers. It has been observed that such steering systems can improve maneuverability and reduce the off tracking at low speeds. Articulated vehicles with passive trailer steering systems generally degrade high-speed lateral stability. AHVs experience large rearward amplification and path-following off tracking with

passive steering systems at high speed operations [45]. So, there exists a trade-off between low-speed maneuverability and high-speed lateral stability as the parameters which improves lateral stability may degrade the maneuverability. Poor directional performance of AHVs with passive trailer steering at high speeds may lead to instability modes, which includes jack-knifing, trailer swaying and rollover.

2.5. Active stability control

To date, active stability control is a very popular strategy to improve the lateral stability and maneuverability of AHVs, as passive trailer steering is not a good option for high-speed lateral stability. Active stability control mainly includes active trailer differential braking and active trailer steering system. Many active trailer steering strategies have been discussed over the years to improve low-speed path-following off-tracking issues [46-49]. Researchers at Cambridge university presented an active trailer steering control strategy for conventional tractor - active trailer (CT-AT) systems and active tractor - active trailer (AT-AT) systems [50]. Simulation results have shown that active trailer steering control strategy is able to enhance the performance at low speeds as well as high speeds. The AHV is able to maintain good path-following performance all the time which reduces off-tracking. Active trailer steering also causes less yawing which further reduce rearward amplification ratio and lateral load transfer which shows that active trailer steering performs better than passive steering in terms of lateral stability at high speeds. Islam [51] presented a closed-loop dynamic simulation-based design method for AHVs with active trailer steering (ATS) systems. The proposed design reduces the rearward amplification ratio by 52.2% and path-following off tracking by 24.8% in an obstacle avoidance lane change maneuver. Khajepour and his team [52] designed a differential braking strategy and employed it on both tractor and trailer simultaneously. They further explained that both tractor and trailer differential

braking are effective in improving handling performance and minimizing hitch angles but tractor differential braking offers more stability compared to trailer differential braking. Another way of achieving better lateral stability and maneuverability is to use a passive and an active trailer steering system. Passive steering takes care of the path-following off-tracking issues to improve maneuverability at low speeds, while activity trailer steering is to improve lateral stability at high speed maneuvers. It is a good way to deal with the trade -off in the design criteria but it makes the geometry of trailer more complex [53, 54].

2.6. Predicted safety systems

Predictive safety systems (PSSs) are very popular these days as they remove the driver from the control loop. Since vast majority of accidents happen due to the mistake of driver, replacing a driver completely with an autonomous control can be a revolutionary step that can save many innocents lives. The past three decades have witnessed the development of advanced driver assistance systems, e.g., lane departure prevention. These systems are known as 'predictive safety systems' [55], which consider not only current vehicle state, but also predicted vehicle state and hazards in a finite future time window. Since the beginning of 21st century, extensive research has been conducted to explore autonomous vehicle technologies. Majority of the research in this area is dedicated to single unit vehicles. Designing PSSs for AHVS is still open for research.

In recent years, few attempts have been made on developing tracking-control techniques for farm tractor/trailer combinations [56], heavy-duty mining and construction trucks [57], and AHVs with automated reverse parking [58]. A path-planning scheme was proposed for tractor/semi-trailer combinations operating in urban environments [59]. These studies share one common feature that they focused on low-speed trajectory-tracking and/or motion-planning based on kinematic control,

while ignoring the high-speed RA dynamic behavior and the unstable motion modes of rollover, jackknifing, and trailer sway.

Few scholars tackled the issues of local motion-planning and tracking-control for AAHVs under high-speed operations. A path-planning method for single and double lane-change maneuvers at constant speed was proposed, and the feasibility of the approach was examined using simulation [60]. A forward speed-planning scheme was developed [61]; considering the curvature of reference path and all vehicle units' states, a fuzzy controller was devised to control lateral acceleration via adjusting forward speed in order to maximize speed and minimize travel time. A robust linear quadratic regulator and a H_∞ controller was devised for path-following and lateral stability control of a tractor/semi-trailer, and the two tracking-controllers were compared in terms of robustness, driving smoothness, and safety [62]. A model predictive control (MPC) based tracking-controller was proposed for AHVs operating on electrified highways, and the MPC tracking-controller was evaluated with numerical simulations under the maneuvers of adaptive cruise control, overtaking, and path-following [63]. A hybrid tracking-controller was designed [64], in which an MPC controller is responsible for curved path negotiation, and an optimal curvature preview controller for straight road operations.

In the aforementioned studies on local motion-planning and tracking-control for AAHVs, the respective local motion-planning and tracking-control designs were mainly based on the output and input variables of the leading vehicle unit, while the output variables of the trailing vehicle unit(s) were generally ignored. This design consideration may be attributed to the fact that the actuators for steering and forward speed manipulations are equipped on the leading vehicle unit. However, this design practice may underestimate the effect of RA dynamic behavior of AHVs. Most of the above trajectory tracking-controllers for AAHVs were essentially path tracking-

controllers due to the fact that over curved road negotiations and lane-change maneuvers, vehicle forward speed was assumed to be constant. In reality, the forward speed of an AHV may vary, e.g., under an overtaking maneuver in highway operations.

This research is intended to address the aforementioned issues by designing a novel tracking-controller for AAHVs.

Chapter 3

Trade-off Analysis between Static and Dynamic Stability of Articulated Heavy Vehicles

3.1. Introduction

This chapter conducts a detailed study on static and dynamic stabilities of AHVs considering two different rear axle arrangements of the tractor and three different schemes of payloads on a semi-trailer with a tridem-axle group. In order to conduct this study, a 3 degrees of freedom (DOF) linear yaw-plane model is developed in the MATLAB/Simulink environment to represent the lateral dynamics of a tractor/semi-trailer. Comparative studies have been conducted to examine various vehicle models for representing the lateral dynamics of AHVs [65-67]. It was found that linear yaw plane model works effectively in terms of steady state handling response up to a lateral acceleration of 0.25g. Also, a linear model provides reasonable prediction up to a lateral acceleration range of 0.4g for AHVs with highly understeered tractor.

3.2. 3-DOF linear yaw plane tractor/semi-trailer model

Figure 3.1 shows the schematic diagram of a linear 3-DOF yaw-plane model to represent the lateral dynamics of the tractor/semi-trailer. It is assumed: 1) each axle of the tractor and the semi-trailer is represented by a single wheel located at the center of the respective axle; 2) the aerodynamic effect as well as the motions of pitch, roll and lift are neglected; 3) the vehicle unit's mass is lumped at its CG with a given mass moment of inertia about the respective vertical axis of the body-fixed coordinate system. In the modelling, the motions considered include the lateral and yaw motions of the tractor, as well as the yaw motion of the trailer. Based on Newton's law of

dynamics, the equations of motion are derived. The governing equations of the lateral and yaw motions of the tractor expressed in the tractor-fixed coordinate system are given as

$$m_t\left(\dot{v}_{yt} + r_t v_{xt}\right) = F_{ytt} - F_{fy} \tag{3.1}$$

$$I_{zt}\dot{r}_t = M_{zt} + F_{fy}L_{wt} \tag{3.2}$$

where m_t denotes the tractor mass, I_{zt} tractor yaw moment of inertia, r_t yaw rate of the tractor, L_{wt} distance between the tractor CG and the fifth-wheel, M_{zt} the yaw moment due to tractor tire forces, v_{xt} and v_{yt} are longitudinal and lateral velocities at tractor CG, F_{ytt} is the total tractor tire forces in lateral direction, F_{fx} and F_{fy} are the tractor and trailer hitch force at the fifth-wheel in the longitudinal and lateral direction.

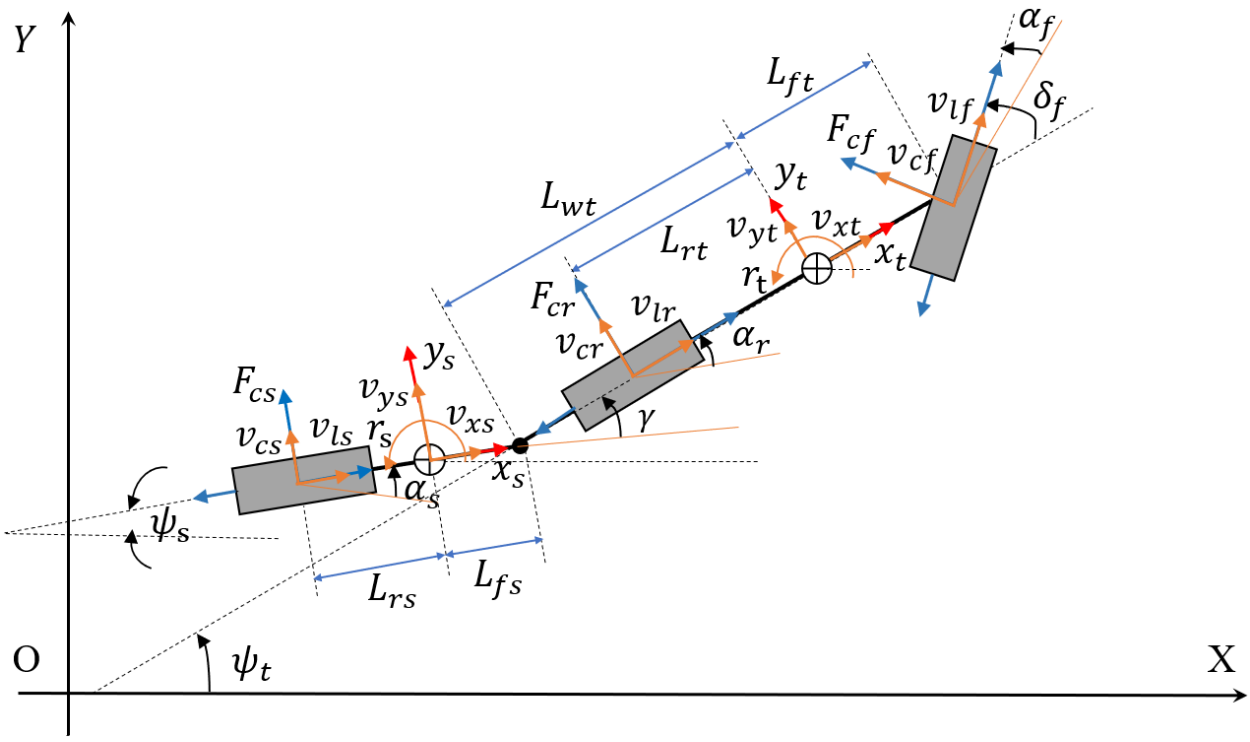

Figure 3.1 Schematic representation of the 3-DOF yaw-plane tractor/semi-trailer model.

The governing equations of the lateral and yaw motions of the trailer expressed in the tractor-fixed coordinate system are given as

$$m_s\left(-L_{fs}r_s^2\,\gamma - L_{wt}\dot{r}_t - L_{fs}\dot{r}_s + \dot{v}_{yt} + r_t v_{xt}\right) = F_{yts} + F_{fy} \tag{3.3}$$

$$I_{zs}\dot{r}_s = M_{zs} + F_{fx}\gamma L_{fs} + F_{fy}L_{fs} \tag{3.4}$$

where m_s denotes the trailer mass, I_{zs} trailer yaw moment of inertia, M_{zs} trailer yaw moment due to trailer tire forces, γ articulation angle between the tractor and the trailer, L_{fs} the distance between the fifth-wheel and the trailer CG, r_s trailer yaw rate, F_{yts} the total lateral tire forces expressed in x and y axis of the tractor-fixed coordinate system. Combining Equations (3.1) to (3.4) and eliminating the reaction forces at the fifth-wheel leads to the following governing equation of motions of the tractor/semi-trailer expressed in the tractor-fixed coordinate system as

$$(m_t + m_s)\left(\dot{v}_{yt} + r_t v_{xt}\right) - m_s\left(L_{fs}r_s^2\gamma + L_{wt}\dot{r}_t + L_{fs}\dot{r}_s\right) = F_{ytt} + F_{yts} \tag{3.5}$$

$$I_{zt}\dot{r}_t + m_t\left(\dot{v}_{yt} + r_t v_{xt}\right)L_{wt} = M_{zt} + F_{ytt}L_{wt} \tag{3.6}$$

$$I_{zs}\dot{r}_s + m_t\left(-r_t v_{yt}\right)L_{fs}\gamma + m_t\left(\dot{v}_{yt} + r_t v_{xt}\right)L_{fs} = M_{zs} + F_{ytt}L_{fs} \tag{3.7}$$

The lateral tire forces and moments can be calculated as

$$F_{ytt} = F_{cf}cos\delta_f + F_{cr} \tag{3.8}$$

$$F_{yts} = F_{cs}cos\gamma \tag{3.9}$$

$$M_{zt} = (F_{cf}cos\delta_f)L_{ft} - (F_{cr})L_{rt} \tag{3.10}$$

$$M_{zs} = -(F_{cs})L_{rs} \tag{3.11}$$

The tire side slip angles for tractor and trailer wheels can be calculated as

$$\alpha_f = \delta_f - arctan\left(\frac{v_{cf}}{v_{lf}}\right) \tag{3.12}$$

$$\alpha_r = -arctan\left(\frac{v_{cr}}{v_{lr}}\right) \tag{3.13}$$

$$\alpha_s = -arctan\left(\frac{v_{cs}}{v_{ls}}\right) \tag{3.14}$$

where δ_f denotes the steer angle of tractor front wheel, α_f, α_r, and α_s are the side slip angle of the tractor front tire, tractor rear tire, and trailer tire, respectively, v_{cf} denotes the lateral velocity of tractor front tire, v_{cr} denotes the lateral velocity of tractor rear tire, v_{cs} denotes the lateral velocity of trailer tire, v_{lf} denotes the longitudinal velocity of tractor front tire, v_{lr} denotes the longitudinal velocity of tractor rear tire, v_{ls} denotes the longitudinal velocity of trailer tire

The tire forces per axle are assumed to be proportional to the tire slip angles as

$$F_{cf} = C_f \alpha_f \tag{3.15}$$

$$F_{cr} = C_r \alpha_r \tag{3.16}$$

$$F_{cs} = C_s \alpha_s \tag{3.17}$$

Where C_f, C_r and C_s are the cornering stiffness values of tractor front, tractor rear and trailer tires. Using the above equations, the 3-DOF linear tractor/semi-trailer model is expressed in the compact form as

$$\boldsymbol{M\dot{x}} = \boldsymbol{Dx} + \mathbf{E}\boldsymbol{u} \tag{3.18}$$

where

$$\boldsymbol{x} = [\gamma \; v_{yt} \; r_t \; r_s]^T \tag{3.19}$$

$$\boldsymbol{u} = [\delta_f] \tag{3.20}$$

In order to do eigenvalue analysis for the dynamic stability of the AHV, the system matrix is derived as

$$\boldsymbol{A} = \boldsymbol{M}^{-1}\boldsymbol{D} \tag{3.21}$$

Based on the aforementioned equations, the linear 3-DOF tractor/semi-trailer model is developed in MATLAB/Simulink to evaluate the effect of axle arrangements and payload schemes on the static and dynamic stabilities of the AHV. Matrices **M**, **D** and **E** are given in the Appendix.

3.3. Trailer payload schemes

Three different payload schemes are considered in this study to analyze the effect of trailer payload on the static and dynamic stability of the tractor/semitrailer. The first scheme is considered as an empty trailer payload case, in which trailer is considered to be having zero payload.

In the second scheme, a 9000 kg trailer payload is considered. Figure 3.2 illustrates the dimensions of the trailer payload. The payload material is stainless steel. Since roll motion is not considered, the payload CG height is assumed to be zero. The density of stainless steel is 7500 kg/m^3 and volume of the payload is 1.2 m^3, which results in the payload mass of 9000 kg.

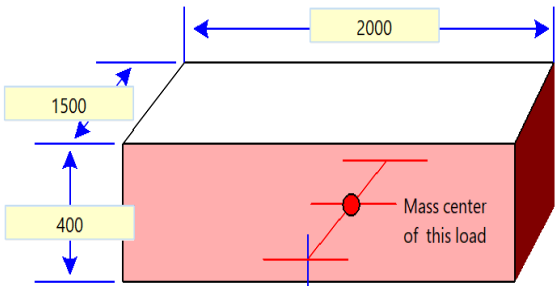

Figure 3.2 Dimensions of 9000 Kg payload in mm.

In the third scheme, 20582.76 kg trailer payload is considered, Stainless steel is considered as the material of the payload. Figure 3.3 shows the dimensions of the payload.

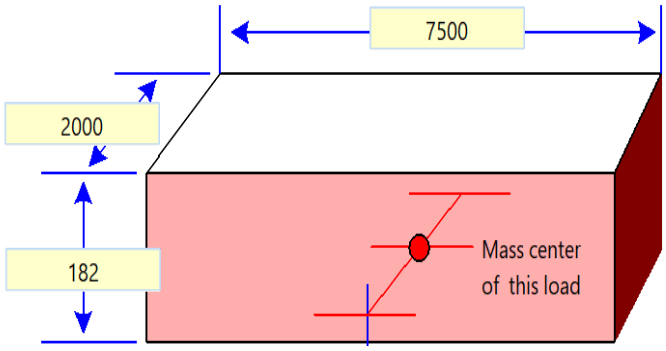

Figure 3.3 Dimensions of 20000 Kg payload in mm.

The positions of CGs of the trailer payloads are assumed to be coincident with the CG of the empty trailer payload in this research. The mass moments of inertia of the payloads are calculated based on this assumption. The maximum gross weight limit of single rear axle tractor semi-trailer and a double rear axle tractor semitrailer is taken in to consideration and payloads on the trailer are selected accordingly [92]

3.4. Stability analysis

Two types of instability modes exist for a system of at least second order. The first one is a 'static' or divergent type of instability mode, in which the variables describing the system increase exponentially in magnitude without oscillations. The second one is a "dynamic" instability, in which the variables experience oscillations with increasing amplitude [34]. A trade-off between the two instability modes exists. Making the system statically stable may lead to degrading the dynamic stability of the system, and vice versa. Therefore, a compromise between the two instabilities may be an acceptable solution. In this study, we explore the effects of trailer payload

and different tractor rear axle arrangements on the static and dynamic stabilities of the tractor/semi-trailer system.

3.5. Static stability

In order to analyze the static stability, steady state condition of tractor/semi-trailer is considered. The understeer gradient (k_{us}) of the tractor/semi-trailer is calculated to analyze the steady state handling responses considering three different trailer payload schemes and two rear axle arrangements of the tractor.

Calculation of combined the understeer gradient of tractor semi/trailer can be done by using the approach reported in [34]. Considering the steady state turn of the tractor alone, yaw rate of the tractor is given by

$$\omega_1 = \frac{V_x \delta_f}{l_1 + k_{us} {V_x}^2} \tag{3.22}$$

where l_1 is the wheelbase of the tractor, and $l_1 = l_{ft} + l_{rt}$. The understeer gradient of the tractor is defined by k_{us} as

$$K_{us} = \frac{1}{g}\left(\frac{w_f}{C_f} - \frac{w_r}{C_r}\right) \tag{3.23}$$

where w_f and w_r are the static loads on the front and rear tires of the tractor.

Considering the steady state turn of the tractor/semi-trailer, yaw rate of the tractor/semi-trailer is given by

$$\omega_2 = \frac{V_x \delta_f}{l_1 + (k_{us} - \Delta k_{us}) {V_x}^2} \tag{3.24}$$

where k_{us} is the understeer gradient of the tractor alone, and Δk_{us} is the change of the understeer gradient due to the attached semi-trailer, which can be calculated by

$$\Delta k_{us} = \frac{m_2 L_{rs}[C_f(L_{ft}+L_{wt})+C_r(L_{wt}-L_{rt})]}{C_f C_r(L_{ft}+L_{rt})(L_{rs}+L_{fs})} \tag{3.25}$$

The load shift of the trailer towards the tractor front and rear axles can be calculated as

$$\Delta W_f = \frac{-m_2 L_{rs}(L_{wt}-L_{rt})g}{(L_{ft}+L_{rt})(L_{rs}+L_{fs})} \tag{3.26}$$

$$\Delta W_r = \frac{m_2 L_{rs}(L_{wt}-L_{rt}+L_{ft}+L_{rt})g}{(L_{ft}+L_{rt})(L_{rs}+L_{fs})} \tag{3.27}$$

The equivalent understeer gradient of the tractor/semi-trailer is given by

$$K_{us} - \Delta k_{us} = \frac{1}{g}\left(\frac{w_{ft}}{C_f} - \frac{w_{rt}}{C_r}\right) \tag{3.28}$$

$$w_{ft} = w_f + \Delta W_f \tag{3.29}$$

$$w_{rt} = w_r + \Delta W_r \tag{3.30}$$

Table 3.1 lists the values of the equivalent understeer gradient coefficient of the tractor/semi-trailer system considering different trailer payload schemes and trailer rear axle arrangements. A higher trailer payload leads to a load shift towards the rear axle of the tractor, which decreases the understeer gradient of the tractor/semi-trailer system.

The comparison between understeer gradient coefficient values of the single tractor rear axle arrangement and the double tractor rear axle arrangement clearly indicates that adding one more tractor axle reduces the oversteer gradient of the tractor/semitrailer. An additional axle at the rear of the tractor increases the wheelbase and number of rear tires of the tractor, which improves the understeer steady state handling response as compared to the single rear axle tractor.

Table 3.1 Understeer gradient coefficient values under different conditions.

Equivalent understeer gradient of single tractor rear axle with zero trailer payload	$0.02\,\frac{rad}{g}$
Equivalent understeer gradient of single tractor rear axle with 9000 Kg trailer payload	$-0.0546\,\frac{rad}{g}$
Equivalent understeer gradient of single tractor rear axle with 20000 Kg trailer payload	$-0.1188\,\frac{rad}{g}$
Equivalent understeer gradient of double tractor rear axles with zero trailer payload	$0.0408\,\frac{rad}{g}$
Equivalent understeer gradient of double tractor rear axles with 9000 Kg payload	$0.01\,\frac{rad}{g}$
Equivalent understeer gradient of double tractor rear axles with 20000 Kg payload	$0.009\,\frac{rad}{g}$

3.6. Handling performance measure

The steady state handling performance of a tractor/semi-trailer system can also be evaluated by calculating the slope of difference between the Ackerman angle and the front wheel steering angle, (L/R- δ), versus lateral acceleration (a_y) [68]. The Ackerman angle (L/R) is defined as the front wheel angle, which is required by a simple two axle vehicle having a wheelbase of L to negotiate a turn with a curve radius R at a zero forward speed, whereas the front wheel steering angle (δ) can be determined by considering the steering-wheel angle input and the steering system gear ratio. In this method, a ramp steering-wheel input of 2 deg/sec is given to the tractor/semitrailer at a constant forward speed up to 100 km/h, which leads to the rate of change of lateral acceleration

well within the range of 0.01g/sec to 0.02g/sec [68]. In this study, the steering gear ratio is set to 16.94, which is taken from the corresponding TruckSim model, and this value is used for a power assist steering system.

3.6.1. Handling diagram of the single tractor rear axle arrangement

The handling diagram is plotted for the single tractor rear axle arrangements with different trailer payload schemes to evaluate the steady state handling behavior of the tractor/semi-trailer combination.

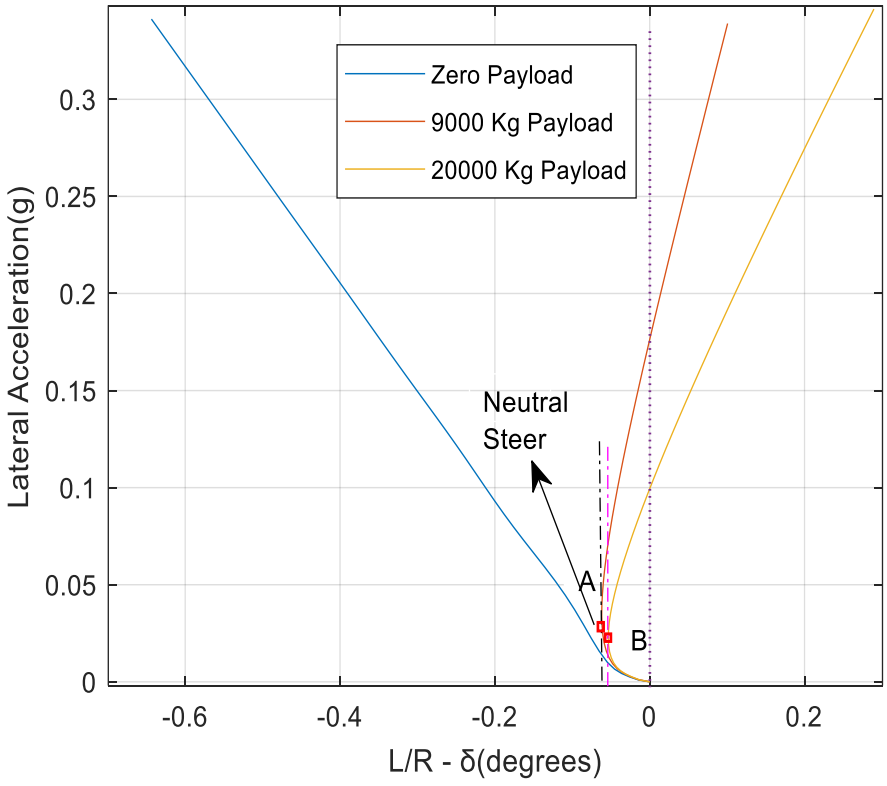

Figure 3.4 Handling diagram of the single tractor rear axle arrangement.

Figure 3.4 shows the handling diagram of the single tractor rear axle arrangement with three trailer payloads schemes of 0, 9000 and 20000 kg. It can be observed that the understeer gradient is

dropping with the increase of trailer payload. The tractor/semi-trailer with zero trailer payload is showing an understeer behavior throughout the lateral acceleration range up to 0.35g, whereas the understeer behavior for the scheme of 9000 kg trailer payload and 20000 kg trailer payload is changing from understeer to oversteer at point A and point B. Lateral acceleration value at point A and B is 0.034g and 0.026g which shows that tractor/semi-trailer having 9000 kg payload shows better understeer behavior than tractor/semi-trailer having 20000 kg payload.

The results shown in Figure 3.4 through handling diagram are consistent with the understeer gradient coefficient values listed in Table 3.1. However, the handling diagram seen in Figure 3.4 provides more detailed information regarding the steady state handling performance of the vehicle under different operating conditions.

3.6.2 Handling diagram of the double tractor rear axle arrangement

Figure 3.5 illustrates the handling diagram of the double tractor rear axle arrangement with three trailer payload schemes.

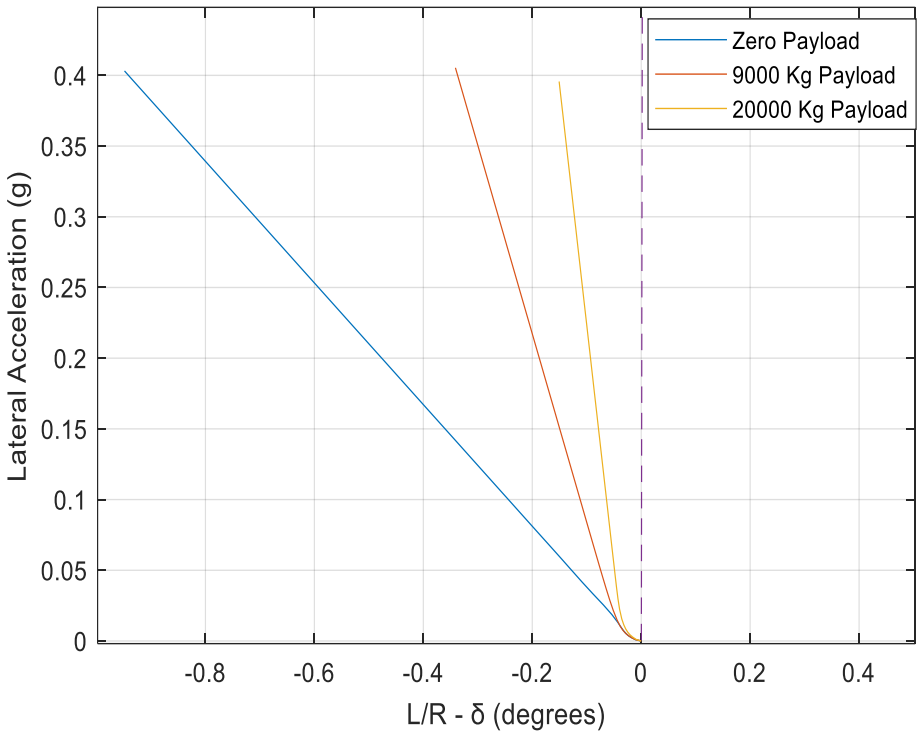

Figure 3.5 Handling diagram of the double tractor rear axle arrangement.

With the increase of trailer payload, the understeer gradient of tractor/semi-trailer decreases. This is due to the transfer of vertical load towards the rear of tractor at the fifth-wheel. However, the extra rear axle on the tractor enhances the understeer handling behavior as compared to single trailer rear axle arrangement. The handling diagram results shown in Figure 3.5 well agree with the conclusion drawn from the understeer gradient coefficient values given in Table 3.1.

3.7. Dynamic stability

In order to study the dynamic stability, the tractor/semi-trailer combination is considered as a free vibration system with zero control input, and the system matrix, **A**, expressed in Equation (3.21) is used to conduct eigenvalue analysis [34, 69-71]. The system eigenvalues (poles) are the eigenvalues of matrix **A**, that is, the roots of the characteristic equation

$$\det(S\boldsymbol{I} - \boldsymbol{A}) = 0 \tag{3.31}$$

where $\boldsymbol{I}$ is an identity matrix and S represents the roots of the characteristic equation. Since **A** is a matrix of dimension 4x4 with all real value elements, So, the above equation is a 4-th order equation with real coefficients. The roots are therefore either real or complex occurring in conjugate pairs. The system will be considered as stable if all the roots have a negative real part. The system will get unstable if the real parts are positive values. Since matrix **A** is depending upon longitudinal forward speed, the positions of the eigenvalues also change with forward speed. Plotting a graph in terms of the relationship between the damping ratio and the forward speed is an effective way to evaluate the dynamic stability of the AHV. If the system has a pair of complex eigenvalue as

$$S_{1,2} = d \pm jw \tag{3.32}$$

where j is the imaginary unit, d the rear part, and w the imaginary part. The damping ratio can be calculated by

$$\xi = \frac{-d}{\sqrt{d^2+w^2}} \tag{3.33}$$

A negative damping ratio ζ indicates an unstable system. The eigenvalue analysis is done for the tractor/semitrailer combination considering two different tractor rear axle arrangements and three different trailer payload schemes.

3.8. Eigenvalue analysis for single tractor rear axle arrangement

The matrix, **A**, expressed in Equation (3.21) is utilized to calculate the eigenvalues considering the single tractor rear axle arrangement with three different trailer payload schemes. Given a pair of complex eigenvalues, the damping ratio is calculated using Equation (3.33).

3.8.1. Zero trailer payload

Figure 3.6 shows the relationship between damping ratio and forward speed for the single tractor rear axle arrangement with zero trailer payload scheme. In this figure, the two curves represent two motion modes of the tractor/semitrailer combination. For the motion mode shown in brown curve, the damping ratio drops as forward speed increases. When the damping ratio takes the value of zero, the vehicle forward speed is approximate 59 m/s, which is the critical speed. Beyond the critical speed, the tractor/semi-trail combination will lose it lateral stability, experiencing trailer sway with the oscillation amplitude increasing with the time.

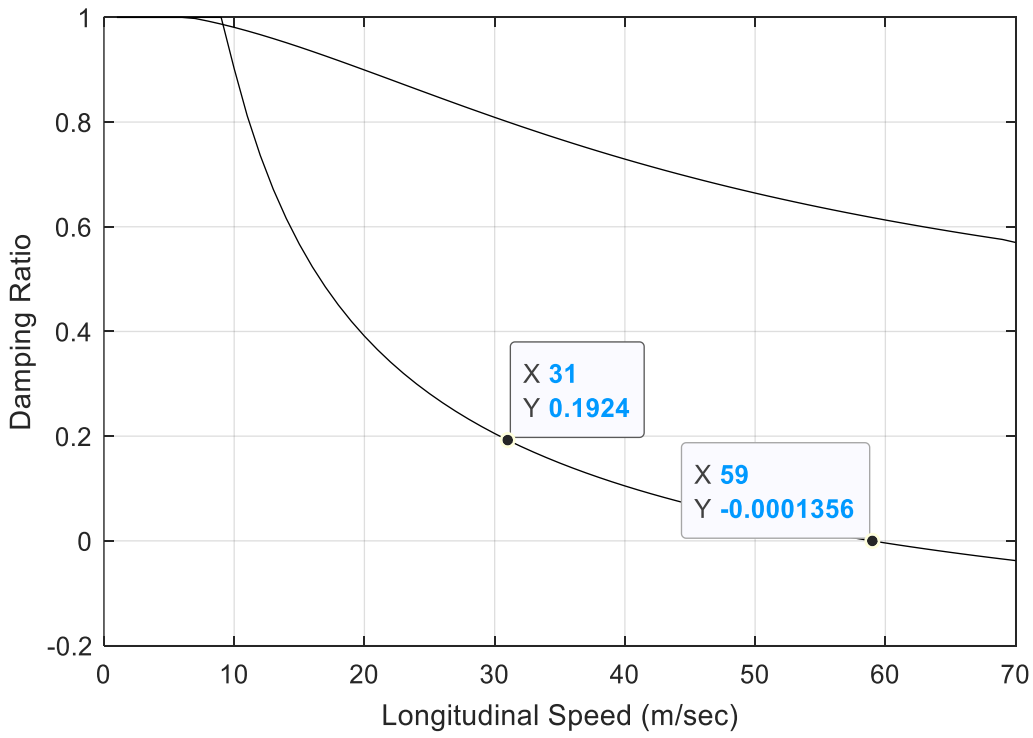

Figure 3.6 Damping ratio vs forward speed for single trailer rear axle arrangement with zero trailer payload.

3.8.2. 9000 kg trailer payload

Figure 3.7 shows the relationship between the damping ratio and forward speed for the single tractor rear axle arrangement with 9000 kg trailer payload. For the two motion modes shown in

the figure, even though the damping ratio drops with vehicle forward speed. However, within the speed range concerned, the damping ratio of the least damped motion mode remains positive. This implies that the vehicle is dynamically stable at forward speed up to 200 m/s. A comparison between the results shown in Figures 3.6 and 3.7 discloses that increasing trailer payload is benefit for improving the dynamic stability of the tractor/semi-trailer combination. Load added at the trailer increases the vertical force, which increases the lateral tire force, hence increasing the yaw damping effect of the tractor/semi-trailer system.

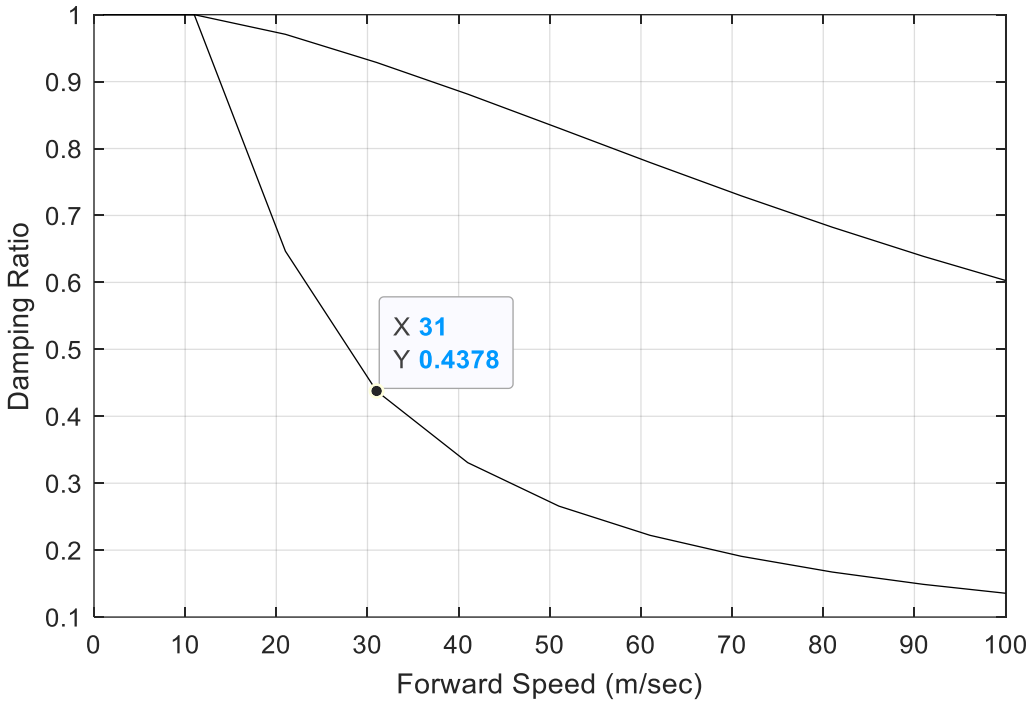

Figure 3.7 Damping ratio vs forward speed for the single tractor rear axle arrangement with 9000 kg trailer payload.

3.8.3. 20000 kg trailer payload

Figure 3.8 shows the relationship between the damping ratio and the forward speed for the single tractor rear axle arrangement with 20000 kg trailer payload. Similar to the scheme of 9000 kg trailer payload shown in Figure 3.7, the scheme of 20000 kg trailer payload seen in Figure 3.8 is

dynamically stable over the forward speed range concerned. To identify the difference between the two trailer payload schemes, we compare the damping ratios at the forward speed of 31.0 m/s for the least damped motion modes of the two schemes. As shown in Figures 3.7 and 3.8, at the given forward speed, the damping ratio for the 9000 kg trailer payload scheme is 0.4378, whereas the counterpart for the 20000kg trailer payload scheme is 0.4781.Thus, considering the three trailer payload schemes, for the single trailer rear axle arrangement, we may conclude that increasing trailer payload is benefit for improving the dynamic stability of the tractor/semi-trailer combination. Thus, the dynamic stability and static stability have conflicting requirement on the trailer payload. In the latter case, as discussed in Section 3.5 and 3.6, the less the trailer payload, the higher the static stability.

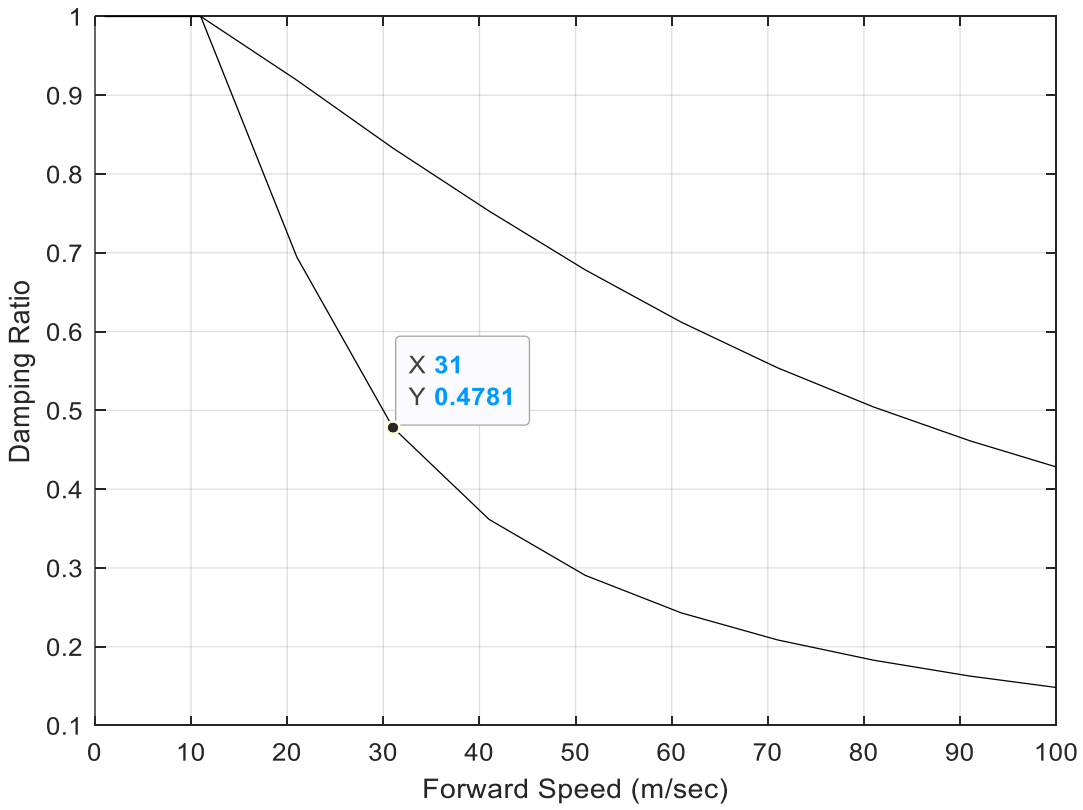

Figure 3.8 Damping ratio vs forward speed for the single tractor rear axle arrangement with 20000 kg trailer payload.

3.9. Evaluating dynamic stability of the single tractor rear axle arrangement using TruckSim model

A convenient way to evaluate the dynamic stability of the tractor/semitrailer combination is to conduct an open-loop sinewave steering input testing maneuver. Figure 3.9 shows the time history of the tractor front wheel steering angle for the simulated testing maneuver using the corresponding TruckSim model of the tractor/semi-trailer combination. Note that the TruckSim model represents the single tractor rear axle arrangement with three trailer payload schemes of 0, 9000, and 20000 kg. Two forward speeds are considered, i.e., 50 and 70 m/s. Note that as shown in Figure 3.6, for the single tractor rear axle arrangement with zero trailer payload, the 3-DOF yaw-plane model identifies the critical speed, i.e., 59.0 m/s. Thus, the selected forward speed of 50 m/s is less than the critical speed, while the forward speed of 70 m/s is higher than the critical speed.

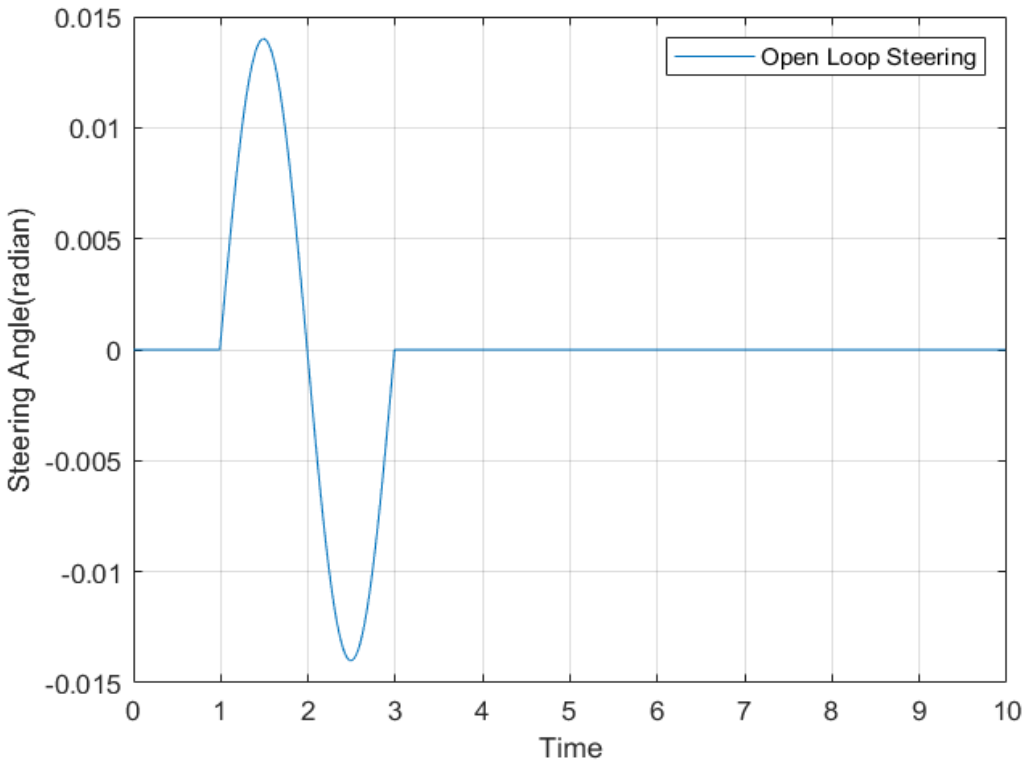

Figure 3.9 Time history of tractor front wheel steering angle.

3.9.1. Yaw rate and lateral acceleration

Figures 3.10, 3.11 and 3.12 show the time history of the trailer yaw rate, tractor lateral acceleration, and the trailer lateral acceleration at the forward speed of 50 m/s for the single tractor rear axle arrangement with three trailer payload schemes. It can be observed that the trailer is showing an oscillating behavior, but it is getting stable with time in the case of trailer with zero payload. In the trailer payload schemes of 9000 and 20000 kg, the AHV oscillates about one cycle and quickly settles down to its steady state. The results shown in Figures 3.10, 3.11, and 3.12 achieve good agreement with those based on the eigenvalue analysis using the 3-DOF linear yaw-plane model.

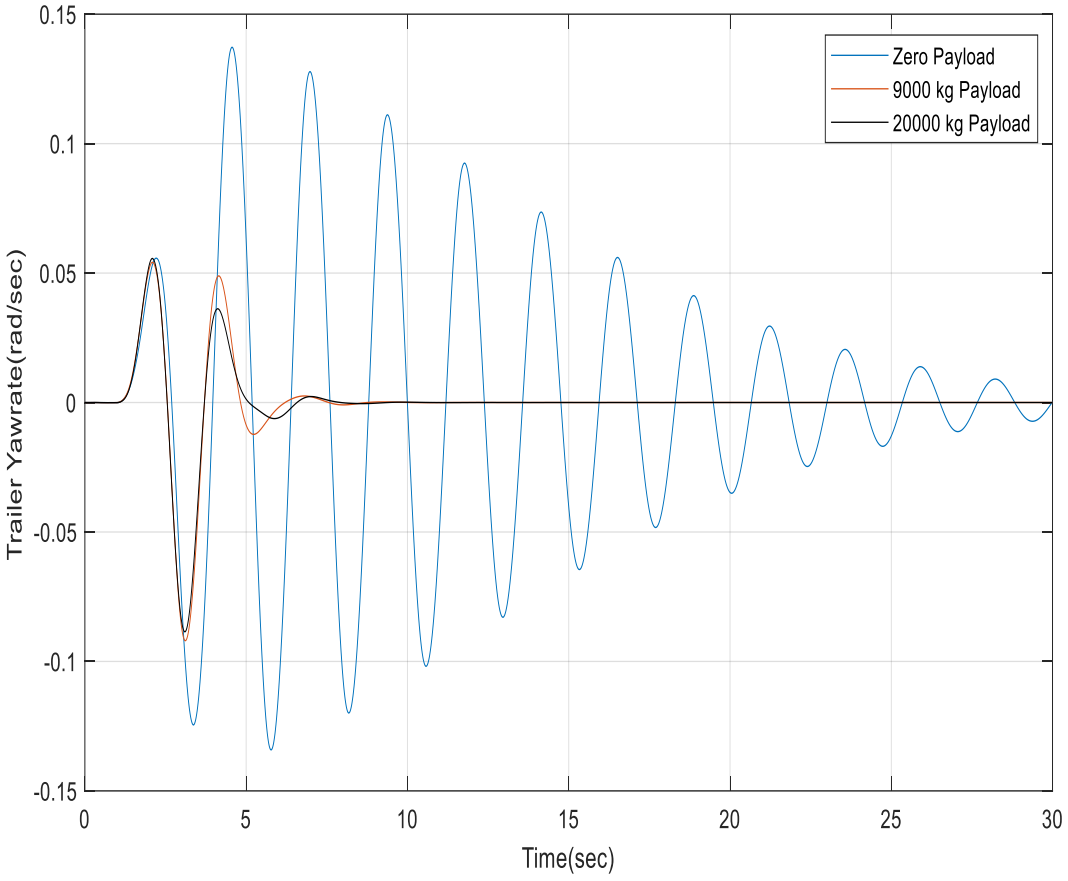

Figure 3.10 Time history of trailer yaw rate at forward speed of 50 m/s for the single tractor rear axle arrangement with three trailer payload schemes.

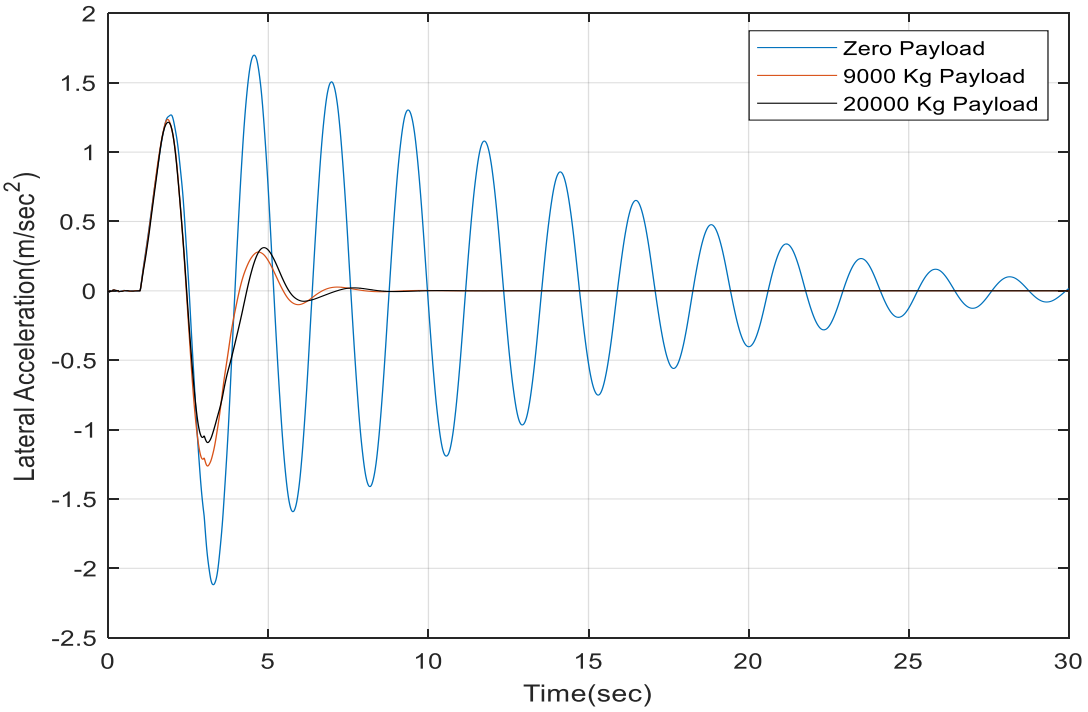

Figure 3.11 Time history of tractor lateral acceleration at forward speed of 50 m/s for the single tractor rear axle arrangement with three trailer payload schemes.

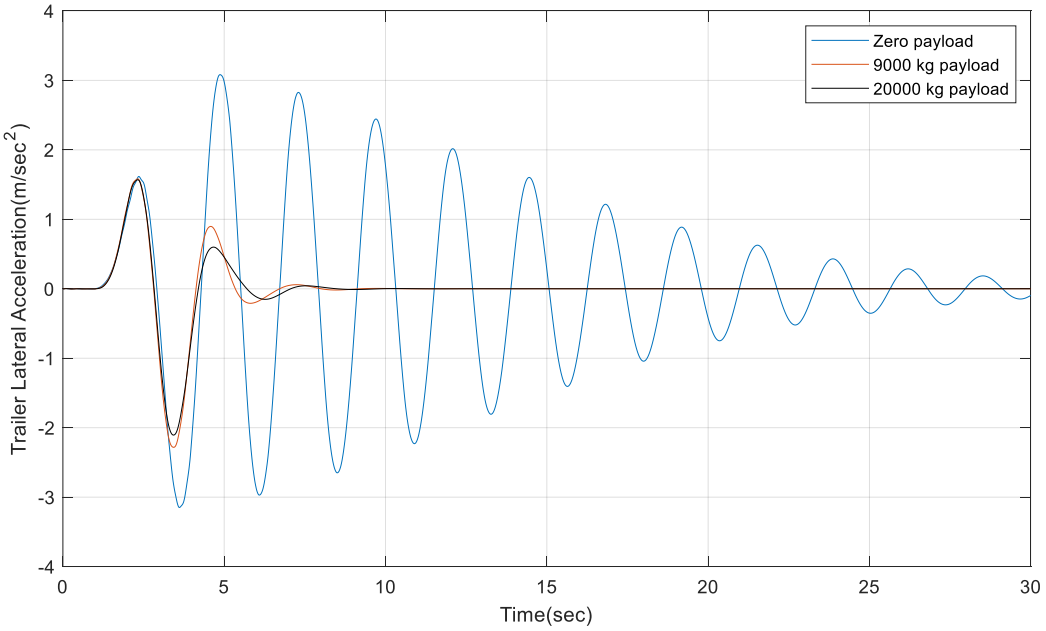

Figure 3.12 Time history of trailer lateral acceleration at forward speed of 50 m/s for the single tractor rear axle arrangement with three trailer payload schemes.

Figures 3.13, 3.14 and 3.15 shows the time history of trailer yaw rate, tractor lateral acceleration, and trailer lateral acceleration at the forward speed of 70 m/h for the single tractor rear axle arrangement with three trailer payload schemes. Results show that for the zero trailer payload scheme, the AHV oscillates in terms of leading and trailer units' yaw rate and lateral acceleration. The amplitudes of the oscillations increase with time, and eventually the vehicle loses its lateral stability. On the other hand, for the trailer payload schemes of 9000 and 20000 kg, after around one cycle of oscillation in terms of both the leading and trailing units' yaw rate and lateral acceleration, the tractor/semi-trailer combination settles down to its stable steady state straight line motion. Once again, the time domain simulation based on the TruckSim model is consistent with that of the eigenvalue analysis using the 3-DOF yaw-plane model.

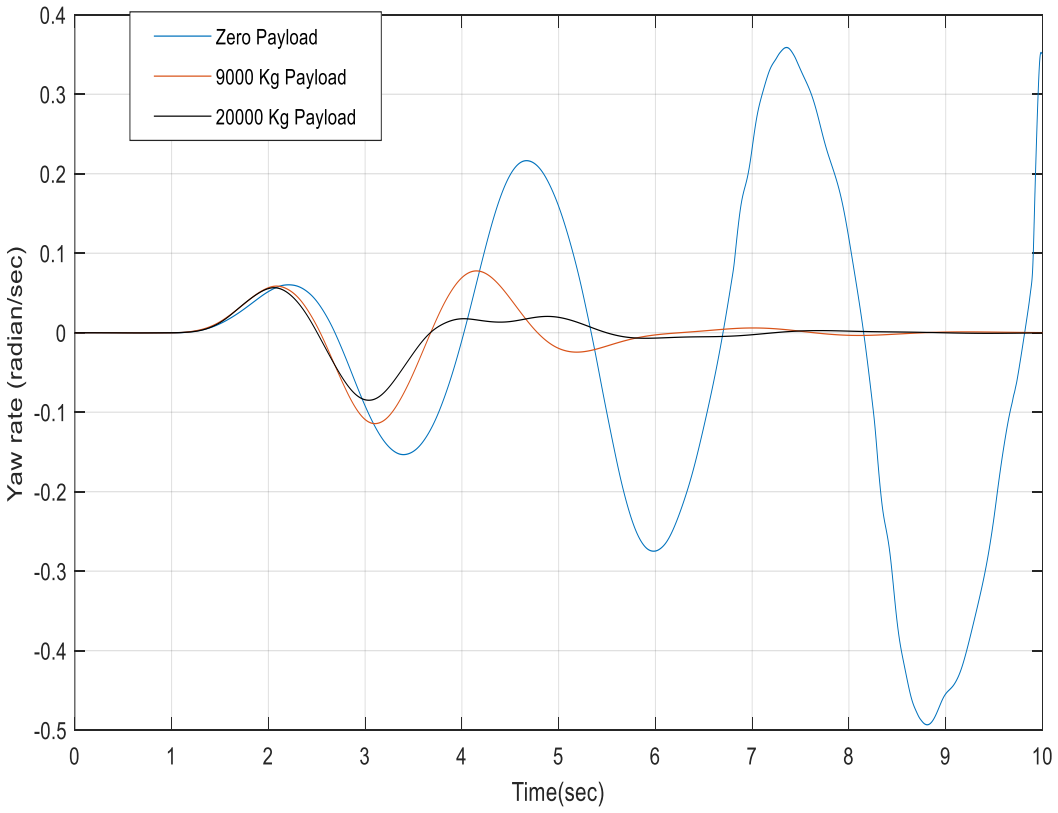

Figure 3.13 Time history of trailer yaw rate at forward speed of 70 m/s for the single tractor rear axle arrangement with three trailer payload schemes.

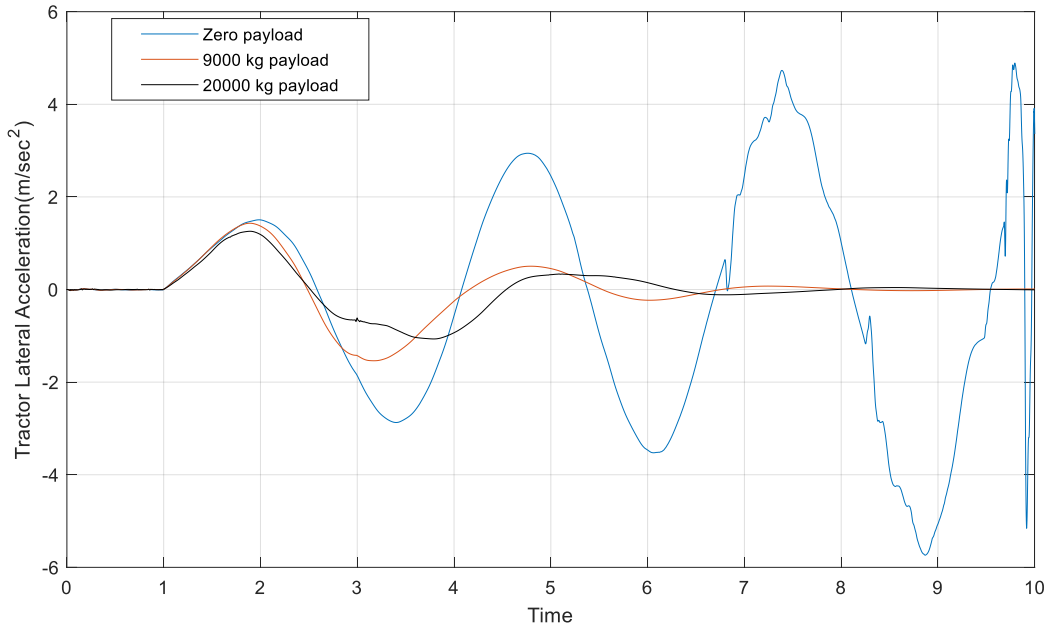

Figure 3.14 Time history of tractor lateral acceleration at forward speed of 70 m/s for the single tractor rear axle arrangement with three trailer payload schemes.

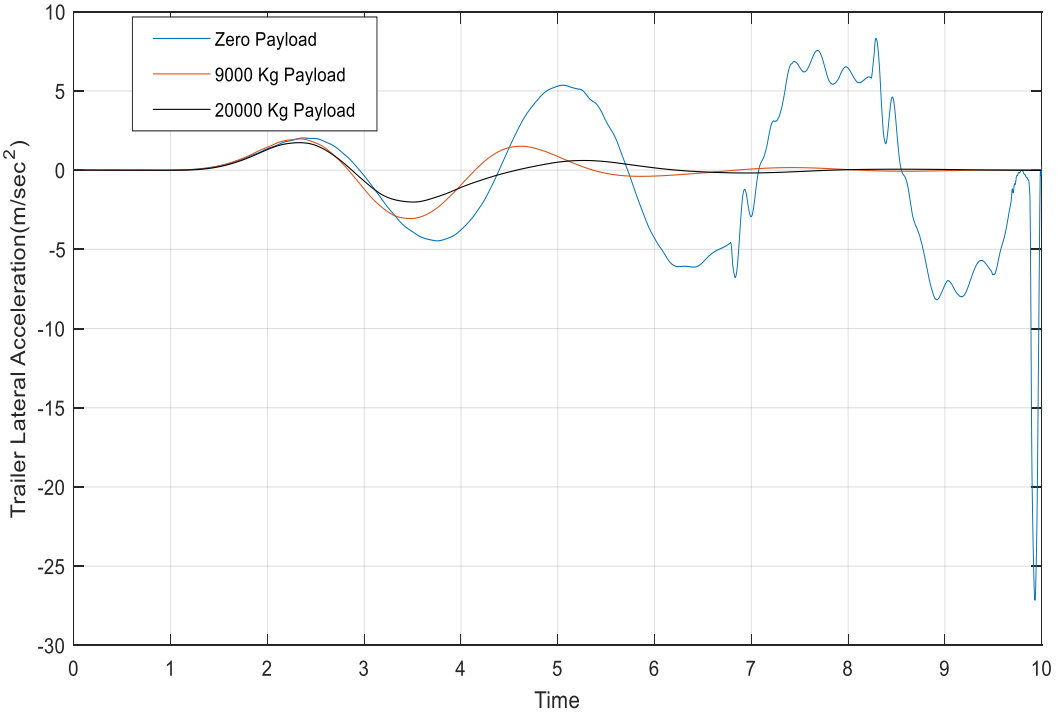

Figure 3.15 Time history of trailer lateral acceleration at forward speed of 70 m/s for the single tractor rear axle arrangement with three trailer payload schemes.

3.10. Eigenvalue analysis for double tractor rear axle arrangement

Eigenvalue analysis is also done for the double tractor rear axle tractor/semi-trailer system with three trailer payload scheme to evaluate the dynamic stability of the articulated vehicle.

3.10.1. Zero trailer payload

Figure 3.16 shows the relationship between damping ratio and forward velocity for the double tractor rear axle arrangement with zero trailer payload. It can be seen that for the two motion modes, the damping ratio drops with the increase of forward speed. For the least damped mode, at the speed of 72 m/s, the damping ratio is zero. This means that the speed of 72 m/s is the critical speed, above which the vehicle will lose its dynamic stability.

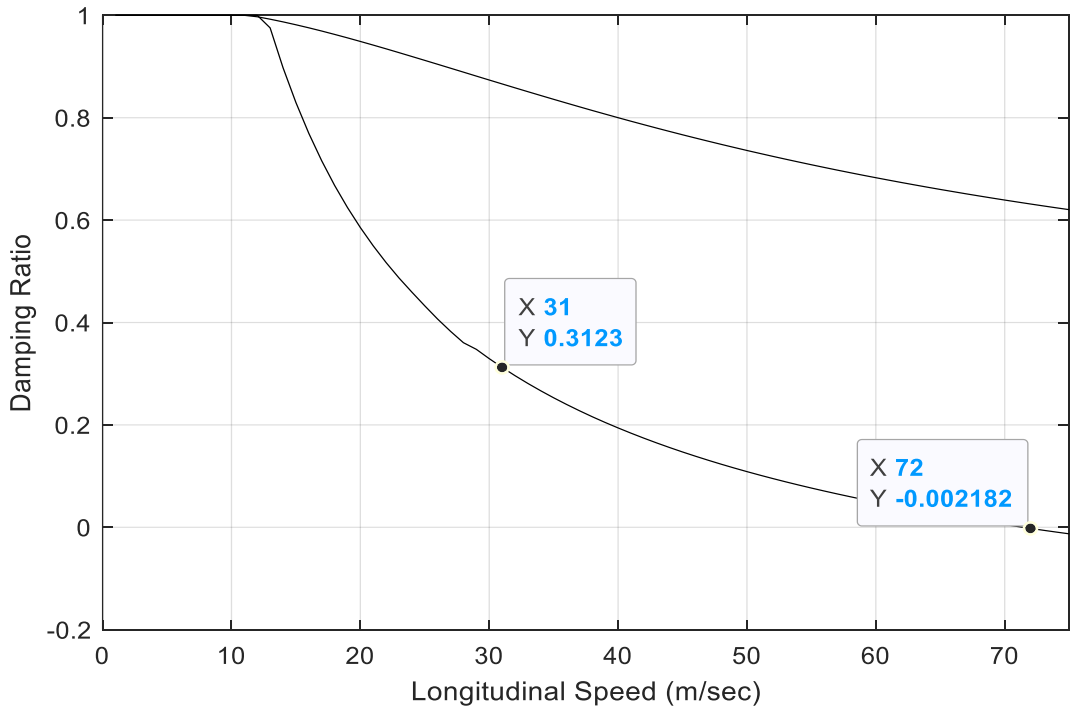

Figure 3.16 Damping ratio vs forward speed for double tractor rear axle arrangement with zero trailer payload.

3.10.2. 9000 kg trailer payload

Figure 3.17 shows the relationship between damping ratio and forward speed for the double tractor rear axle arrangement with 9000 kg trailer payload.

The damping ratios of the two motion modes decrease with the increase of forward speed. Within the forward speed range concerned, the damping ratio of the least damped motion mode remains positive. This means that the AHV is dynamically stable in the forward speed range shown in the figure.

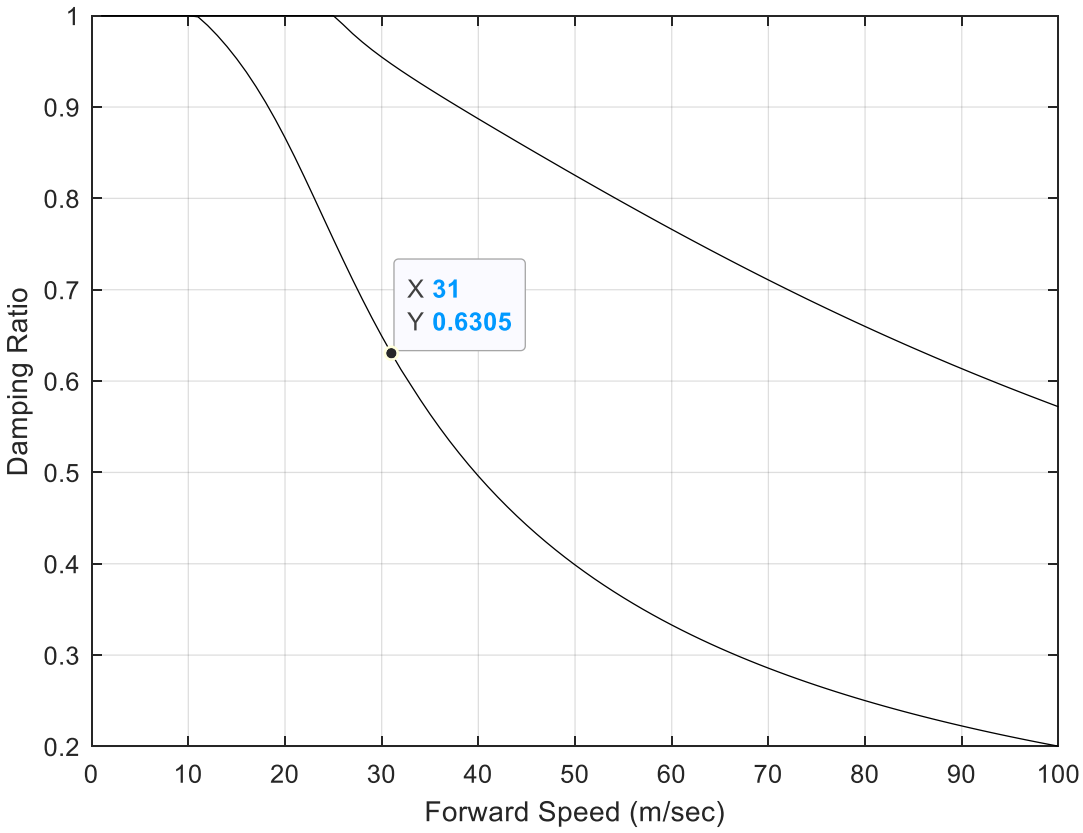

Figure 3.17 Damping ratio vs forward speed for the double tractor rear axle arrangement with 9000 kg trailer payload.

3.10.3. 20000 kg trailer payload

Figure 3.18 shows the relationship between damping ratio and forward speed for the double tractor rear axle arrangement with 20000 kg trailer payload. Similar to the trailer payload scheme of 9000 kg, the damping ratios of the two motion modes drop with the increase of forward speed. Within the forward speed range concerned, the damping ration of the least damped motion mode remains positive, implying that the AHV is dynamically stable in the forward speed range shown in the figure.

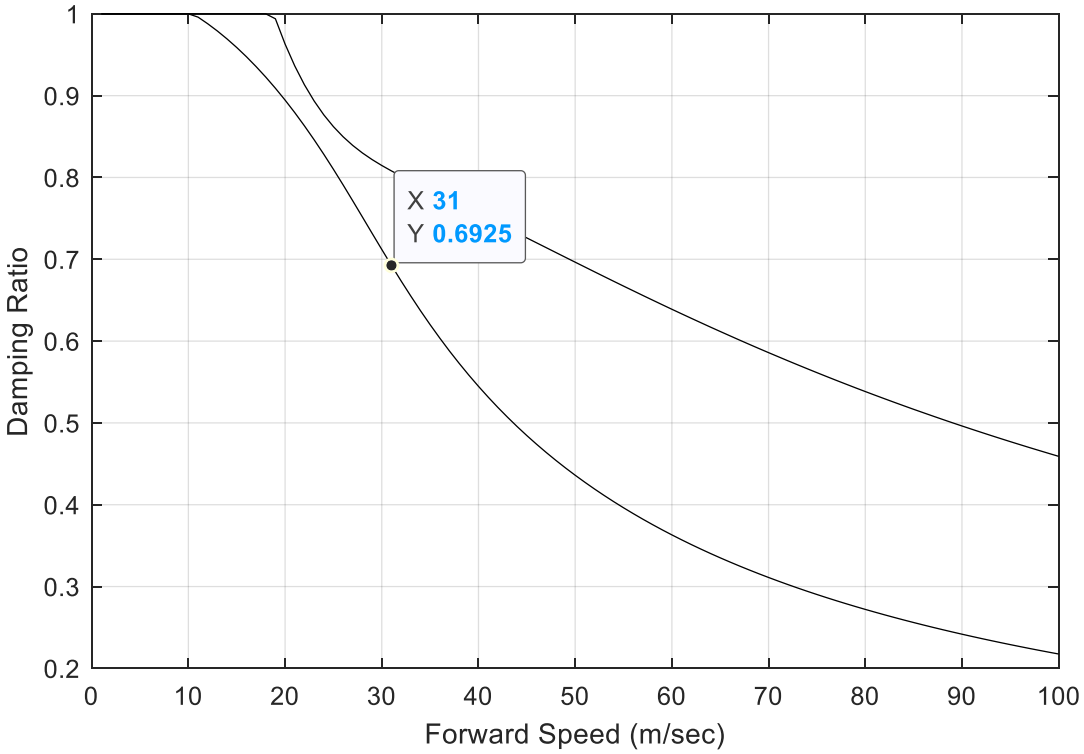

Figure 3.18 Damping ratio vs forward speed for the double tractor rear axle arrangement with 20000 kg trailer payload

To effectively evaluate the effects of the two tractor rear axle arrangements and the three trailer payload schemes on the dynamic stability of the tractor/semi-trailer combination, in each of Figures 3.6 to 3.8 and 3.16 to 3.18, the respective damping ratio of the least damped motion mode

at the forward speed of 31 m/s is identified. The identified damping ratios are listed in Table 3.2. Given the data provided in the table, the following points can be made: 1) regardless of tractor rear axle arrangement, the larger the trailer payload, the higher the dynamic stability of the AHV; 2) with a given trailer payload, the double tractor rear axle arrangement exhibits higher lateral dynamic stability compared against the single tractor rear axle arrangement.

Table 3.2 Damping ratios of the least damped motion mode for the single and double tractor rear axle arrangements with three trailer payload schemes at the forward speed of 31m/s.

Damping ratio for the single tractor rear axle arrangement at 31m/s	Damping ratio for the double tractor rear axle arrangement at 31m/s
Zero trailer payload 0.1924	**Zero trailer payload** 0.3123
9000 kg trailer payload 0.4378	**9000 kg trailer payload** 0.63
20000 kg trailer payload 0.4781	**20000 kg trailer payload** 0.69

3.11. Evaluating dynamic stability of the double tractor rear axle arrangement using TruckSim model

As for the single tractor rear axle arrangement, we also simulate the same open-loop sinewave steering input testing maneuver for the double tractor rear axle arrangement using the respective TruckSim model. In this case, the TruckSim model represents the tractor/semi-trailer combination with the double tractor rear axle arrangement and the three trailer payload schemes. Two forward speeds are considered, that is, 65 and 80 m/s. Note that as shown in Figure 3.16, for the double tractor rear axle arrangement with zero trailer payload, the critical speed is 72 m/s. Figures 3.19, 3.20 and 3.21 show the time history of the trailer yaw rate, tractor lateral acceleration, and the trailer lateral acceleration at the forward speed of 65m/s for the double tractor rear axle arrangement with three trailer payload schemes. It can be seen that the yaw rate and lateral acceleration of the trailer with zero payload is oscillating but settling down over time. However,

the time history of yaw rate and lateral acceleration for the 9000 and 20000 Kg trailer payload schemes are oscillating with less amplitudes and shorter settling time due to the additional trailer payload.

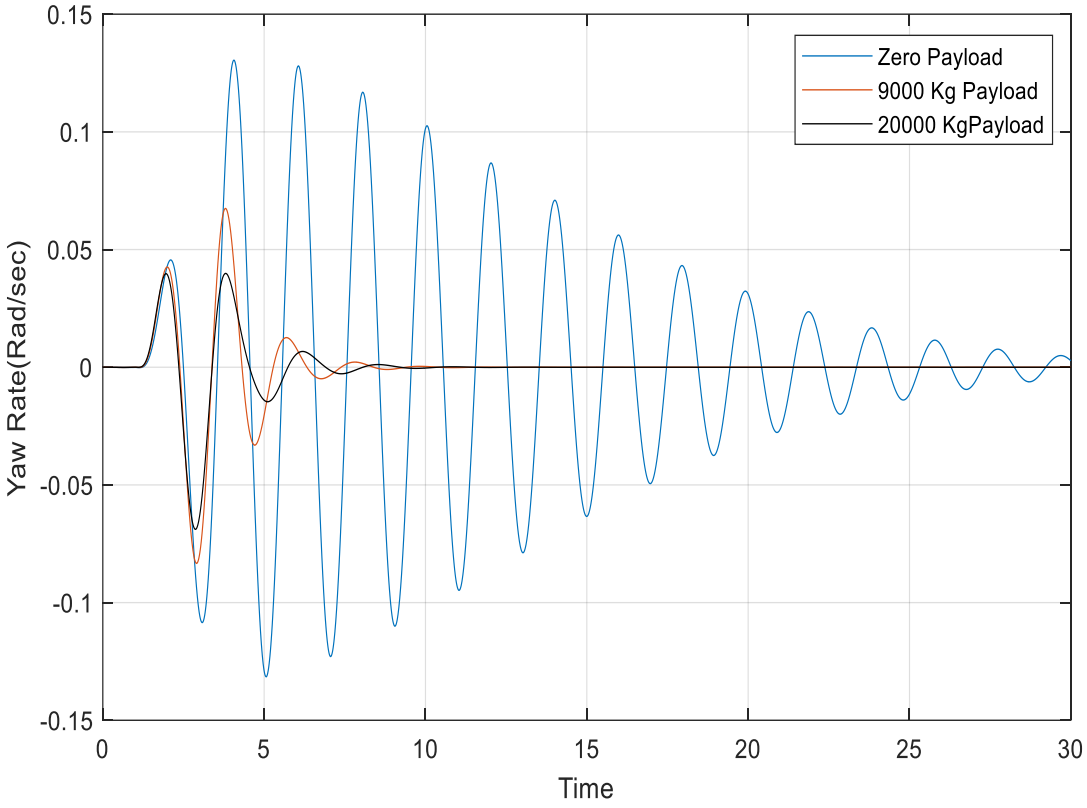

Figure 3.19 Time history of trailer yaw rate at forward speed of 65 m/s for the double tractor rear axle arrangement with three trailer payload schemes.

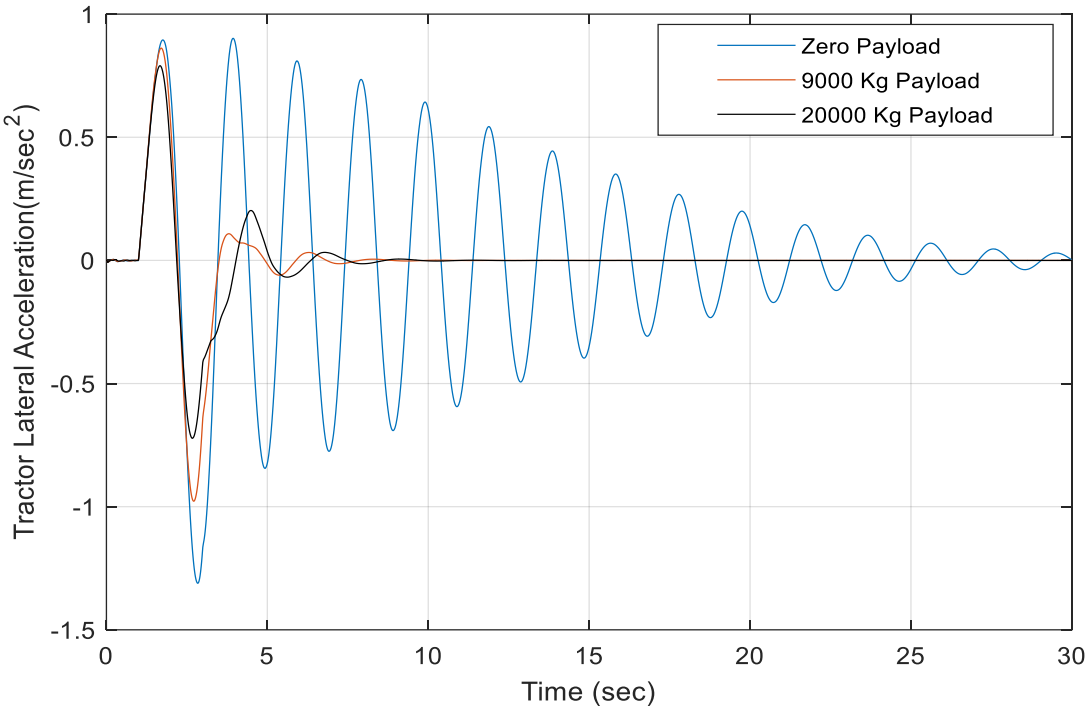

Figure 3.20 Time history of tractor lateral acceleration at forward speed of 65 m/s for the double tractor rear axle arrangement with three trailer payload schemes.

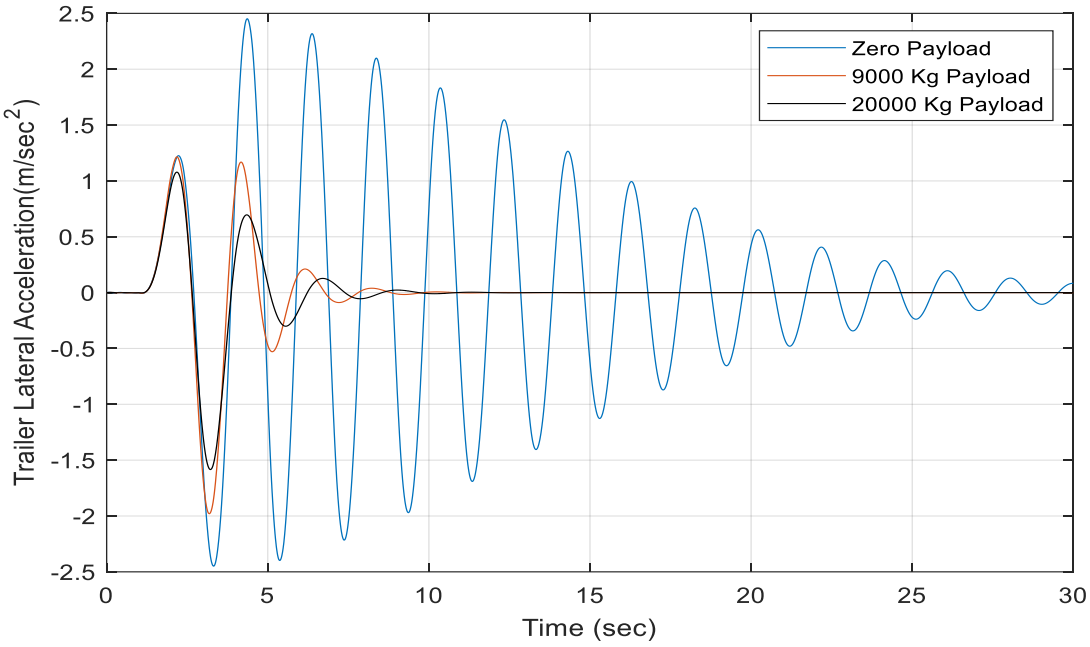

Figure 3.21 Time history of trailer lateral acceleration at forward speed of 65 m/s for the double tractor rear axle arrangement with three trailer payload schemes.

Figures 3.22, 3.23 and 3.24 show the time history of trailer yaw rate, tractor lateral acceleration and trailer lateral acceleration at the forward speed of 80 m/s for the double tractor rear axle arrangement with three trailer payload schemes. It can be seen that the yaw rate and lateral acceleration of the trailer with zero payload is highly oscillatory and finally getting unstable. For the trailer payload schemes of 9000 and 20000 kg, the tractor/semi-trailer combination exhibits stable motion modes with much lower oscillation amplitudes and shorter settling times.

The above time domain simulation results based on the TruckSim model are consistent with the eigenvalue analysis based on the 3-DOF linear yaw-plane model.

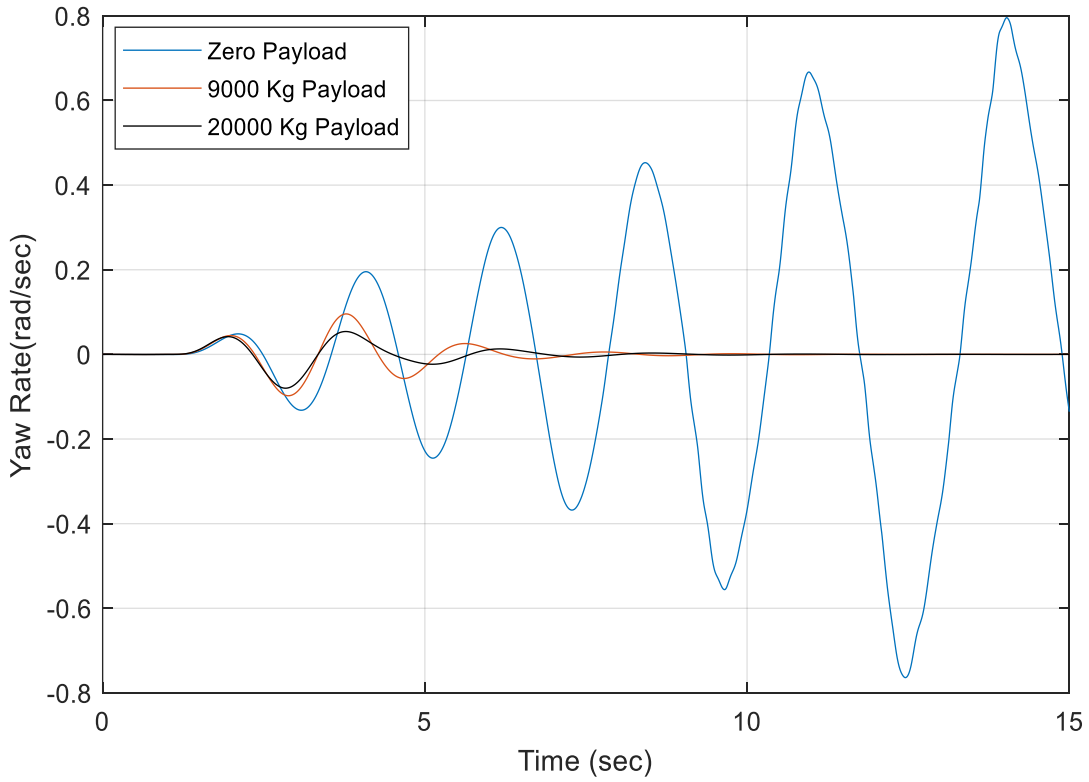

Figure 3.22 Time history of trailer yaw rate at forward speed of 80 m/s for the double tractor rear axle arrangement with three trailer payload schemes.

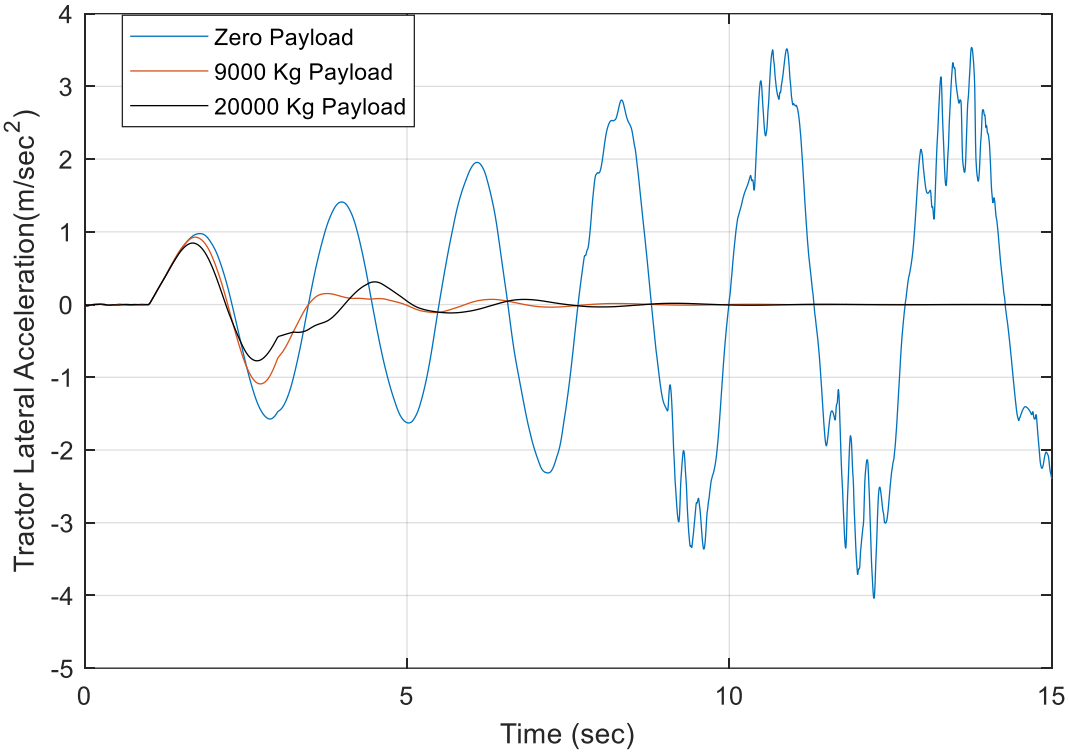

Figure 3.23 Time history of tractor lateral acceleration at forward speed of 80 m/s for the double tractor rear axle arrangement with three trailer payload schemes

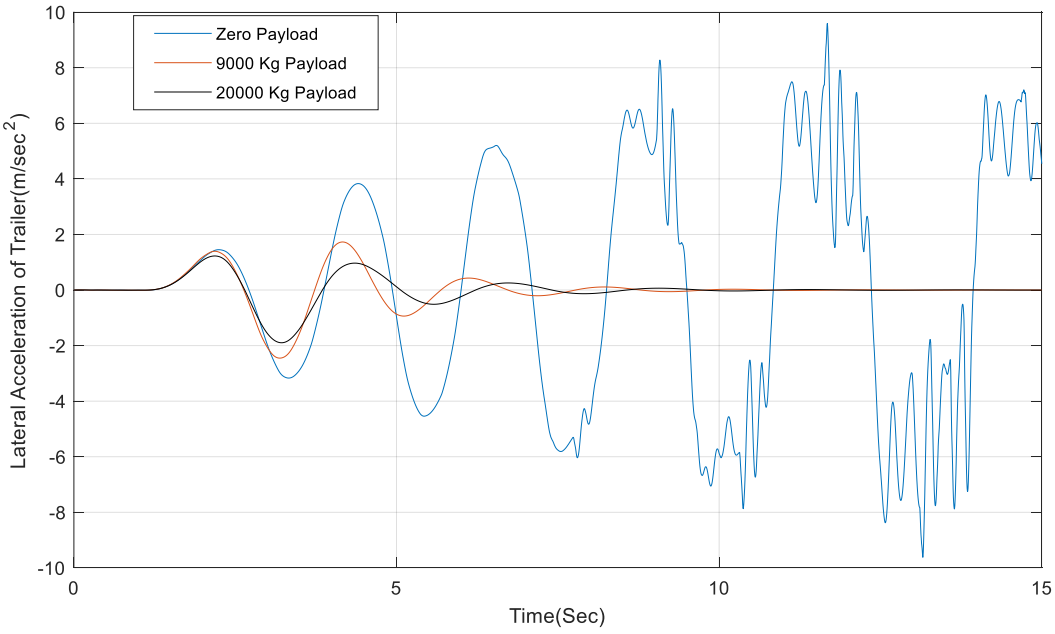

Figure 3.24 Time history of trailer lateral acceleration at forward speed of 80 m/s for the double tractor rear axle arrangement with three trailer payload schemes

Chapter 4

Vehicle Modeling and Validation

4.1. Introduction

This chapter describes the generation of a 7-DOF nonlinear tractor/semi-trailer model for the design of the NLMPC-based tracking-controller for AAHVs. The 7-DOF non-linear tractor/semi-trailer model will be used as the prediction model in NLMPC controller design, while the corresponding TruckSim model is developed to mimic the vehicle plant. These two vehicle models are described in following sections.

4.2. 7-DOF Non-linear tractor/semi-trailer model

Figure 4.1 shows the 7-DOF non-linear model to represent the dynamics of the tractor/semi-trailer combination. As seen in the figure, the tractor/semi-trailer combination is telescoped laterally, and each axle set of both the tractor and trailer is denoted by a single wheel. Three coordinate systems are introduced: 1) the inertial coordinate system, $\boldsymbol{X-O-Y}$, 2) tractor body fixed coordinate system with the origin located at its CG, $\boldsymbol{x_t-o_t-y_t}$, and 3) semi-trailer body fixed coordinate system with the origin located at its CG, $\boldsymbol{x_s-o_s-y_s}$.

In the 7-DOF non-linear single-track model, seven motions are considered, which include tractor lateral motion, tractor longitudinal motion, tractor yaw motion, trailer yaw motion, as well as spinning motion of tractor front wheel, tractor rear wheel, and trailer wheel. The following assumptions are made: 1) the vertical, pitch, and roll motions are ignored; 2) tractor front wheel steer angle δ_f and articulation angle γ are small; 3) the longitudinal velocities of the tractor and

semi-trailer are the same; and 4) the vehicle units are treated as rigid bodies, and their masses are lumped at the respective CGs with the corresponding mass moments of inertia around the vertical axes of the vehicle body fixed coordinate systems.

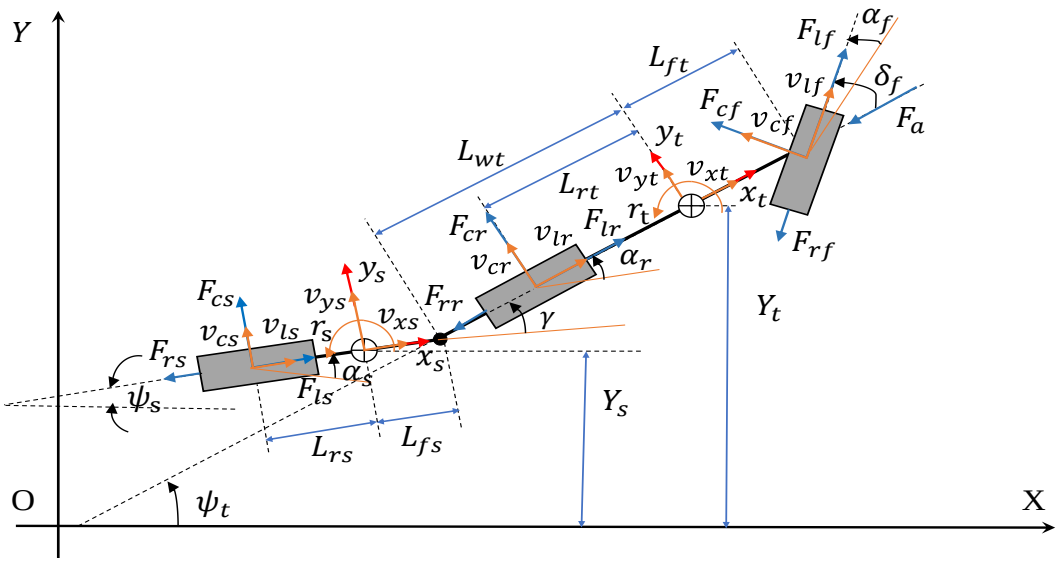

Figure 4.1 7-DOF non-linear tractor/semi-trailer model.

4.2.1. Rigid body model for the tractor and semi-trailer combination

Based on Newton's law of dynamics, the equations of motion of the tractor/semi-trailer combination are derived. The governing equations of the longitudinal, lateral and yaw motions of the tractor expressed in the tractor-fixed coordinate system are given as

$$m_t\left(\dot{v}_{xt} - r_t v_{yt}\right) = F_{xtt} - F_{fx} - F_a \tag{4.1a}$$

$$m_t\left(\dot{v}_{yt} + r_t v_{xt}\right) = F_{ytt} - F_{fy} \tag{4.1b}$$

$$I_{zt}\dot{r}_t = M_{zt} + F_{fy}L_{wt} \tag{4.1c}$$

where m_t denotes the tractor mass, I_{zt} the tractor yaw moment of inertia, L_{ft}, L_{rt} and L_{wt} represent the distances between the tractor CG and its front axle, its rear axle, and the fifth-wheel,

respectively, r_t is the tractor yaw rate, M_{zt} the tractor yaw moment due to its tire forces, v_{xt} and v_{yt} are longitudinal and lateral velocities at the tractor CG, accordingly, F_{xtt} and F_{ytt} the respective total tractor tire forces in longitudinal and lateral directions, F_{fx} and F_{fy} reaction forces at the fifth-wheel in the longitudinal and lateral directions in the tractor-fixed coordination system, correspondingly, F_a is the aerodynamic drag and determined by

$$F_a = (1/2)C_D A_a \rho_a v_{xt}^2 \tag{4.2}$$

where C_D denotes the aerodynamic resistance coefficient, A_a the frontal area of the tractor, and ρ_a the mass density of the air.

The governing equations of the longitudinal, lateral and yaw motions of the trailer expressed in the tractor-fixed coordinate system are expressed as

$$m_s\left(L_{wt} r_t^2 + L_{fs} r_s^2 - L_{fs}\dot{r}_s\gamma + \dot{v}_{xt} - r_t v_{yt}\right) = F_{xts} + F_{fx} \tag{4.3a}$$

$$m_s\left(-L_{fs} r_s^2\,\gamma - L_{wt}\dot{r}_t - L_{fs}\dot{r}_s + \dot{v}_{yt} + r_t v_{xt}\right) = F_{yts} + F_{fy} \tag{4.3b}$$

$$I_{zs}\dot{r}_s = M_{zs} + F_{fx}\gamma L_{fs} + F_{fy} L_{fs} \tag{4.3c}$$

where m_s denotes the trailer mass, I_{zs} the trailer yaw moment of inertia, M_{zs} the trailer yaw moment due to trailer tire forces, γ the articulation angle between the tractor and the trailer, L_{fs} and L_{rs} represent the distance between the trailer CG and the fifth-wheel, as well as the trailer axle, respectively, r_s is the trailer yaw rate, F_{xts} and F_{yts} are the total tire forces expressed in x_t and y_t axis of the tractor-fixed coordinate system, respectively.

Combining equations (4.1) and (4.3) and eliminating the coupling forces at the fifth-wheel leads to the following governing equations of motion of the tractor/semi-trailer combination expressed in the tractor-fixed coordinate system as

$$(m_t + m_s)\left(\dot{v}_{xt} - r_t v_{yt}\right) + m_s\left(L_{wt} r_t^2 + L_{fs} r_s^2 - L_{fs}\dot{r}_s\,\gamma\right) = F_{xtt} + F_{xts} - F_a \quad (4.4a)$$

$$(m_t + m_s)\left(\dot{v}_{yt} + r_t v_{xt}\right) - m_s\left(L_{fs} r_s^2 \gamma + L_{wt}\dot{r}_t + L_{fs}\dot{r}_s\right) = F_{ytt} + F_{yts} \quad (4.4b)$$

$$I_{zt}\dot{r}_t + m_t\left(\dot{v}_{yt} + r_t v_x\right)L_{wt} = M_{zt} + F_{ytt}L_{wt} \quad (4.4c)$$

$$I_{zs}\dot{r}_s + m_t\left(\dot{v}_{xt} - r_t v_{yt}\right)L_{fs}\gamma + m_t\left(\dot{v}_{yt} + r_t v_{xt}\right)L_{fs} = M_{zs} + (F_{xtt} - F_a)\gamma L_{fs} + F_{ytt}L_{fs} \quad (4.4d)$$

The tire-related forces and moments, i.e., F_{xti}, F_{yti} and M_{zi}, $i \in \{s, t\}$, are expressed by

$$F_{xtt} = \left[\left(F_{lf} - F_{rf}\right)cos\delta_f - F_{cf}sin\delta_f\right] + \left[(F_{lr} - F_{rr})cos\delta_r - F_{cr}sin\delta_r\right] \quad (4.5a)$$

$$F_{ytt} = \left[\left(F_{lf} - F_{rf}\right)sin\delta_f + F_{cf}cos\delta_f\right] + \left[(F_{lr} - F_{rr})sin\delta_r + F_{cr}cos\delta_r\right] \quad (4.5b)$$

$$F_{xts} = \left[(F_{ls} - F_{rs})cos\delta_s - F_{cs}sin\delta_s\right]cos\gamma + \left[(F_{ls} - F_{rs})sin\delta_s + F_{cs}cos\delta_s\right]sin\gamma \quad (4.5c)$$

$$F_{yts} = \left[(F_{ls} - F_{rs})sin\delta_s + F_{cs}cos\delta_s\right]cos\gamma - \left[(F_{ls} - F_{rs})cos\delta_s - F_{cs}sin\delta_s\right]sin\gamma \quad (4.5d)$$

$$M_{zt} = \left[\left(F_{lf} - F_{rf}\right)sin\delta_f + F_{cf}cos\delta_f\right]L_{ft} - \left[(F_{lr} - F_{rr})sin\delta_r + F_{cr}cos\delta_r\right]L_{rt} \quad (4.5e)$$

$$M_{zs} = -\left[(F_{ls} - F_{rs})sin\delta_s + F_{cs}cos\delta_s\right]L_{rs} \quad (4.5f)$$

where $\delta_i, i \in \{f, r, s\}$, denote the steer angle of the tractor front wheel, tractor rear wheel, and trailer wheel, respectively. To determine the tire forces of the tractor and trailer, the following wheel/tire dynamics should be considered.

4.2.2. Wheel and tire dynamics

The slip angles for tractor and trailer tires can be calculated by

$$\left[\delta_i - arctan(v_{ci}/v_{li})\right],\ i \in \{f, r, s\} \quad (4.6)$$

where the subscripts *f*, *r*, and *s* represent the tractor front wheel, tractor rear wheel, and semi-trailer wheel, respectively, δ_i and α_i, $i \in \{f, r, s\}$, denote the steer and slip angle of the tire, accordingly, v_{li} and $v_{ci,}$ $i \in \{f, r, s\}$, the longitudinal and lateral velocity of the tire, correspondingly. Note that in this study, the tractor rear wheel and the trailer wheel are not steerable, i.e., $\delta_r = 0$ and $\delta_s = 0$.

The tire forces are calculated using Dugoff tire model [72, 73]. It is assumed that the normal loads on the tractor and trailer tires remain constant. Based on the geometry of the tractor/semi-trailer model shown in Figure 4.1, the normal loads on the tractor and trailer tires are determined by

$$F_{Zf} = m_t g L_{rt} / \left(L_{ft} + L_{rt}\right) - m_s g L_{rs} (L_{wt} - L_{rt}) / \left[\left(L_{ft} + L_{rt}\right)\left(L_{fs} + L_{rs}\right)\right] \tag{4.7a}$$

$$F_{Zr} = m_t g L_{ft} / \left(L_{ft} + L_{rt}\right) + m_s g L_{rs} \left(L_{wt} + L_{ft}\right) / \left[\left(L_{ft} + L_{rt}\right)\left(L_{fs} + L_{rs}\right)\right] \tag{4.7b}$$

$$F_{Zs} = m_s g L_{fs} / \left(L_{fs} + L_{rs}\right) \tag{4.7c}$$

The longitudinal and cornering (i.e., lateral) tire forces are determined by

$$F_{li} = C_{\sigma i} [\sigma_{li} / (1 + \sigma_{li})] f(\lambda_i), \; i \in \{f, r, s\} \tag{4.8a}$$

$$F_{ci} = C_{\alpha i} [tan(\alpha_i) / (1 + \sigma_{li})] f(\lambda_i) \tag{4.8b}$$

$$\lambda_i = \mu F_{zi} (1 + \sigma_{li}) / \left\{ 2 \left[(C_{\sigma i} \sigma_{li})^2 + \left(C_{\alpha i} tan(\alpha_i) \right)^2 \right]^{\frac{1}{2}} \right\} \tag{4.8c}$$

$$f(\lambda_i) = \begin{cases} (2 - \lambda_i)\lambda_i & for \;\; \lambda_i < 1 \\ 1 & for \;\; \lambda_i \geq 1 \end{cases} \tag{4.8d}$$

where $F_{ji}, j \in \{l, c\}$ and $i \in \{f, r, s\}$, represent longitudinal and cornering force of tractor front tire, tractor rear tire, and semi-trailer tire, respectively, α_i denotes tire slip angle determined by

Equation (4.6), $C_{\sigma i}$ tire longitudinal stiffness, $C_{\alpha i}$ tire cornering stiffness, μ tire/road friction coefficient, F_{zi} tire normal force, and σ_{li} tire longitudinal slip ratio, which is determined by

$$\sigma_{li} = \begin{cases} (R_{ei}\omega_i - v_{li})/v_{xti}\,,\ i \in \{f,r,s\}; & if\ v_{li} > R_{ei}\omega_i\ and\ \ v_{li} \neq 0\ (for\ braking) \\ (R_{ei}\omega_i - v_{li})/(R_{ei}\omega_i)\,; & if\ v_{li} < R_{ei}\omega_i\ \ and\ \omega_i \neq 0\ (for\ driving) \end{cases} \tag{4.9}$$

where $R_{ei}, i \in \{f,r,s\}$ denote the effective rolling radius of tractor front wheel, tractor rear wheel, and semi-trailer wheel, respectively, and ω_i the corresponding wheel angular velocities.

In equation (4.9), the wheel angular velocities, ω_i, are governed by the respective wheel dynamics represented by Figure 4.2. Following Newton's law of dynamics, we can establish the governing equation of motion for the wheel as

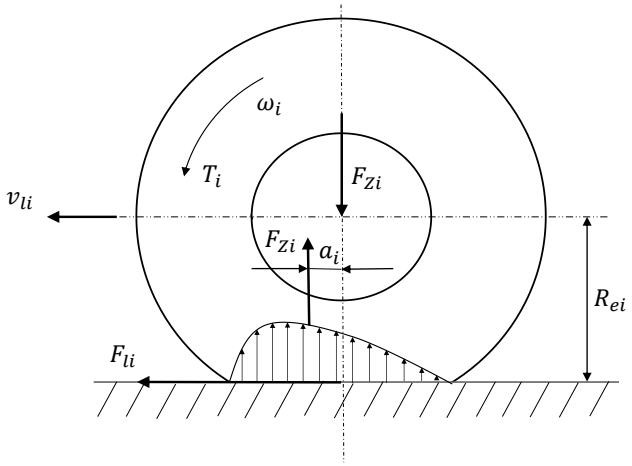

Figure 4.2. Schematic representation of the wheel dynamics.

$$I_{ewi}\dot{\omega}_i = T_i - F_{li}R_{ei} - F_{Zi}a_i,\ i \in \{f,r,s\} \tag{4.10a}$$

where I_{ewi} is the equivalent mass moment of inertia of the wheel, T_i the torque exerted on the wheel, which may be a propulsion torque or a brake torque, F_{li} the longitudinal tire force determined by Equation (4.8a), F_{Zi} the normal load on the tire, and a_i the offset of the normal load from the center of the wheel. Note that under braking operations, the applied torque T_i should be in the opposite direction as shown in Figure 4.2. The offset of the normal load results from the

wheel rolling and the tire tread deformation; due to viscous damping of the tire tread, all the energy absorbed over the deformation in the leading section of the tire/road contact patch is not fully recovered; the distribution of the normal load is thus more in the leading half of the contact patch [74]. The tire rolling resistance arises due to the damping effect of the pneumatic tire. Considering the offset of the normal load, we can determine the tire rolling resistant force as

$$F_{ri} = F_{Zi}(a_i/R_{ei}), i \in \{f, r, s\} \tag{4.10b}$$

$$f_{ri} = (a_i/R_{ei}) \tag{4.10c}$$

where f_{ri} is the coefficient of rolling resistance of the tire, which is generally determined by experimental data [75]. To determine the propulsion torque applied on a drive axle, a simplified powertrain model is generated, which is presented in 4.6. In the case of braking operations, the brake torque determination follows the scheme proposed by Zhu and He [76].

Equations (4.4) and (4.10a) govern the 7 motions of the tractor/semi-trailer model. The vehicle model can be expressed in a compact form as

$$\dot{\boldsymbol{x}}_t(t) = f[\boldsymbol{x}_t(t), \boldsymbol{u}_t(t)] \tag{4.11a}$$

where the subscript *t* means that the governing equations of motion are defined in the $x_t - o_t - y_t$ coordinate system, $\boldsymbol{x}_t$ and $\boldsymbol{u}_t$ are the state and control variable vectors, respectively, which are specified by

$$\boldsymbol{x}_t = \left[v_{xt}\ \ v_{yt}\ \ r_t\ \ r_s\ \ \omega_f\ \ \omega_r\ \ \omega_s\right]^T \tag{4.11b}$$

$$\boldsymbol{u}_t = \left[\delta_f\ \ T_f\ \ T_r\ \ T_s\right]^T \tag{4.11c}$$

In this study, the 7-DOF tractor/semi-trailer nonlinear model is generated using Matlab/Simulink, and the associated elements/sub-models, e.g., the wheel model, Dugoff tire model, rigid body

model, etc., are integrated following the structure arrangement shown in Figure 4.3. Given an initial condition and an operating maneuver, the structured simultaneous equations of motion of the vehicle model can be solved, and the resultant state variable vector, $\boldsymbol{x}_t$, can be attained.

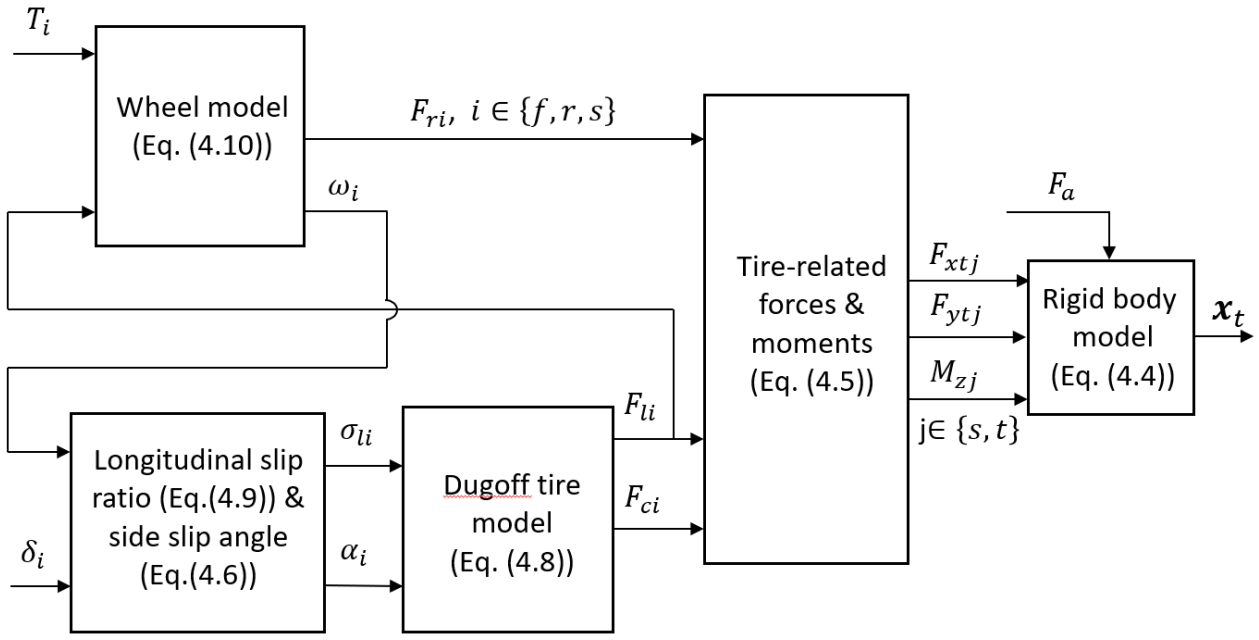

Figure 4.3 Structure arrangement of the elements/sub-models of the 7-DOF nonlinear tractor-semi-trailer model.

4.3. TruckSim model

The 3-dimensional (3-D) nonlinear tractor/semi-trailer model is generated using TruckSim software, which uses a symbolic multibody program, VehicleSim (VS) Lisp, to generate equations of motion [20]. As shown in Figure 4.4, the configuration of the tractor/semi-trailer combination is defined as 'S_SS+SSS', where 'S' represents a solid axle, an underscore '_' a separation of axle group, and a '+' a fifth-wheel connecting the two vehicle units. The TruckSim model assumes the nonlinear dynamics of suspension systems, pneumatic tires, and mechanical joints. The 3-D vehicle model consists of two rigid bodies for representing the sprung-masses of the tractor and semi-trailer, as well as six axles. Each rigid body is allowed to move longitudinally, laterally, and

vertically, as well as to rotate in roll, pitch, and yaw. The fifth-wheel is modelled as a ball-joint, about which roll, yaw, and pitch motions are permitted. Each axle is considered as a beam, which can roll and bounce with respect to the sprung-mass to which it is attached. Each wheel is modelled with a rotating DOF. Using TruckSim software, we thus model the tractor/semi-trailer combination as a 33-DOF nonlinear model.

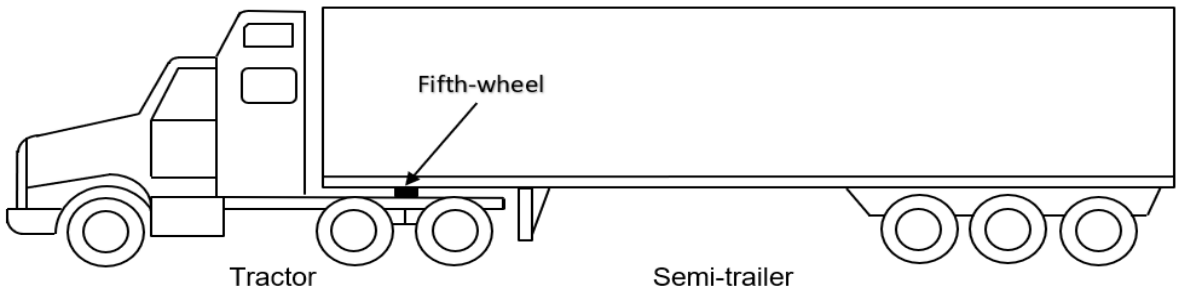

Figure 4.4 Configuration of the tractor/semi-trailer combination.

In addition, the tractor is modelled with the drive setting of 6x4, in which the two rear axles of the leading vehicle unit are drive axles. The built-in powertrain model consists of a diesel engine with the power capacity of 330 kw, a mechanical clutch, a gearbox with 18 gear ratios, and a final drive unit with the gear ratio of 4.4. In the built-in braking system model, the control input pressure from the master cylinder is proportioned for each wheel-end brake actuator, and the brake torque is assumed as a nonlinear function of actuator pressure [20]. For the 3-D TruckSim model, the forward speed is controlled using the throttle and brake positions, i.e., t_p and b_p, which take values within the range of $[0,\ 1]$, where 1 means full throttle or brake and 0 means none. If one of the variables take a non-zero value, the other is zero.

The TruckSim software was built upon the symbolic multibody program, VS Lisp, for deriving equations of motion for 3-D vehicle systems [20]. An input to the VS Lisp describes the 3-D vehicle model structure mostly in geometric terms, e.g., sprung mass DOF, point locations, and directions of force vectors. Upon receiving the input, the VS Lisp derives equations of motion in terms of ordinary differential equations and generates a computer source code (C or Fortran) to solve them. The TruckSim software comprises three main components, i.e., VS browser, TruckSim databases, and VS solver. The VS browser serves as a graphical user interface to TruckSim. The browser may also be used for other applications, e.g., incorporating the tracking-controller to be devised using Matlab/Simulink into the 3-D TrcukSim model via the interface for co-simulation. The VS solver is employed to solve the derived governing equation of motion of the vehicle model and to execute the defined simulations

4.4. Trajectory tracking of tractor/semi-trailer combination

This section introduces the associated concepts of local motion-planning, reference trajectory determination, and kinematics for path-tracking.

4.4.1. Local motion-planning

For an autonomous vehicle, the motion-planning and decision module is featured with hierarchically structured sub-modules, which include route-planning at the top level, behavioral-planning at the middle level, and local motion-planning at the bottom level [77]. In the operation of the module, the route-planning determines the global route, and the behavioral-planner then decides on a local driving task with a motion specification (e.g., turn-left, lane-change, or cruise-

in-line). With the directives of the behavioral-planner, the local motion-planning sub-module generates the reference trajectory for tracking-controller to track. The local motion-planning techniques may be categorized into two types [78]: 1) separated approaches, by which spatial maneuver, e.g., a single lane-change (SLC) for obstacle avoidance, and temporal maneuver, such as speeding up along the predefined SLC path to overtake a preceding vehicle, are separately planned; 2) integrated methods, with which the spatial and temporal maneuvers are planned simultaneously. The second type shows poor computational efficiency, while the first one significantly improves computational efficiency due to its layered nature [79].

In this study, we adopt the separated methods. In the case concerned, a tracking-controller is designed for the tractor/semi-trailer combination, and it will be evaluated in a SLC overtaking maneuver in highway operations. Thus, the local motion-planning is to determine a collision free SLC path, and to plan a forward speed scheme over the maneuver.

4.4.2. Reference motion trajectory determination

To evaluate path-following performance and lateral stability of AHVs, a high-speed obstacle avoidance testing procedure is recommended by ISO [80] in which the SLC path is prescribed. Over the SLC testing maneuver, the vehicle forward speed remains constant. To tailor an experiment procedure for the SLC overtaking maneuver in highway operations, a testing course and a speed profile are established upon the ISO recommended procedure [81, 82]. It is assumed that during the overtaking maneuver, the tractor/semi-trailer travels in the longitudinal direction at a constant acceleration, and the lateral acceleration time-history of the tractor is a single-cycle sine wave with a given amplitude and time period. Under highway operations, the geometric path of the overtaking maneuver is defined in the inertial coordinate system and expressed by

$$Y_{ref}(t) = \frac{L}{T}\left[t - \frac{T}{2\pi} sin\left(\frac{2\pi t}{T}\right)\right] \quad (4.2a)$$

$$X_{ref}(t) = v_0 t + \frac{1}{2} a t^2 \quad (4.2b)$$

where $X_{ref}(t)$ and $Y_{ref}(t)$ is the horizontal and vertical coordinates of a moving point on the path at time *t*, *L* denotes the lateral displacement of the SLC maneuver, *T* the time period of the sine wave, v_0 the vehicle speed at the beginning of the maneuver, and the constant longitudinal acceleration over the maneuver. At an arbitrary time, instant, the vehicle forward speed is thus determined by

$$v_{ref}(t) = v_0 + at \quad (4.2c)$$

Figure 4.5 shows the schematic representation of the SLC overtaking maneuver. Initially, the tractor/semi-trailer combination follows a passenger car in the right lane at the same forward speed, v_0. It is assumed that there is no any vehicle in the left lane. To overtake the preceding passenger car, the AHV performs a SLC maneuver, over which the vehicle is accelerating at a constant acceleration, *a*.

To successfully execute the overtaking maneuver with good driving quality and without collision, we need to determine the last point to overtake (LPTO) and the corresponding clearing distance [83], L_{LPTO}. The LPTO is defined as the point on the central line of the right lane, at which the AHV is able to successfully execute a SLC overtaking maneuver with the least clearing distance, L_{LPTO}, as shown in Figure 4.5. The successful SLC overtaking maneuver implies that the execution of the maneuver be achieved with good driving quality (e.g., time-efficiency, speed limit, longitudinal and lateral comfort), feasibility (e.g., longitudinal and lateral acceleration limits), and safety (collision free operation).

Thus, the SLC overtaking maneuver should be well planned, and the respective governing maneuvering parameters, including, L_c, L, T, v_0 and a should be fine-tuned. In Figure 4.5, A, B, and D denote the tractor front right corner, the trailer rear right corner, and the car rear left corner, respectively, X_{car} and X_t the horizontal coordinates of car and tractor front bumpers (in the inertial coordinate system), accordingly, t_{LPTO} and T the time instants correspond the clear distance L_{LPTO} and the point that the SLC overtaking maneuver is exactly terminated, correspondingly.

To facilitate performing the SLC maneuver, the initial clearing distance, L_c, is introduced, which is defined as the distance between the tractor front bumper and the car rear bumper at the beginning of the overtaking maneuver. At corners A, B, and D, the corresponding coordinates in the inertial coordinate system are denoted by (X_A, Y_A), (X_B, Y_B), and (X_D, Y_D), respectively.

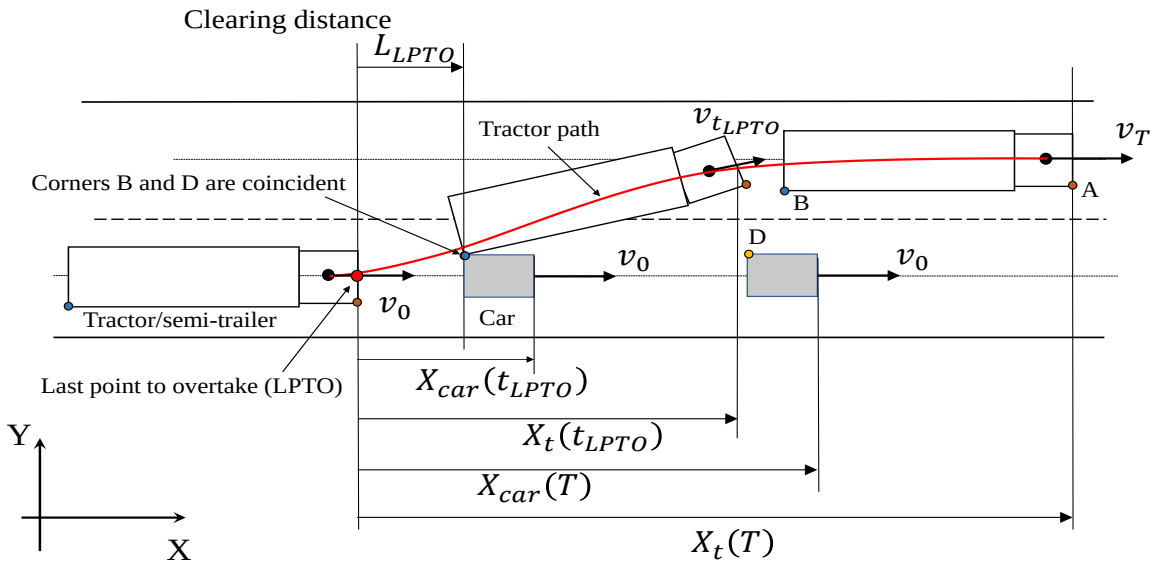

Figure 4.5. Single lane-change overtaking maneuver.

Built upon the numerical simulation using the TruckSim model, the fine-tuned values for the parameters of the reference trajectory over the SLC overtaking maneuver are determined, and they are listed in Table 4.1. Given the maneuver parameter values, the reference path for the tractor can be specified as shown in Figure 4.5.

Table 4.1 Parameter values for the reference trajectory over the SLC overtaking maneuver.

Parameters	Initial vehicle speed, v_0 (m/s)	Acceleration, a, (m/s^2) [84]	Time period, T, s	Max. displacement, L, m	Initial clearing displacement, L_c, m
Values	22.22	0.3	3.5	3.2	6.45

4.5. Kinematics for tractor/semi-trailer path-tracking

Figure 4.6 shows the geometry representation of the tractor/semi-trailer combination and the target path to be tracked by the vehicle. The target path is defined in the inertial coordinate system. At an arbitrary instant *t*, the vertical coordinates of the tractor and trailer CGs in the inertial coordinate system can be determined by

$$\dot{Y}_i(t) = v_{xi}(t)sin\psi_i(t) + v_{yi}cos\psi_i(t), i \in \{s,t\} \tag{4.3a}$$

$$\dot{X}_i(t) = v_{xi}(t)cos\psi_i(t) - v_{yi}sin\psi_i(t) \tag{4.3b}$$

where the subscript *s* and *t* represent the semi-trailer and tractor, respectively, the heading angle of the tractor and semi-trailer are calculated via

$$\dot{\psi}_i(t) = r_i(t), i \in \{s,t\} \tag{4.3c}$$

The horizontal coordinates of the tractor and semi-trailer in the inertial coordinate system are denoted as $X(t)$ and $X(t-\tau)$, respectively, where the time delay τ is determined by

$$\tau = \left(L_{wt} + L_{fs}\right)/v_{xt} \tag{4.3d}$$

where τ denotes the time required for the semi-trailer to travel from its current position to the tractor's current position as shown in Figure 4.5. At the time instant *t*, the target points to be tracked by the CG of the tractor and semi-trailer are represented by points S_{pt} and S_{ps} on the target path, respectively. The target points S_{pt} and S_{ps} are determined by $[X(t), Y_{ref}(t)]$ and $[X(t-\tau), Y_{ref}(t-\tau)]$, and the tangent angles of the target path at these points are denoted by $\psi_{ref}(t)$ and $\psi_{ref}(t-\tau)$, accordingly.

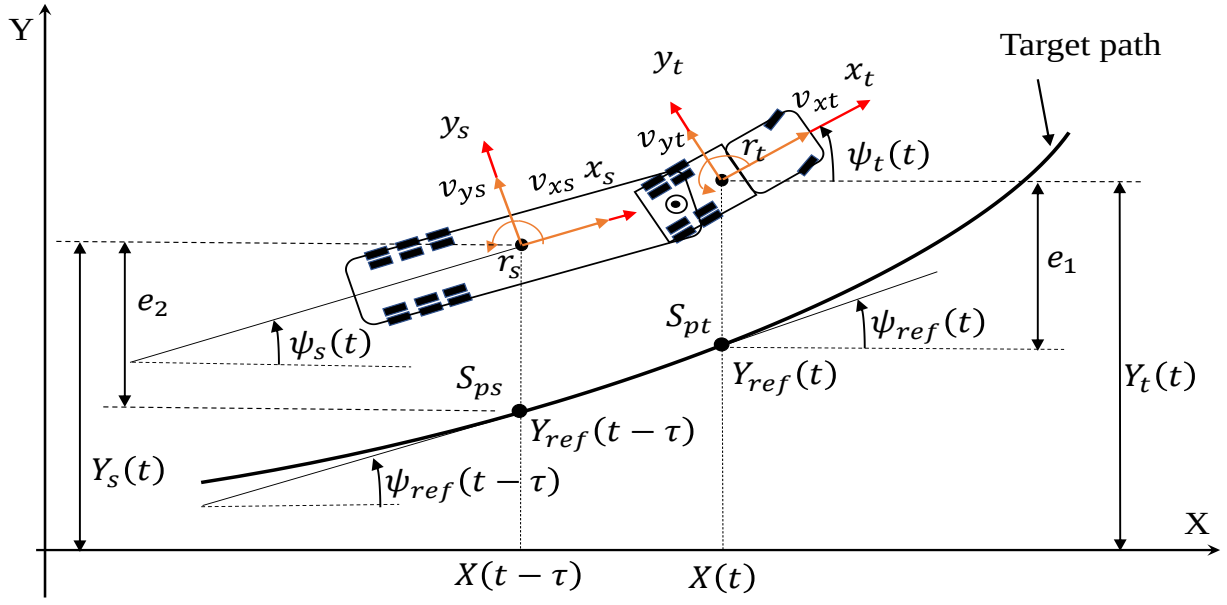

Figure 4.6 Geometry representation of the tractor/semi-trailer combination and target path.

As illustrated in Figure 4.6, the cross-track errors of the tractor and semi-trailer can be specified by

$$e_t = Y_t(t) - Y_{ref}(t) \tag{4.3e}$$

$$e_s = Y_s(t) - Y_{ref}(t-\tau) \tag{4.3f}$$

The orientation angle errors of the tractor and semi-trailer is determined by

$$\Delta\psi_t(t) = \psi_t(t) - \psi_{ref}(t) \tag{4.3g}$$

$$\Delta\psi_s(t) = \psi_s(t) - \psi_{ref}(t-\tau) \tag{4.3h}$$

Considering the reference trajectory determined in Section 4.4.2, and the above kinematic model for tractor/semi-trailer path-tracking, we rewrite the vehicle model as follows

$$\dot{\boldsymbol{x}}_p(t) = f\left[\boldsymbol{x}_p(t), \boldsymbol{u}_p(t)\right] \tag{4.4a}$$

where the subscript *p* implies that the vehicle model is tailored for the NLMPC controller design, $\boldsymbol{x}_p$ and $\boldsymbol{u}_p$ are the state and control variable vectors, respectively, which are specified as

$$\boldsymbol{x}_p = \left[\gamma\ v_{xt}\ \ v_{yt}\ \ r_t\ \ r_s\ \omega_r\ Y_t\ Y_s\ \psi_t\ \psi_s\ X_A\ Y_A\ X_B\ Y_B\right]^T \tag{4.4b}$$

$$\boldsymbol{u}_p = \left[\delta_f\ \ T_r\right]^T \tag{4.4c}$$

where γ is the articulation angle between tractor and trailer, X_A, Y_A are the horizonal and vertical coordinates (in the inertial coordinate system) of the tractor front right corner (see Figure 4.5), and X_B, Y_B the horizonal and vertical coordinates of the trailer rear right corner. It should be noted that given the subset of vehicle state $[Y_t\ Y_s\ \psi_t\ \psi_s]^{\mathrm{T}}$ and the length and width of the tractor and trailer, the subset of vehicle state $[X_A\ Y_A\ X_B\ Y_B]^{\mathrm{T}}$ can be derived. Compared with the vehicle model described in Equation (4.11), in the prediction vehicle model defined in Equation (4.4), the state variable vector is extended, while the control input vector is shrunk.

4.6. Simplified power train model

Figure 4.7 shows the simplified powertrain system, which consists of an internal combustion (IC) engine or an electric motor with an output torque (T_{tq}), a gear box with a selected gear ratio (i_g), a final drive unit with a gear ratio (i_0), and a driving wheel with an applied torque (T_i). The output torque from the engine or motor is related with the torque exerted on the driving wheel by

$$T_i = T_{tq} i_g i_0 \eta_t \tag{4.5a}$$

where η_t denotes the transmission efficiency of the drive line, which takes the value of 0.92.

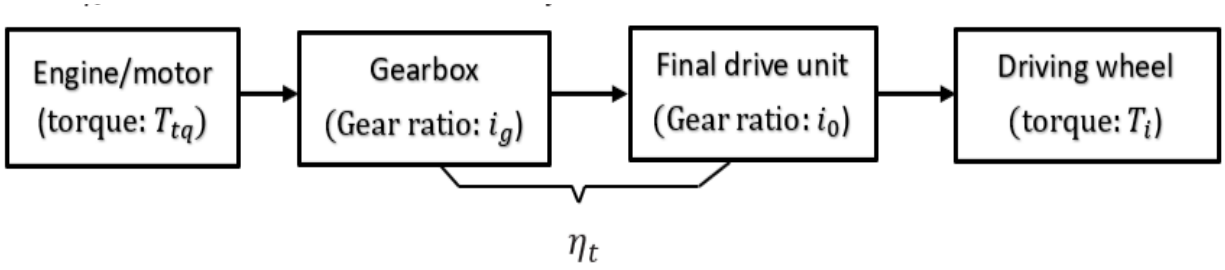

Figure 4.7 Schematic representation of the simplified powertrain system

In this study, a diesel engine is adopted, and its output torque (T_{tq}, *Nm*) is a function of the crank shaft rotation speed (*n*, r/min). Based on the power plant used in the built-in powertrain sub-model of the 3-D TruckSim model introduced in Section 4.3, the engine torque-speed function at the full throttle control (i.e., $t_p = 1.0$) is determined by

$$T_{tq} = \begin{cases} 1.2725n + 163.75, & 500 \le n \le 1300 \\ 1898, & 1300 < n < 1500 \\ -0.6633n + 2893, & 1500 \le n \le 2100 \end{cases} \tag{4.5b}$$

If the driving wheels rotate without slip, the vehicle forward speed, i.e., v_{li} (in km/h), and the engine crank shaft rotation speed, *n* (in r/min), are related by

$$v_{li} = 0.377\, n R_{ei} / (i_g i_0) \tag{4.5c}$$

The gear ratios of the gearbox and the final drive unit are listed in Table 4.2. Under the highway operation, it is assumed that the vehicle travels at the overdrive gear ratio, i.e., $i_{g18} = 0.73$.

Table 4.2 The gear ratios of the gearbox and final drive unit.

Gear	1	2	3	4	5	6	7	8	9	10	11	12	13	14	15	16	17	18
Gear ratio	14.4	12.29	8.56	7.3	6.05	5.16	4.38	3.74	3.2	2.73	2.29	1.95	1.62	1.38	1.17	1	0.86	0.73
Final drive ratio	4.4																	

Given the powertrain shown in Figure 4.7, the equivalent mass moment of inertia of the driving wheel is determined by

$$I_{ewi} = I_{wi} + I_f i_g^2 i_0^2 \eta_t \tag{4.5d}$$

where I_{wi} denotes the mass moment of inertia of the driving wheel alone, and I_f the mass moment of inertia of the flywheel of the IC engine.

Equation (4.5b) provides the maximum torque production capacity of the 330 KW diesel engine at full throttle and is driven based upon the data provided in the powertrain model considered in TruckSim.

4.7. Vehicle model validation

To validate the 7-DOF tractor/semi-trailer model, an open-loop simulation is conducted and the achieved simulation results are compared against the corresponding TruckSim model. Figure 4.8 depicts the open-loop steer input for both the TuckSim and the 7-DOF non-linear model. The steer input is defined as a single cycle sine wave with the amplitude of 1.5 degrees and the frequency of

0.4 Hz. Under the open-loop single-lane change maneuver, the vehicle forward speed is initialized at 20 m/s and a constant full throttle scenario is considered during test Maneuver.

The simulation results are shown in Figures 4.9 to 4.12 in terms of the time history of tractor front wheel slip angle, tractor lateral acceleration, trailer lateral acceleration and yaw rate of both tractor and trailer. A comparison of simulation results derived from the 7-DOF mathematical model and TruckSim model indicates that the two models achieve excellent agreement.

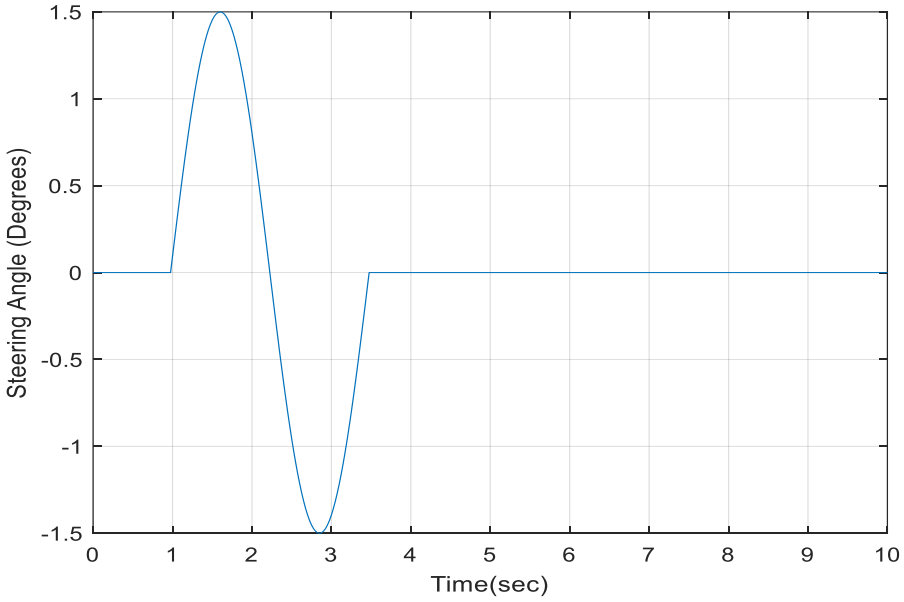

Figure 4.8 Open loop steering input

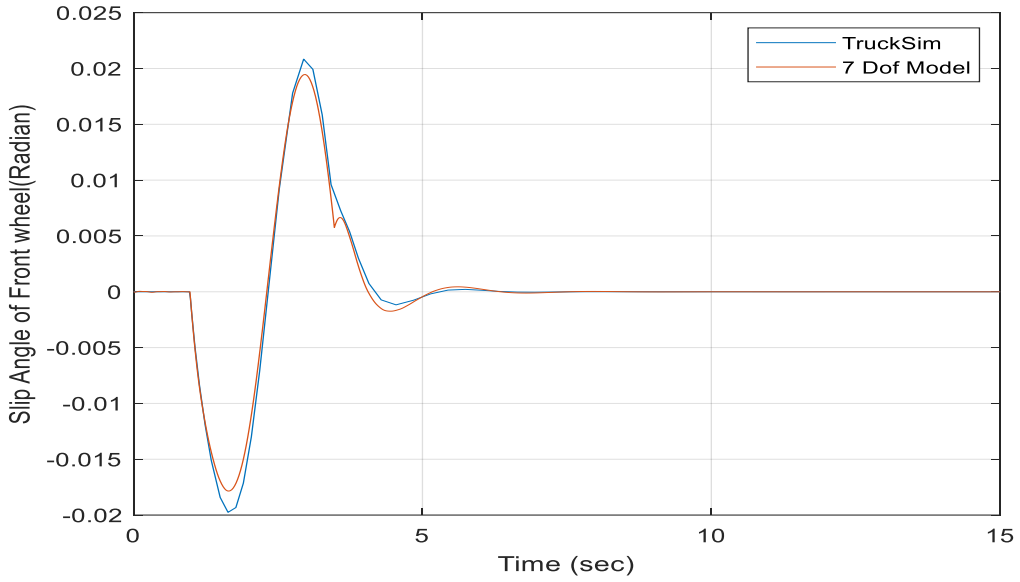

Figure 4.9 Time history of front wheel slip angle

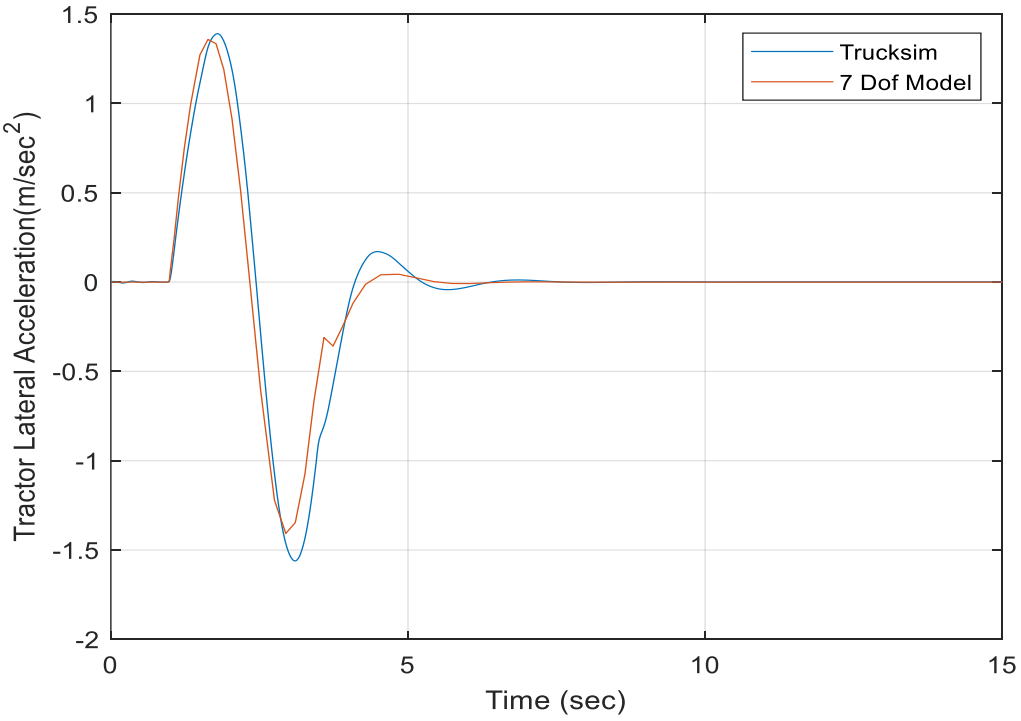

Figure 4.10 Tractor lateral acceleration time history

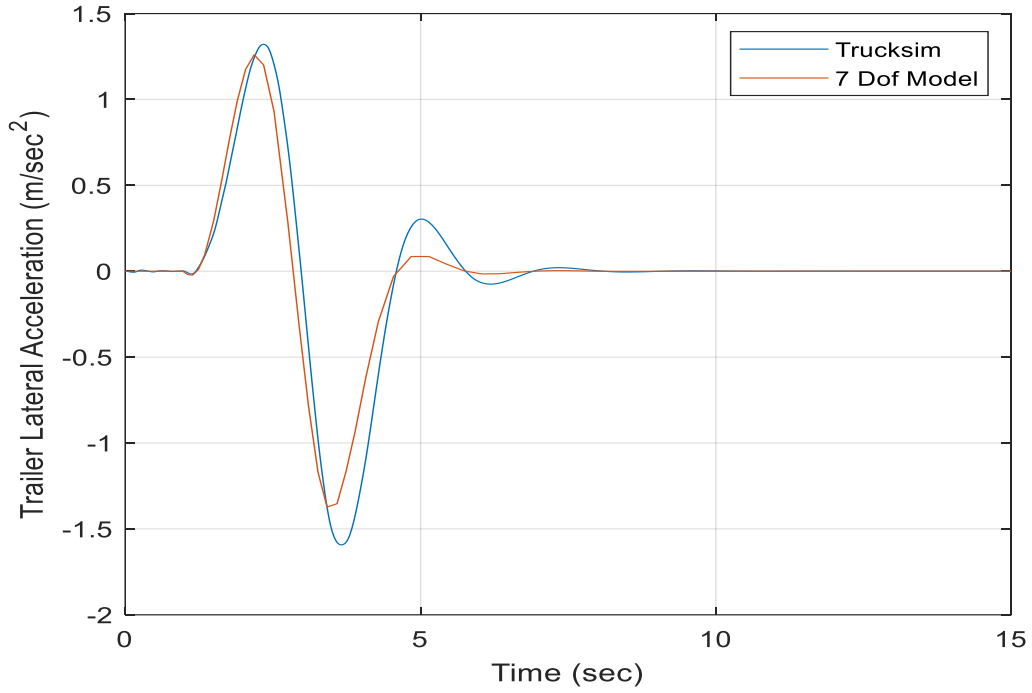

Figure 4.11 Trailer lateral acceleration time history

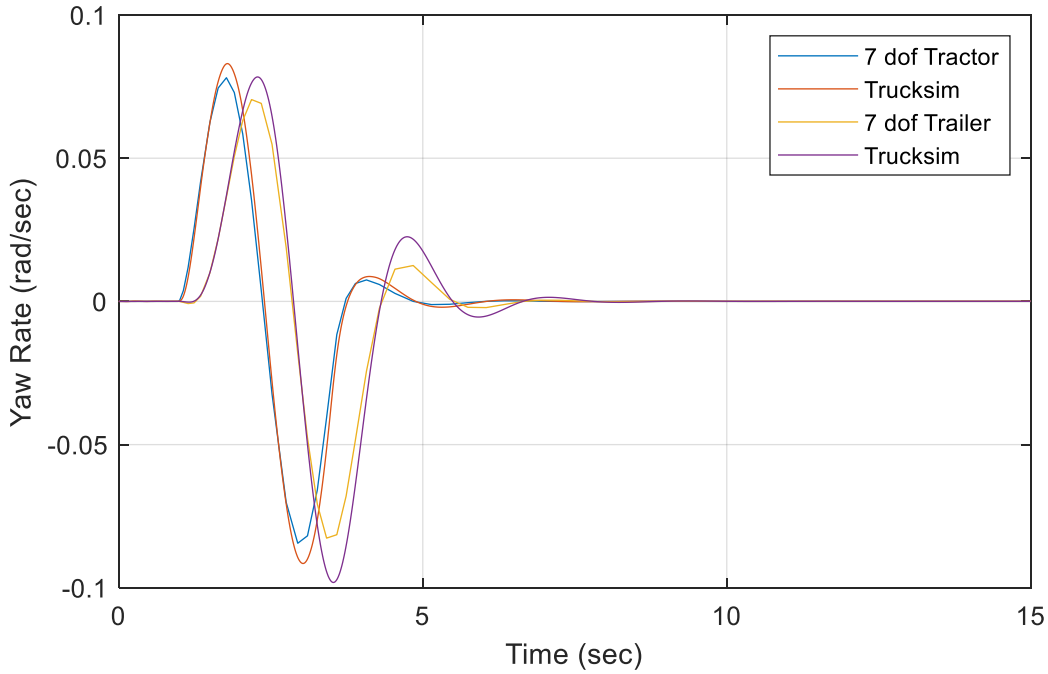

Figure 4.12 Yaw rate time history

Chapter 5

Nonlinear MPC Based Tracking Control Design

In this chapter, the Nonlinear MPC based tracking control is designed to improve the trajectory tracking and high-speed lateral stability of a tractor/semi-trailer during a single lane change maneuver at high speed.

5.1. Design of NLMPC-based tracking-controller

This section discretizes the prediction vehicle model described in Equation (4.4) and specifies output variables. The design of NLMPC-based tracking-controller is then formulated as a constrained optimization problem with a cost function and a set of state and control variables constraints. It should be emphasized that the design objective of the tracking-controller is to calculate the tractor front wheel steering angle and the tractor rear wheel driving torque in order to track as close as possible the reference motion trajectory planned in Section 4.4.2.

5.2. Discretized prediction vehicle model

At sampling step *k*, discretizing the nonlinear vehicle model represented by Equation (4.4) with the forward Euler method leads to

$$\boldsymbol{x}_p(k+1) = f\left[\boldsymbol{x}_p(k), \boldsymbol{u}_p(k)\right] \tag{5.1a}$$

$$\boldsymbol{u}_p(k) = \boldsymbol{u}_p(k-1) + \Delta\boldsymbol{u}_p(k) \tag{5.1b}$$

$$\boldsymbol{y}_p(k) = \boldsymbol{C}\boldsymbol{x}_p(k) \tag{5.1c}$$

where $\boldsymbol{y}_p(k)$ denotes the output variable vector, and

$$\boldsymbol{x}_p = \left[\gamma(k)\ v_{xt}(k)\ v_{yt}(k)\ r_t(k)\ r_s(k)\ \omega_r(k)\ Y_t(k)\ Y_s(k)\ \psi_t(k)\ \psi_s(k)\ X_A(k)\ Y_A(k)\ X_B(k)\ Y_B(k)\right]^T \tag{5.1d}$$

$$\boldsymbol{u}_p(k) = \left[\delta_f(k)\ T_r(k)\right]^T \tag{5.1e}$$

$$\boldsymbol{C} = \begin{bmatrix} 0 & 1 & 0 & 0 & 0 & 0 & 0 & 0 & 0 & 0 & 0 & 0 & 0 & 0 \\ 0 & 0 & 0 & 0 & 0 & 0 & 1 & 0 & 0 & 0 & 0 & 0 & 0 & 0 \\ 0 & 0 & 0 & 0 & 0 & 0 & 0 & 1 & 0 & 0 & 0 & 0 & 0 & 0 \\ 0 & 0 & 0 & 0 & 0 & 0 & 0 & 0 & 1 & 0 & 0 & 0 & 0 & 0 \\ 0 & 0 & 0 & 0 & 0 & 0 & 0 & 0 & 0 & 1 & 0 & 0 & 0 & 0 \\ 0 & 0 & 0 & 0 & 0 & 0 & 0 & 0 & 0 & 0 & 1 & 0 & 0 & 0 \\ 0 & 0 & 0 & 0 & 0 & 0 & 0 & 0 & 0 & 0 & 0 & 1 & 0 & 0 \\ 0 & 0 & 0 & 0 & 0 & 0 & 0 & 0 & 0 & 0 & 0 & 0 & 1 & 0 \\ 0 & 0 & 0 & 0 & 0 & 0 & 0 & 0 & 0 & 0 & 0 & 0 & 0 & 1 \end{bmatrix} \tag{5.1f}$$

With the state variable vector and matrix $\boldsymbol{C} \in \mathbb{R}^{9\times 14}$ defined in Equations (5.1d) and (5.1f), respectively, the output variable vector is written in the compact form specified by

$$\boldsymbol{y}_p(k) = \left[\overline{\boldsymbol{y}}_p^T(k)\ \widetilde{\boldsymbol{y}}_p^T(k)\right]^T \tag{5.1g}$$

where

$$\overline{\boldsymbol{y}}_p(k) = [v_{xt}(k)\ Y_t(k)\ Y_s(k)\ \psi_t(k)\ \psi_s(k)\ ]^T \tag{5.1h}$$

$$\widetilde{\boldsymbol{y}}_p(k) = [X_A(k)\ Y_A(k)\ X_B(k)\ Y_B(k)]^T \tag{5.1i}$$

The state variable vector of the reference trajectory of the overtaking maneuver is defined by

$$\boldsymbol{r}(k) = [\overline{\boldsymbol{r}}^T(k)\ \widetilde{\boldsymbol{r}}^T(k)]^T \tag{5.2a}$$

where

$$\overline{\boldsymbol{r}}(k) = \left[v_{ref}(k)\ Y_{reft}(k)\ Y_{refs}(k)\ \psi_{reft}(k)\ \psi_{refs}(k)\right]^T \tag{5.2b}$$

$$\widetilde{\boldsymbol{r}}(k) = [X_D(k)\ Y_D(k)]^T \tag{5.2c}$$

where the reference speed v_{ref} is specified by Equation (4.2c), Y_{reft} and Y_{refs} correspond to the lateral coordinates of points S_{pt} and S_{ps} on the reference path shown in Figure 4.5, i.e., $Y_{ref}(t)$

and $Y_{ref}(t-\tau)$, respectively, and $Y_{ref}(t)$ and τ are determined by Equations (4.2a) and (4.3d), accordingly, similarly, ψ_{reft} and ψ_{refs} correspond the tangential angles of the reference path at points S_{pt} and S_{ps}, i.e., $\psi_{ref}(t)$ and $\psi_{ref}(t-\tau)$, respectively, X_D and Y_D denote the corresponding horizonal and vertical coordinates of the rear left corner of the car in Figure 4.4.

The NLMPC controller consists of two core components: the discretized prediction vehicle model represented by Equation (5.1) and an optimizer with a cost function and a batch of constraints. The prediction vehicle model is used to predict the future evolution of the tractor/semi-trailer combination. At a sampling time, beginning with the current state of the virtual vehicle plant, i.e., the 3-D TruckSim model, an open-loop optimal control problem is solved over a short time window. This online optimization problem minimizes the errors between the predicted outputs and the reference trajectories over a sequence of future control input, subject to associated constraints. The resulting optimal control input is applied to the virtual plant, during the following sampling interval. At the next time step, a new optimal control problem based on a new set of state of the vehicle system is solved over a shifted time window. This 'receding horizon implementation' makes the NLMPC algorithm a feedback controller.

With the vectors of control input, output variable, and the reference variable, which are defined by Equations (5.1b), (5.1g) and (5.2), respectively, the NLMPC controller design is formulated as a constrained optimization problem with the following cost function subject to the specified constraints

$$\min_{\Delta \boldsymbol{u}_p(k|k),\cdots,\Delta \boldsymbol{u}_p(k+H_c-1|k)} J\left(\boldsymbol{x}_p(k), \Delta \boldsymbol{u}_p(k)\right) = \sum_{i=1}^{H_p} \left\| \bar{\boldsymbol{y}}_p(k+i|k) - \bar{\boldsymbol{r}}(k+i|k) \right\|_{\boldsymbol{Q}}^2 + \sum_{i=0}^{H_c} \left\| \Delta \boldsymbol{u}_p(k+i|k) \right\|_{\boldsymbol{R}}^2 \quad (5.3a)$$

subject to:

$$\boldsymbol{x}_p(k+1|k) = f\left(\boldsymbol{x}_p(k+i|k), \boldsymbol{u}_p(k+i|k)\right), i \in \{0, \cdots, H_p - 1\} \quad (5.3b)$$

$$\boldsymbol{u}_p(k+i|k) = \boldsymbol{u}_p(k-1+i|k) + \Delta\boldsymbol{u}_p(k+i|k), i \in \{0, \cdots, H_p - 1\} \quad (5.3c)$$

$$\boldsymbol{y}_p(k+i|k) = \boldsymbol{C}\boldsymbol{x}_p(k+i|k), i \in \{1, \cdots, H_p\} \quad (5.3d)$$

$$v_{min} \leq v_{xt}(k+i|k) \leq v_{max},\ i \in \{1, \cdots, H_p\} \quad (5.3e)$$

$$d_{min} \leq Y_A(k+i|k) - Y_D(k+i|k), \text{ if } X_A(k+i|k) \geq X_D(k+i|k), i \in \{1, \cdots, H_p\} \quad (5.3f)$$

$$d_{min} \leq Y_B(k+i|k) - Y_D(k+i|k), \text{ if } X_B(k+i|k) \geq X_D(k+i|k), i \in \{1, \cdots, H_p\} \quad (5.3g)$$

$$\boldsymbol{u}_{p,min}(k+i|k) \leq \boldsymbol{u}_p(k+i|k) \leq \boldsymbol{u}_{p,max}(k+i|k), i \in \{0, \cdots, H_c - 1\} \quad (5.3h)$$

$$\Delta\boldsymbol{u}_{p,min}(k+i|k) \leq \Delta\boldsymbol{u}_p(k+i|k) \leq \Delta\boldsymbol{u}_{p,max}(k+i|k), i \in \{0, \cdots, H_c - 1\} \quad (5.3i)$$

$$\Delta\boldsymbol{u}_p(k+i|k) = \boldsymbol{0}, i \in \{H_c, \cdots, H_p - 1\} \quad (5.3j)$$

where Equations (5.3b) to (5.3d) represent the vehicle dynamics, the constraints (5.3e) limit the forward speed, expressions (5.3f) and (5.3g) ensure a collision-free overtaking maneuver, (5.3h) poses constraints on the steering angle and driving torque, (5.3i) limits the steering angle and driving torque variations between two consecutive time steps, H_p and H_c are the output prediction horizon and the control horizon, respectively, (5.3j) represents that the control action gets constant between the control horizon (H_c) and predict ion horizon (H_p) range as shown in the figure A3 of Appendix, the symbol $|k$ indicates the sampling step *k*, at which control input $\boldsymbol{u}_p(k)$ is applied for the closed-loop control of the AHV plant, $\Delta\boldsymbol{u}_p(k) = \Delta\boldsymbol{u}_p(k|k), \cdots, \Delta\boldsymbol{u}_p(k+H_c-1|k)$ denotes the optimization vector, $\boldsymbol{y}_p(k+i|k)$ the output vector predicted at time $k+i$, $\boldsymbol{Q} \in \mathbb{R}^{5\times5}$ and $\boldsymbol{R} \in \mathbb{R}^{2\times2}$ the matrices corresponding to weights on the output and control input vectors, accordingly.

Note that $H_p > H_c$, and the predicted control inputs are assumed constant in the time interval from H_c to H_p.

In addition to tracking the reference longitudinal speed v_{ref} for time efficiency, expression (5.3e) constrains forward speed for longitudinal comfort. Considering the fact that the reference motion trajectory in terms of Equations (4.2a) to (4.2c) is derived based on kinematic analysis, we impose the rigid constraints of (5.3f) and (5.3g) on the lateral displacements of the tractor and trailer; thus, over the SLC overtaking maneuver, the AHV will not collide with the preceding car traveling at a constant speed in the straight right lane. To guarantee stable and smooth motions of tractor/semi-trailer combination over the overtaking maneuver, the magnitude and variation of tractor front wheel steer angle are limited via the constraints (5.3h) and (5.3i), respectively. In addition, the longitudinal speed is controlled and manipulated considering the output driving torque capacity at a given forward speed specified in Equations (4.5a) to (4.5c). Note that Equation (4.5b) specifies the maximum engine torque output over the given speed ranges.

On the right-hand side of Equation (5.3a), the first summand imposes the penalty on trajectory tracking deviation, while the second summand is to prevent large control effort for the automated driving. Solving the optimization problem in Equation (5.3), we obtain the optimal control input increments evaluated at the sampling step *k* for the currently observed vehicle state vector $\boldsymbol{x}_p(k)$, and denote the optimally predicted control input increments by

$$\Delta \boldsymbol{u}_p^*(k) \triangleq \left[\Delta \boldsymbol{u}_p^*(k|k), \cdots, \Delta \boldsymbol{u}_p^*(k + H_c - 1|k)\right]^T \tag{5.4}$$

where the first control input increment is used to update the required control action as described in Equation (5.1b). The resulting state feedback control law is thus cast as

$$\boldsymbol{u}_p(k+1) = \boldsymbol{u}_p(k) + \Delta \boldsymbol{u}_p^*(k|k) \tag{5.5}$$

At the next sampling step $k+1$, the control action $\boldsymbol{u}_p(k+1)$ will be applied to the vehicle plant to acquire the new vehicle state vector $\boldsymbol{x}_p(k+1)$, with which the optimization problem formulated in (5.3) will be solved again over a shifted horizon.

To summarize the NLMPC controller design, we visualize the interrelations among the MPC optimizer, the prediction vehicle model, and the vehicle plant using the block diagram shown in Figure 5.1. Note that in the figure, the time instant t_k corresponds to the sampling time step k.

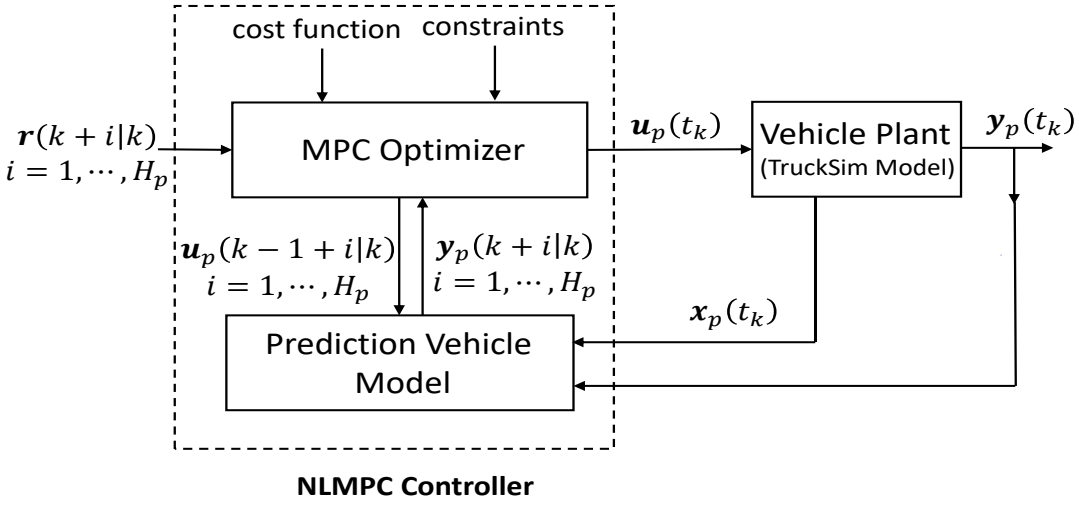

Figure 5.1 Block diagram describing the interrelations among NLMPC controller and vehicle plant.

5.3. Results and discussion

To evaluate the proposed NLMPC tracking-controller, co-simulations are conducted under the SLC maneuver specified in Section 4.4.2. This section first selects the parameter values of the NLMPC controller and other relevant elements. The chosen simulation results are then presented.

5.3.1 Selecting parameter values of NLMPC controller and other relevant elements

As shown in Figure 5.1, the co-simulation for evaluating the NLMPC controller is directly associated with the reference motion trajectory, the NLMPC controller (consisting of the MPC optimizer and the prediction vehicle model), and the 'vehicle plant', i.e., the 3-D TruckSim model. The parameter values for the prediction vehicle model and the 3-D TruckSim model are provided in Appendix. The reference trajectory is parameterized as a sinusoidal function in time, and is determined by the lateral/longitudinal position and longitudinal speed of the AAHV, as well as the forward speed of the obstacle car at the starting point of the overtaking maneuver. The parameter values for the reference trajectory over the overtaking maneuver are listed in Table 4.1. The NLMPC controller parameters may be categorized into two groups: 1) tuning parameters, and 2) constraint parameters. The following subsections select the values for these NLMPC controller parameters.

5.3.2 Values selection for tuning parameters of NLMPC controller

In MPC controller designs, the tuning parameters generally include [85, 86]: prediction horizon, H_p, control horizon, H_c, sampling time, T_s, output weighting matrix, $\boldsymbol{Q}$, and control input variation weighting matrix, $\boldsymbol{R}$. Tuning of MPC controllers is of importance due to the fact that a good choice of tuning parameters is likely to significantly increase control quality [87]. In real-time execution of MPC controls, practical limitations often restrict the availability of sampling time, T_s, as a tuning parameter [86]. In MPC controller designs for autonomous vehicles traveling at forward speed lower than 70 km/h, it is recommended that sampling time, T_s, take 0.05 s [18]. In this study, the

NLMPC controller is designed for the tractor/semi-trailer combination traveling at higher speeds on highways, a shorter sampling time is thus selected, that is, $T_s = 0.01\ s$.

Reliable guidelines for selecting the tuning parameters of the prediction horizon, H_p, and control horizon, H_c, are well established [85]. The prediction horizon establishes the number of time instants in a finite future time interval, in which the vehicle outputs are predicted. The control horizon is an integer number, and it specifies the length of time steps that the NLPMC controller drive the vehicle outputs to their reference values. The control horizon represents the number of time instants in a future time interval, in which control action can be used to minimize the vehicle output and input deviations from the reference trajectories or targets. The relationship between the two parameters should satisfy the requirement of $H_c \leq H_p$. Generally, the larger the prediction horizon is selected, the more information about the future vehicle dynamics is attained. Consequently, better SLC overtaking performance may be achieved. However, a larger prediction horizon often leads to a heavier computational burden of the controller. In addition, a large control horizon allows for aggressive control actions, but increases the computation cost of the controller. Fully, considering the aforementioned trade-offs, we select the values for these two parameters, i.e., $H_p = 10$ and $H_c = 2$.

The selection of the diagonal weight matrices, $\boldsymbol{Q} \in \mathbb{R}^{5\times5}$ and $\boldsymbol{R} \in \mathbb{R}^{2\times2}$, reflects our controller design objective to keep the output tracking error 'small' using the control actions that are 'not too large'. The diagonal elements of the matrix $\boldsymbol{Q}$ $\left(Q_{ij} \neq 0 \text{ for } i = j \text{ and } Q_{ij} = 0 \text{ for } i \neq j\right)$ are real-valued variables used to manipulate the relative importance associated with each controlled output in the objective function expressed in Equation (5.3a). The diagonal elements of the matrix $\boldsymbol{R}$ $\left(R_{ij} \neq 0 \text{ for } i = j \text{ and } R_{ij} = 0 \text{ for } i \neq j\right)$ are also real-valued variables, which weigh the importance of each control input. An effective setting of this weight matrix may prevent both

aggressive control and an oscillation behavior of the controlled outputs. The matrices $\boldsymbol{Q}$ and $\boldsymbol{R}$ exhibit conflicting effects on the minimization of the objective function. As a result, while tuning the weight matrices, we establish a compromise between the desired outputs and limiting the actuator actions. Table 5.1 summarizes and lists the selected values for the tuning parameters of the NLMPC controller. Since tuning the weighting factors for MPC controller is a very tedious and time-consuming task, these weighting factors are finalized after doing a lot of trial and error method. Different values have been used for the output variable and control variable weighting factors and the values which provides the best optimized results are finalized.

Table 5.1 Values for the tuning parameters of the NLMPC controller.

Tuning parameters	Sampling time (s)	Prediction horizon	Control horizon	Weight Q_{11}	Weight Q_{22}	Weight Q_{33}	Weight Q_{44}	Weight Q_{55}	Weight R_{11}	Weight R_{22}
Values	0.01	10	2	15	750	200	25	25	150	25

5.3.3 Values selection for constraint parameters of NLMPC controller

In the NLMPC controller design, the constraints specified in (5.3e) to (5.3i) reflect the associated vehicle physical limits and design requirements. Considering the longitudinal comfort and time efficiency, we set the forward speed limits to be $v_{min} = 22.22\, m/s$ and $v_{max} = 27.78\, m/s$. Numerous simulations based on the 3-D TruckSim model indicate that over the SLC overtaking maneuver shown in Figure 4.4, three points on the interacting vehicles are critical for potential collision between the two vehicles. These critical points are the tractor front right corner, A, the trailer rear right corner, B, and the car rear left corner, D. To guarantee collision-free SLC overtaking maneuvering, we pose the rigorous constraints on the coordinates of these critical

points in expressions (5.3f) and (5.3g), and set the minimum lateral separation distance in the vertical direction to be $d_{min} = 0.3\ m$.

To ensure comfort and stable lateral motions during the overtaking maneuver, we set the tractor front wheel steering angle limits to be $\delta_{fmin} = -10.0^o$, $\delta_{fmax} = 10^o$, $\Delta\delta_{fmin} = -1.5^o$, and $\Delta\delta_{fmax} = 1.5^o$. It is assumed that in the highway operation, the AHV travels at the overdrive speed ratio of 0.73. Considering the fact that over the maneuver, the vehicle travels at a continuously increasing forward speed, we set the minimum and the minimum variation of driving torque exerted on the tractor rear axle to be $T_{rmin} = 0.0\ Nm$ and $\Delta T_{rmin} = 0.0\ Nm$. Given the powertrain data provided in section 4.6, the maximum and the maximum variation of driving torque exerted on the rear axle of the tractor over the maneuver are constrained as

$$T_{rmax} = \begin{cases} 5{,}608.7\ Nm, & v \in [22.22, 24.94]\ m/s \\ -117.88v + 8548.93\ Nm, & v \in [24.94, 27.78]\ m/s \end{cases} \tag{5.6}$$

$$\Delta T_{rmax} = \begin{cases} 560.87\ Nm, & v \in [22.22, 24.94]\ m/s \\ -11.79v + 854.89\ Nm, & v \in [24.94, 27.78]\ m/s \end{cases} \tag{5.6}$$

Table 5.2 summarizes and lists the values of the constraint parameters of the NLMPC controller.

Constraint parameters	d_{min} m	v_{min} m/s	v_{max} m/s	δ_{fmin} (°)	δ_{fmax} (°)	$\Delta\delta_{fmin}$ (°)	$\Delta\delta_{fmax}$ (°)	T_{rmin} Nm	T_{rmax}, Nm		ΔT_{rmin} Nm	$\Delta T_{rmax}, Nm$	
									$v \in [22.22, 24.94], m/s$	$v \in [24.94, 27.78], m/s$		$v \in [22.22, 24.94], m/s$	$v \in [24.94, 27.78], m/s$
values	0.3	22.22	27.78	-10.0	10.0	-1.5	1.5	0	5,608.7	$-117.88v + 8548.93$	0	560.87	$-11.79v + 854.89$

Table 5.2 Values of the constraint parameters of the NLMPC controller.

5.4 Selected simulation results

In the simulation experiments, two cases are considered. In the first case, as shown in Figure 4.5, for both the leading and trailing vehicle units, trajectory-tracking controls are implemented; while

in the second case, only tractor trajectory-tracking control is conducted. In the following subsections, without a specification, it is referred to the first case.

5.4.1 Execution of SLC overtaking maneuver

Figure 5.2 shows the relative kinematic relationships between the tractor/semi-trailer combination and the obstacle car over the SLC overtaking maneuver. Under the maneuver, initially the AHV and the front car are traveling at the same forward speed of 22.22 m/s along the central line in the right lane, as seen in Figure 4.4. To overtake the obstacle car, the AHV conducts the SLC maneuver, over which the longitudinal acceleration is 0.3 m/s^2. Figure 5.2(a) illustrates the time-histories of the reference and actual forward speed of the AHV. Note that over the maneuver, the front car travels in the same direction at the constant forward speed.

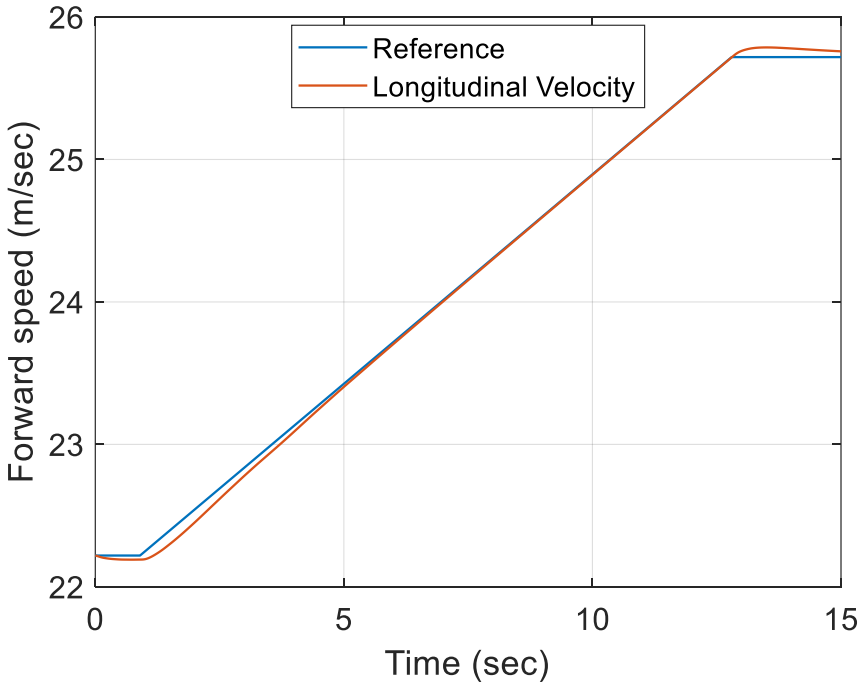

(a)

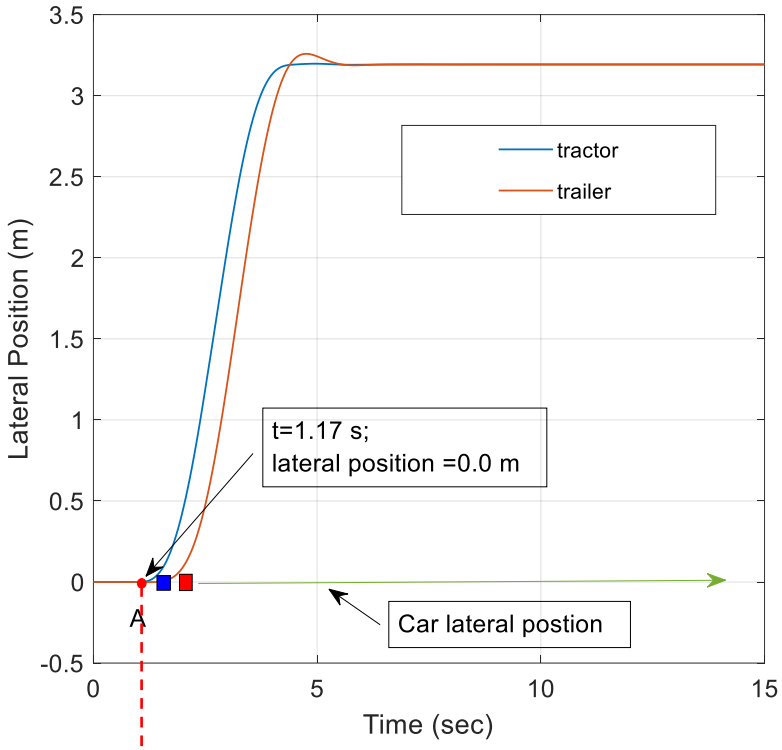
tractor
trailer
t=1.17 s;
lateral position =0.0 m
Car lateral postion
A
Lateral Position (m)
Time (sec)
3.5
3
2.5
2
1.5
1
0.5
0
-0.5
0
5
10
15

(b)

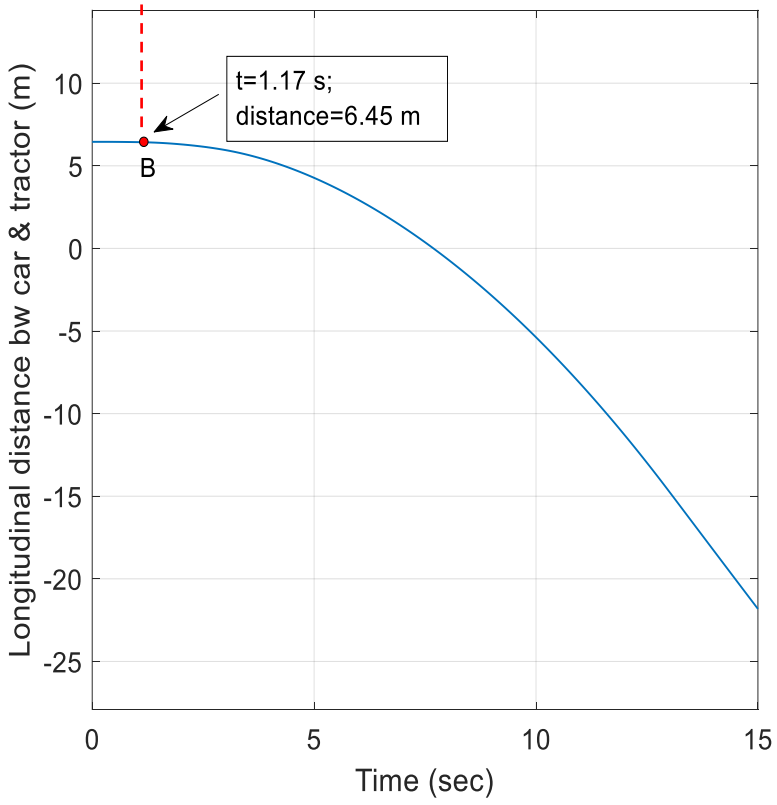
t=1.17 s;
distance=6.45 m
B
Longitudinal distance bw car & tractor (m)
Time (sec)
10
5
0
-5
-10
-15
-20
-25
0
5
10
15

(c)

(d)

Figure 5.2 Dynamic responses of the tractor/semi-trailer combination over the SLC overtaking maneuver: (a) time-histories of reference and actual forward speed of the AHV; (b) time-histories of lateral positions of the leading and trailing units of the AHV, as well as the obstacle car; (c) time-history of longitudinal distance between the rear bumper of the preceding car and the front bumper of the tractor; (d) relative positions between the obstacle car and the AHV.

Figure 5.2(b) displays the time-histories of the lateral positions of both the leading and trailing units of the AHV, as well as the obstacle, while Figure 5.2(c) illustrates the relative longitudinal distance between the front bumper of the tractor and the rear bumper of the front car. As shown in Figure 5.2(b), at point A (i.e., $t = 1.17$ s), the AHV starts the SLC maneuver and begins to accelerate at the given longitudinal acceleration. As time goes, the lateral distance between the tractor/trailer and the obstacle car increases until the maneuver completes with steady-state lateral displacement of 3.2m

Point B seen in Figure 5.2(c) corresponds to point A in Figure 5.2(b). Point B in Figure 5.2(c) indicates that at the beginning of the SLC overtaking maneuver, the longitudinal distance between the front car and the AHV is 6.45 m. Due to the increased forward speed of the AHV, the relative longitudinal distance between the tractor and the obstacle car decreases from $t = 1.17\ s$ until $t = 7.69\ s$. The relative longitudinal distance between the two vehicles then increases as time goes. Figure 5.2(d) exhibits the relative positions between the obstacle car and the AHV over the SLC overtaking maneuver, which clearly indicate that the maneuver is successfully executed without collision between the two vehicles.

5.4.2 Dynamic behaviors of tractor/semi-trailer combination over SLC overtaking maneuver

To determine the directional performance of the tractor/semi-trailer combination over the SLC overtaking maneuver, we evaluate the dynamic behaviors of the vehicle shown in Figure 5.3. The path-following off-tracking (PFOT) measures of the tractor and the trailer may be acquired from Figure 5.3(a) and (b), which illustrate the respective reference and actual path of the leading and trailing unit's CG. In this study, the measure of PFOT is defined as the deviation between the actual lateral position and the reference lateral position with a given longitudinal position. Note that for the specified SLC testing maneuver recommended by ISO-14791 [80], the testing vehicle shall follow a predefined reference test course so that the leading unit does not deviate more than 0.150 m from the desired path.

As shown in Figure 5.3(a) and (b), both the vehicle units track their reference paths well: the maximum PFOT of the trailer is 0.105 m, while the counterpart for the tractor is only 0.055 m. The larger PFOT measure of the trailer may be caused by two factors: 1) the RA dynamic feature of the AHV, and 2) the indirect steering control of tractor front wheel.

Figure 5.3(c) shows the time-histories of the lateral acceleration at the CG of both the tractor and the trailer. The maximum peak values of the lateral acceleration of the tractor and trailer are 1.677 and 1.729 m/s^2, respectively. The above maximum peak values of the lateral acceleration indicate that the AHV operates within its linear lateral dynamic range. The RA measure of the AHV thus takes the value of 1.03, which is close to the desired value of 1.0 [88].

Figure 5.3(d) illustrates the time-histories of the yaw rate of both the leading and trailing units of the AHV. The maximum peak values of yaw rate of the tractor and trailer are 5.443 and 5.319 degree/s, accordingly. As seen in the figure, each of the time-histories of the yaw rates look like a single-cycle sine wave, which is consistent with the published results achieved under similar obstacle avoidance maneuvers [89, 90]. Moreover, comparing the above maximum yaw rate values with those reported in these references, it may be deduced that the yaw stability can be achieved for this AHV over the SLC overtaking maneuver. Table 5.3 summarizes the performance measures of the tractor/semi-trailer combination acquired from the overtaking maneuver.

Table 5.3. Performance measures of the tractor/semi-trailer combination acquired from the simulation results under the SLC overtaking maneuver.

Measures	Tractor Max. PFOT (m)	Trailer Max. PFOT (m)	Tractor Max. a_y (m/s^2)	Trailer Max. a_y (m/s^2)	RA ratio	Tractor Max. r_t (degree/s)	Trailer Max. r_s (degree/s)
Values	0.055	0.105	1.677	1.729	1.030	5.443	5.319

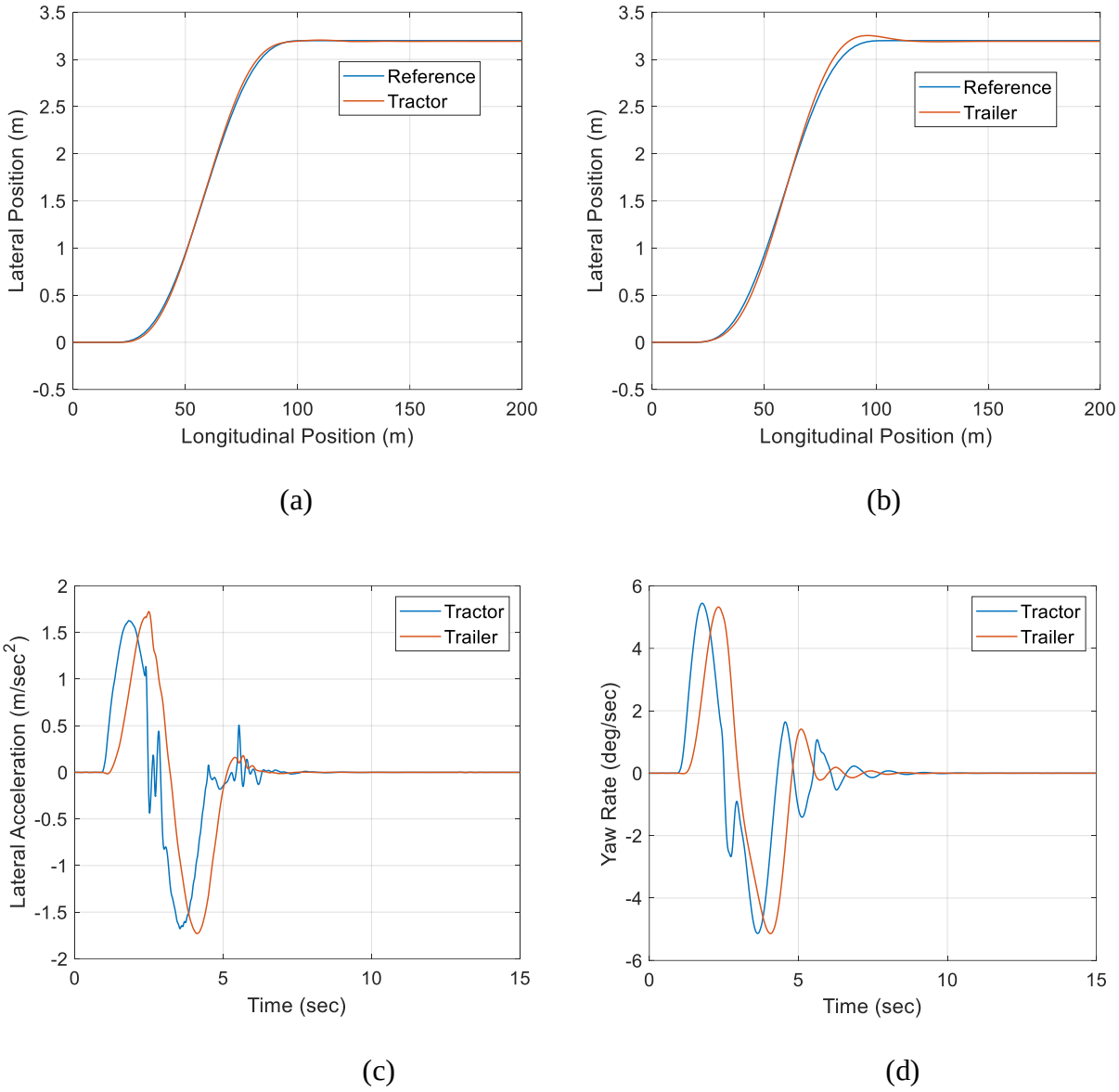

Figure 5.3. Tractor/semi-trailer directional performance determination using dynamic responses acquired from SLC overtaking maneuver: (a) reference and actual tractor path; (b) reference and actual trailer path; (c) time-histories of tractor and trailer lateral acceleration; (d) time-histories of tractor and trailer yaw rate.

To find the root factors determining the performance measures listed in Table 5.3, we examine the tire dynamic states, steering and driving actuations shown in Figure 5.4. Over the overtaking maneuver, under the control of the NLMPC controller, the steering actuation is applied on the tractor front wheels to track the reference path. To follow the desired path and remain lateral

stability under the maneuver, the AHV needs to secure required lateral forces from the road surface by manipulating tire slip angles.

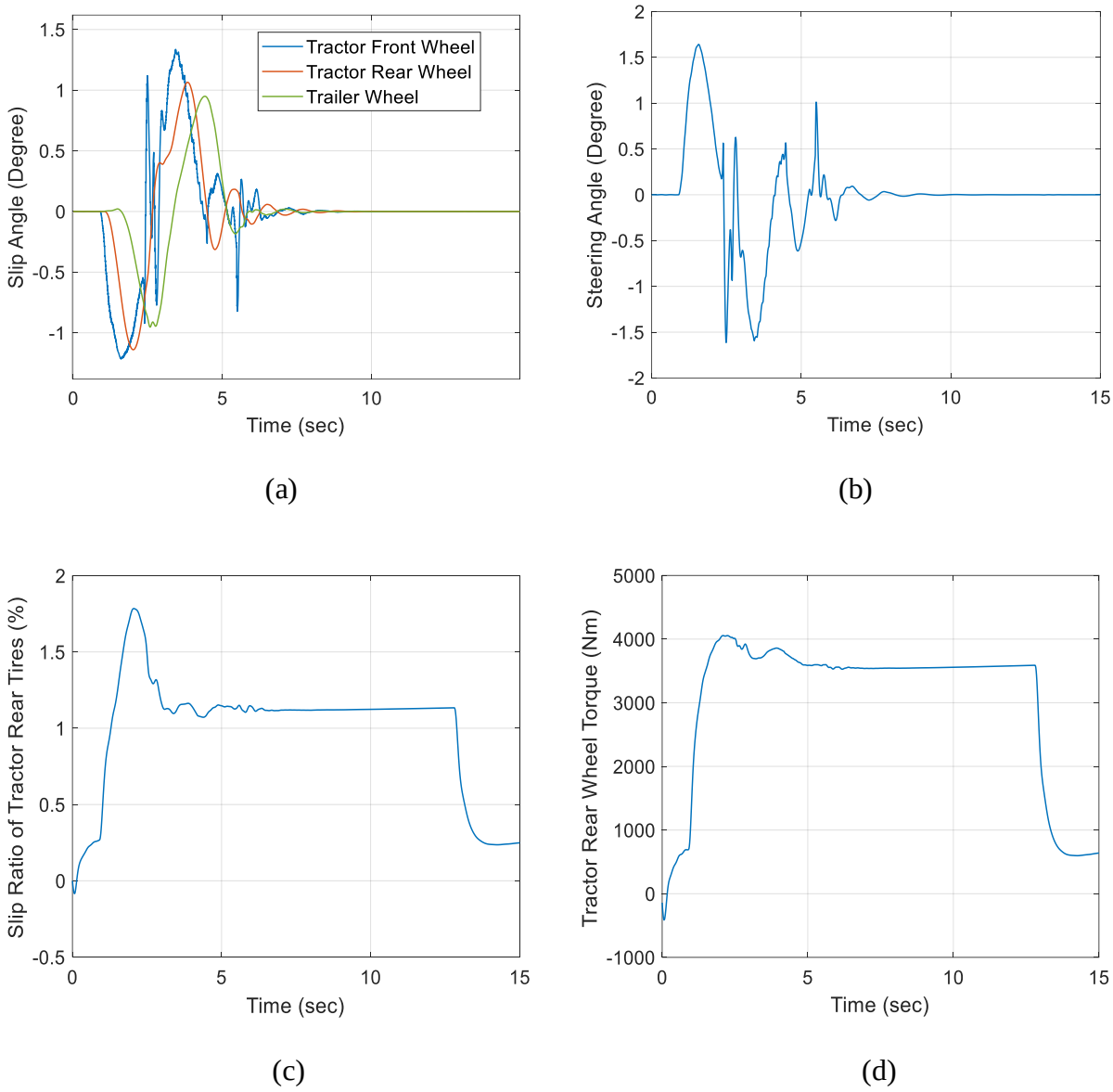

Figure 5.4 Tire dynamic states, steering and driving actuations over SLC overtaking maneuver: (a) time-histories of tire slip angles for both the leading and trailing units; (b) time-history of tractor front wheel steering angle; (c) time-history of longitudinal slip ratio of tractor rear tire; (d) time-history of driving torque on tractor rear wheel.

Figure 5.4(a) shows the time-histories of slip angles of tractor front tires, tractor rear tires, and trailer tires, and Figure 5.4(b) illustrates the associated time-history of the tractor front wheel

steering angle. It is found that the time-history curve of the tractor front wheel steering angle takes an approximate single-cycle sine wave with the maximum peak value of 1.64 degrees. This kinematic feature of tractor front wheel steering angle determines the SLC paths of the tractor and trailer as shown in Figure 5.3(a) and (b), respectively.

A close observation of Figure 5.4(a) discloses the following three facts: 1) each of the three tire slip angle curves looks more or less like a single-cycle sine wave, which is however out-phase in relation with the curve of tractor front wheel steering angle; 2) the maximum peak value of the three tire slip angle curves is less than 1.4 degrees; 3) the amplitude of the respective single-cycle sine wave of tire slip angle curve drops from the tractor front tires, via the tractor rear tires, to the trailer tires. The first fact governs the timely varying cornering forces (in terms of direction and magnitude) on tractor front tires, tractor rear tires, and trailer tires in relation with the tractor front wheel steering angle. The second factor indicates that the AHV operates in the linear lateral dynamic range over the SLC maneuver, which confirms the previous linear lateral acceleration analysis shown in Figure 5.3(c). The third fact implies that the effect of the tractor front wheel steering actuation on controlling the PFOT measure of the tractor is stronger than on controlling the PFOT measure of the trailer. This fact well explains the difference between the PFOT measures of the leading and trailing units listed in Table 5.3.

Figure 5.4(c) and (d) display the time-history of longitudinal slip ratio of tractor rear tire and the time-history of driving torque on tractor rear axle, respectively. Interestingly, the shapes of the curves seen in the two figures look similar. As shown in Figure 5.4(c), the maximum longitudinal slip ration of the tire is less than 1.8%. Thus, the longitudinal tire force and the slip ratio may be correlated by a linear relationship. This linear correlation may explain the shape similarity of the two curves. At the low longitudinal tire slip ratio shown in Figure 5.4(c), the rear tractor driving

wheels perform approximately pure rolling on the road surface. In addition, the maximum driving torque on the wheels is about 4,000 Nm, which is far below the powertrain torque capacity limitation listed in Table 5.2. Therefore, it may be deduced that the vehicle forward speed can be well controlled by the NLMPC controller. Actually, as seen in Figure 5.2(a), the vehicle forward speed well tracks the reference one over the SLC overtaking maneuver.

5.4.3 A comparison between schemes with and without trailer trajectory-tracking control

This subsection compares the two NLMPC control schemes, i.e., considering trajectory-tracking control for both the leading and trailing units and without considering trajectory-tracking control for the trailing unit, using the selected simulation results shown in Figure 5.5. Figure 5.5(a) shows the time-histories of trailer lateral position for both cases and the reference one. Without trailer tracking control, the maximum overshoot is 0.060 m, while the counterpart for the first case is 0.055 m. By introducing the trailer tracking control, the maximum overshoot is reduced by 9.1%.

Figure 5.5(b) compares the time-histories of trailer lateral accelerations for the two cases over the maneuver. In the first case, the maximum peaking lateral acceleration is 1.729 m/s^2, decreasing 3.03% from 1.783 m/s^2, the counterpart of the second case. Figure 5.5(c) illustrates the time-histories of lateral acceleration of the tractor and trailer for the second case. With the curves shown in this figure, we can determine the respective RA ratio of 1.033, which marginally increases from the corresponding measure of 1.030 for the first case.

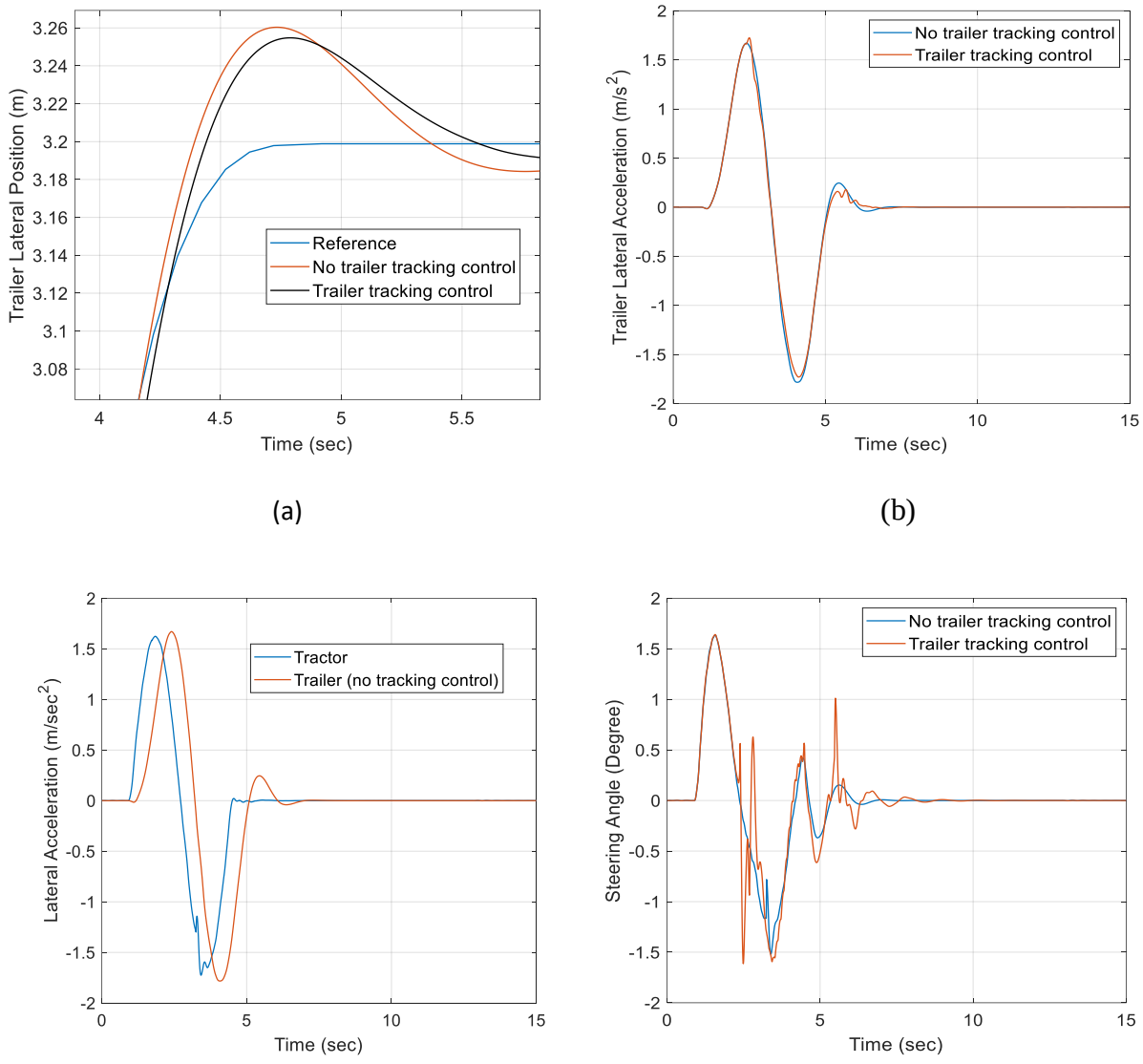

Figure 5.5 A comparison between schemes with and without trailer tracking control: (a) time-histories of trailer lateral positions; (b) time-histories of trailer lateral accelerations; (c) time-histories of tractor and trailer lateral accelerations; (d) time-histories of tractor front wheel steering angles.

Figure 5.5(d) shows the time-histories of tractor front wheel steering angles for both the cases. The root of mean square (RMS) value for the first case is 0.64 degrees, while the RMS for the second

case is 0.58 degrees. It is evident that the first control scheme gains the improved performance at the expense of applying larger tractor front wheel steering actuation effort.

Table 5.4 Parameter values of 7-DOF and TruckSim tractor/semi-trailer models.

L_{ft}, the distance between the tractor front axle and its CG,	1.385 m
L_{rt}, the distance between the tractor rear axle group and its CG	4.25 m
L_{wt}, the distance between the tractor CG and the fifth-wheel	4.57 m
L_{fs}, the distance between the fifth-wheel and the trailer CG	5.5 m
L_{rs}, the distance between the trailer CG and its axle	2.4 m
m_t, the mass of the tractor	7878 kg
m_s, the mass of the trailer	7807 kg
I_{zt}, the yaw moment of inertia of the tractor	19965 $kg \cdot m^2$
I_{zs}, the yaw moment of inertia of the trailer	150000 $kg \cdot m^2$
C_D, the aerodynamic resistance coefficient	0.66
A_a, the frontal area of the tractor	3.2 m^2
ρ_a, the mass density of the air	1.206 kg/m^3
μ, tire/road friction coefficient	0.5
$C_{\sigma i}, i \in \{f, r, s\}$, the longitudinal tire stiffness	{270000×2, 85000×8, 65000×12} N/unit slip
$C_{\alpha i}, i \in \{f, r, s\}$, the tire cornering stiffness	{200000×2, 50000×8, 40000×12} N/rad
$R_{ei}, i \in \{f, r, s\}$, the effective rolling radius of the tractor and trailer	{0.51, 0.51, 0.51} m
$f_{ri}, i \in \{f, r, s\}$, the coefficient of rolling resistance of the vehicle tires	{0.0041, 0.0041, 0.0041}

Chapter 6

Conclusions, Original Contribution and Future Work

This thesis presents a trade-off analysis between static and dynamic stability of a tractor/semi-trailer combination considering two tractor rear axle arrangements and three trailer payload schemes. Building upon the linear stability analysis of articulated heavy vehicles, a nonlinear model predictive control-based tracking-controller is proposed and designed for autonomous articulated heavy vehicles to increase the safety and enhance the transportation efficiency of these large vehicles.

6.1. Conclusions

6.1.1 Trade-off analysis between static and dynamic stability

The trade-off analysis between the static and dynamic stability of the tractor/semitrailer is conducted to assess the effects of tractor rear axle arrangement and trailer payload scheme on the safe operations of AHVs. In order to understand the static stability of the tractor/semi-trailer, the equivalent understeer gradient of the AHV is calculated considering the weight shift from the trailer towards the tractor at the fifth-wheel. In addition, a constant speed test is simulated to generate the handling diagram for understanding the steady state handling characteristics of the tractor/semi-trailer. The results of based on the equivalent understeer gradient and the handling diagram attain good agreement. Dynamic stability of the tractor/semitrailer is evaluated using eigenvalue analysis approach, by which the relationship between the damping ratio of the least damped motion mode and forward speed can be identified. Considering the relationship between the damping ratio and vehicle forward speed, we can assess the effects of tractor rear axle

arraignment and trailer payload scheme on the dynamic stability of the tractor/semi-trailer combination. The sinewave steering angle based open-loop simulation is performed using the respective TruckSim, and the open-loop simulation validates the eigenvalue analysis results. The trade-off analysis between the static and dynamic stability of the tractor/semi-trailer leads to the following conclusions:

- Increasing the payload of the semi-trailer decreases the understeer gradient of the AHV, while increasing the trailer payload results in the increase of yaw damping ratio of the trailing unit, thereby enhancing the lateral dynamic stability of the vehicle.
- Compared with the single tractor rear axle arrangement, the double tractor rear axle arrangement not only increases the understeer gradient, but also improves the lateral dynamic stability.

6.1.2 NLMPC tracking-controller design

To design the NLMPC controller, a structured nonlinear 7-DOF tractor/semi-trailer model is generated, which consists of the sub-models of tractor and trailer rigid bodies, Dugoff tire, wheel, and a simplified powertrain. Considering the trajectory-tracking control for both the leading and trailing units, we establish the kinematics for tractor/semi-trailer path-tracking. In the formulation of the NLMPC controller design, the constraints reflecting associated vehicle physical limits and design requirements, e.g., ride comfort, time efficient driving, collision-free, etc., are imposed. To evaluate the proposed tracking-controller, the reference parametric motion trajectory tailored from the single lane change testing maneuver by ISO-14791 is introduced.

The co-simulation built upon the Matlab/Simulink-TruckSim environment is conducted to examine the NLMPC tracking-controller design. Simulation results disclose the following insightful findings:

1) Over the specified SLC overtaking maneuver, the tracking-controller can well control the AHV in the linear lateral and longitudinal dynamic ranges so that the vehicle can achieve good path-following performance and lateral stability;

2) Over the overtaking maneuver, to respond to the tractor front wheel steering actuation, the responding efforts of the tractor and trailer tires in terms of the amplitude of tire slip angle are different, which decrease from the tractor front tires, via the tractor rear tires, to the trailer tires;

3) Due to the difference of the responding efforts of the tractor and trailer tires in terms of tire slip angles, the tractor's path-following performance can be better controlled than that of the trailer.

To further assess the NLMPC controller design, a benchmark comparison is conducted between two cases:

i) Considering tracking-control for both the leading and trailing vehicle units;

ii) Only considering tracking-control for the leading vehicle unit.

Numerical experiments demonstrate that compared with the second case, the first case (i.e., the proposed design) can achieve better overall performance in terms of the PFOT measures and lateral stability at the expense of larger tractor front wheel steering actuation.

6.2. Original Contribution

Path following control schemes are already developed by the previous researchers but only the path following of the tractor alone is considered and no attention is paid for the trailer path tracking [62]. The novelty of the tracking control scheme discussed in chapter 4 and 5 is that the tracking control of the trailer have also got attention by considering the tracking and orientation errors of trailer as well which is shown in equation (4.3f) and (4.3h). Lateral position and yaw angle of the trailer are considered as output variables as shown in equation (5.1h). A comparison between schemes with and without trailer trajectory-tracking control discussed in section 5.4.3 reflects that considering the trailer tracking control improves the trailer performance in terms of the overshoot of lateral position and peak value of lateral acceleration by 9.1% and 3.03% respectively.

6.3. Future work

To enhance the NLMPC based tracking-controller performance, the following topics can be tackled in the future research:

1) Roll motions of the tractor and semi-trailer are considered as the roll moments cannot be neglected during high lateral acceleration operations of the tractor/semi-trailer;
2) A motion-planning module is integrated with the tracking-control module;
3) Harder-in-loop (HIL) real-time simulations are conducted to evaluate the performance of the integrated motion planning and tracking-control module.

References

[1] World Health Organization. Global status report on road safety 2018. [cited 2021 Dec. 5]. Available from: https://www.who.int/publications/i/item/9789241565684

[2] Ni, Z. and He, Y., "Design and Validation of a Robust Active Trailer Steering System for Multi-trailer Articulated Heavy Vehicles," Vehicle System Dynamics 57(10):1545-1571, 2019, doi:10.1080/00423114.2018.1529322.

[3] He, Y., Islam, M.M., and Webster, T.D. "An Integrated Design Method for Articulated Heavy Vehicles with Active Trailer Steering Systems," SAE Int. J. Passenger. Car – Mech. Syst. 3(1):158-174, 2010.

[4] European Agency for Safety and Health at Work. A review of accidents and injuries to road transport drivers. ISBN-13:978-92-9191-355-8, 2010; Luxembourg: Publications Office of the European Union, 61 pages.

[5] Kang, X. and Deng, W. (2007) Vehicle-trailer Handling Dynamics and Stability Control – an Engineering Review, SAE Technical Paper, Paper No. 2007-01-0822.

[6] Zhu S, He Y. "A Unified Lateral Preview Driver Model for Road Vehicles," IEEE Trans Intell Transp Syst. 2020;21(11):4858–4868.

[7] S. Vempaty, E. Lee, and Y. He, "Model-reference based adaptive control for enhancing lateral stability of car-trailer systems," Proceedings of ASME International Mechanical Engineering Congress and Exposition, Paper No: INECE2016-65090, V012T16021; 8 pages, 2016.

[8] S. Vempaty, T. Sun, and Y. He, "Enhanced lateral stability of car-trailer systems using model reference adaptive control," Dynamics of Vehicles on Roads and Tracks Vol 1: Proceedings of the 25th International Symposium on Dynamics of Vehicles on Roads and Tracks (IAVSD 2017), 14-18 August 2017, Rockhampton, Queensland, Australia.

[9] E. Lee, S. Kapoor, T. Sikder, and Y. He, "An optimal robust controller for active trailer differential braking systems of car-trailer combinations," Int. J. Vehicle Systems Modelling and Testing, Vol. 12, Nos. ½, pp. 72-93, 2017.

[10] T. Sun, E. Lee, and Y. He, "Non-linear bifurcation stability analysis for articulated vehicles with active trailer differential braking systems," SAE Int. J. Mater. Manf., Vol. 9, No. 6, doi:10.4271/2016-01-0433, 2016.

[11] T. Sun, Y. He, and J. Ren, "Dynamics analysis of car-trailer systems with active trailer differential braking strategies," SAE Int. J. Passenger. Cars – Mech. Syst., Vol. 7, No. 1, doi:10.4271/2014-01-0143, 2014.

[12] X. Ding, Y. He, J. Ren and T. Sun, "A comparative study of control algorithms for active trailer steering systems of articulated heavy vehicles," 2012 American Control Conference (ACC), Montreal, QC, Canada, 2012, pp. 3617-3622, doi: 10.1109/ACC.2012.6315139.

[13] Rahimi, and Y. He, "A review of essential technologies for autonomous and semi-autonomous articulated heavy vehicles," Proceedings of the Canadian Society for Mechanical Engineering International Congress 2020 (CSME Congress 2020), June 21-24, 2020, Charlottetown, PE, Canada, 8 pages.

[14] U.S. Federal Motor Carrier Safety Administration. Large Trucks and bus crash facts 2016. [Online]. Available: https://cms8.fmcsa.dot.gov/safety/data-and-statistics/large-truck-and-bus-crash-facts-2016#A8

[15] S. J. Anderson, J. M. Walker, S. B. Karumanchi, et al. “The intelligent copilot: A constraint-based approach to shared-adaptive of ground vehicles,” IEEE Trans Intell Transp Syst Magaz. 2013;5(2):45-54.
[16] Rahimi, A., Huang, W., Sharma, T., and He, Y. An autonomous driving control strategy for multi-trailer articulated heavy vehicles with enhanced active trailer safety. The 27th IAVSD Symposium on Dynamics of Vehicles on Roads and Tracks, Saint-Petersburg, Russia, 2021, 12 pages.
[17] Yu, J., Sharma, T., and He, Y. Design optimization of autonomous steering control schemes for articulated vehicles. Proceedings of the Canadian Society for Mechanical Engineering International Congress 2021, June 27-30, 2021, Charlottetown, PE, Canada, 10 pages.
[18] Falcone, P, Tseng, HE, Borrelli, F, Asgari, J, Hrovat, D. MPC-based yaw and lateral stabilization via active front steering and braking. Veh Syst Dyn. 2008; 46(supplement): 611-628, 2008.
[19] Rawlings, JB. Tutorial overview of model predictive control. IEEE Control Syst. Mag. 2000; 20(3): 38–52.
[20] Mechanical Simulation Corporation. TruckSim: Math Models. [cited 2022, July 18]. https://www.carsim.com/downloads/pdf/TruckSim_Math_Models.pdf.
[21] He Y, Islam MM, Zhu S, et al. A design synthesis framework for directional performance optimization of multi-trailer articulated heavy vehicleswith trailer lateral dynamic control systems.Proc Inst Mech Eng D, J Automob Eng. 2017;231(8):1096–1125.
[22] Weidner, J. L. 2007. Tractor trailer instability of variably loaded trucks, PHD thesis, Pennsylvania State University, pp.56-72.
[23] Ervin, R., Winkler, C., Fancher, P., Hagan, M., Krishnaswami, V., Zhang, H. and Bogard, S. 1998. Two active systems for enhancing dynamic stability in heavy truck operations, Technical report, UMTRI-98-39.
[24] Boumediene, F. 2001. Outil permettant d’Analyser la stabilité des véhicules lourds, Rapport technique du ministère des transports canadienne, Québec.
[25] Runge, J.W. 2003. Traffic Safety Facts: A Compilation of Motor Vehicle Crash.
[26] Sharp, R. S. and Alonso, F. 2002. Car-caravan snaking, School of Engineering, Cranfield University, Bedford, UK Proc Instn Mech Engrs, Vol 216 Part C, pp.707-736.
[27] He Y, Khajepour A, McPhee J, et al. Dynamic modelling and stability analysis of articulated frame steer vehicles. Int J Heavy Veh Syst. 2005;12(1):28–59.
[28] Shamim, R., Islam, M.M., and He, Y. A comparative study of active control strategies for improving lateral stability of car-trailer systems. SAE Technical Paper 2011-01-0959, 2011.
[29] Nasser, L. A. 2006. Dynamic Modeling and Stability Controller Development for Articulated Steer Vehicles, A thesis presented to the University of Waterloo in fulfillment of the thesis requirement for the degree of Doctor of Philosophy in Mechanical Engineering.
[30] Gibson, H. G., Elliott, K. C. and Persson, S. P. E. 1971. Side slope stability of articulated-frame logging tractors, Journal of Terra mechanics.
[31] Vlk, F. December1982. Lateral dynamics of commercial vehicle combinations. A Literature Survey, VSD, Vol. l I, No. pp.5-6.
[32] Fratila, D. 1994. Lateral stability of car/caravan combinations. PhD Thesis, Dept of Mechanical Engineering, University of Bath, UK.
[33] Vempaty, S., He, Y., & Zhao, L. (2020). An overview of control schemes for improving the lateral stability of car trailer combinations. International Journal of Vehicle Performance, 6(2), 151–199. https://doi.org/10.1504/IJVP.2020.106985.

[34] Hac, A., Fulk, D., & Chen, H. (2008). Stability and control considerations of vehicle-trailer combination. *SAE Technical Papers*, *2008*(724), 776–790. https://doi.org/10.4271/2008-01-1228

[35] Darling, J., Tilley, D., & Gao, B. (2009). An experimental investigation of car-trailer high-speed stability. *Proceedings of the Institution of Mechanical Engineers, Part D: Journal of Automobile Engineering*, *223*(4), 471–484. https://doi.org/10.1243/09544070JAUTO981

[36] Van De Molengraft-Luijten, M. F. J., Besselink, I. J. M., Verschuren, R. M. A. F., & Nijmeijer, H. (2012). Analysis of the lateral dynamic behaviour of articulated commercial vehicles. *Vehicle System Dynamics*, *50*(SUPPL. 1), 169–189. https://doi.org/10.1080/00423114.2012.676650

[37] Fancher PS,Winker CB. Directional performance issues in evaluation and design of articulated heavy vehicles. Veh Syst Dyn. 2007;45(7-8):607–647.

[38] Zhao, L., and He, Y. An investigation of active safety control strategies for improving the lateral stability of car-trailer systems. Int. J. Vehicle Systems Modelling and Testing, Vol. 13, No. 4, pp. 295-318.

[39] Sun, T., He, Y., Esmailzadeh, E. and Ren, J. (2012) ′Lateral stability improvement of car-trailer systems using active trailer braking control′, *Journal of Mechanics Engineering and Automation*, Vol. 2, No. 9, pp.555–562.

[40] Miege AJP, Cebon D. Optimal roll control of an articulated vehicle: theory and model validation. *Vehicle System Dynamics* 2005, 43(12), pp. 867-893.

[41] Kim, K.I., Guan, H., Wang, B., Guo, R. and Liang, F. "Active steering control strategy for articulated vehicles." Frontiers of Information Technology & Electronic Engineering 17 (2016): 576-586.

[42] Aurell, J. and Edlund, S. 1989. The Influence of Steered Axles on the Dynamic Stability of Heavy Vehicles, SAE paper No. 892498.

[43] Jujnovich, B. and Cebon, D. 2002. Comparative performance of semi-trailer steering systems. In proceedings of the 7th International Symposiumon Heavy Vehicle Weights and Dimensions, Delft, pp. 195-214.

[44] Sankar, S., Rakhija, S. and Piche, A. 1991.Directional dynamics of a tractor-semi-trailer with self and force steering axles, SAE Transactions, SAE 912686.

[45] Eisele,D. and Peng, H.August 2000.Vehicle Dynamics Control with Rollover Prevention for Articulated Heavy Trucks, Proceedings of 5th Int'l Symposium on Advanced Vehicle Control, Ann Arbor, Michigan, pp.22-2.

[46] Rangavajhula, K. and Tsao, H-S. J. 2007. Active steering control of an articulated system with a tractor and three full trailers for tractor-track following, Int. J. Heavy Vehicle Systems, 14(3), 271-293.

[47] Rangavajhula, K. and Tsao, H-S. J. 2008. Command steering of trailers and command-steering-based optimal control of an articulated system for tractor-track following, Intn. Mech. Engrs., Vol.222, 2008. Proc. IMechE, Part D: J. Automobile Engineering, 222, 935-954.

[48] Rangavajhula, K. and Tsao, H.-S. J. Effect of multi-axle steering on off-tracking and dynamic lateral response of articulated tractor–trailer Combinations. Int. J. Heavy Veh. Systems, 14(4), 376–401.

[49] Tsao,H.-S.J.,Dessouky,Y.,Rangavajhula,K.,Zeta, J.B., and Zhou, L.2006. Automatic steering for conventional truck trailers: development and assessment of operating concepts for

improving safety, productivity and pavement durability final report, PATH Research Report UCB-ITS-PRR-2006- 8, Institute of Transportation Studies, University of California, Berkeley.
[50] Jujnovich, B. A.; Cebon, D. (2013). Path-Following Steering Control for Articulated Vehicles. Journal of Dynamic Systems, Measurement, and Control, 135(3), 031006–. doi:10.1115/1.4023396.
[51] Md. Manjurul Islam, Xuejun Ding & Yuping He (2012) A closed-loop dynamic simulation-based design method for articulated heavy vehicles with active trailer steering systems, Vehicle System Dynamics, 50:5, 675-697, DOI: 10.1080/00423114.2011.622904.
[52] Abroshan, M., Hajiloo, R., Hashemi, E., & Khajepour, A. (2020). Model predictive-based tractor trailer stabilisation using differential braking with experimental verification. Vehicle System Dynamics, 0(0), 1–24. https://doi.org/10.1080/00423114.2020.1744024.
[53] El-Gindy, M., Mrad, N. and Tong, X. 2001. Sensitivity of rearward amplification control of a tractor/full trailer to tyre cornering stiffness variable, Proc. IMechE, Part D: J. Automobile Engineering, 215, 579-588.
[54] Odhams, A., Roebuck, R., Cebon, D. and Winker, C. 2008. Dynamic safety of active trailer steering systems, Proc. IMechE, Part K: J. Multi-body Dynamics, 222, 367-38.
[55] Anderson SJ, Walker JM, Karumanchi SB, et al. The intelligent copilot: a constraint-based approach to shared-adaptive of ground vehicles. IEEE Trans Intell Transp Syst Magaz. 2013;5(2):45-54.
[56] Kayacan, E., Kayacan E., Ramon, H., Saeys, W. Robust tube-based decentralized nonlinear model predictive control of an autonomous tractor-trailer system. IEEE/ASME Transactions on Mechatronics. 2015; 20(1): 447-456.
[57] Lima, PF. Optimization-based motion planning and model predictive control for autonomous driving: with experimental evaluation on a heavy-duty construction truck. PhD thesis, Department of Automatic Control, KTH Royal Institute of Technology, Stockholm, Sweden, 2018
[58] Elhassan, A. Autonomous driving system for reversing an articulated vehicle. M.S. thesis, Department of Automatic Control, KTH Royal Institute of Technology, Stockholm, Sweden, 2015.
[59] Oliveira, R, Ljungqvist, O, Lima, PF, Wahlberg, B. Optimization-based on-road path planning for articulated vehicles. IFAC PapersOnLine. 2020; 53(2): 15572-15579.
[60] Shojaei, S, Hanzaki, AR, Azadi, S, Saeedi, MA. A novel decision-making unit for automated maneuver of articulated vehicles in real traffic situations. Proc IMechE Part D: J Automobile Engineering. 2020; 234(1): 152-171.
[61] Rahim, A, Huang, W, He, Y. A longitudinal speed controller for autonomous multi-trailer articulated heavy vehicles. Proceedings of the Canadian Society for Mechanical Engineering International Congress 2021, June 27-30, 2021, Charlottetown, PE, Canada, 8 pages.
[62] Barbosa, FM, Marcos, LB, Silva, MM, Terra, MH, Junior, VG. Robust path-following control for articulated heavy-duty vehicles. Control Engineering Practice. 2019; 85: 246-256.
[63] Felex, J, García-Sanchez, C, Lozano JA. Control design for an articulated truck with autonomous driving in an electrified highway. IEEE Access. 2018; 6: 60171-60186.
[64] Liu, L., Wang, B., and He, Y. Research on path-tracking control of articulated vehicle with a trailer based on advanced model prediction control strategy. Proceedings of the Canadian Society for Mechanical Engineering International Congress 2021, June 27-30, 2021, Charlottetown, PE, Canada, 10 pages.

[65] Taylor, P., & Wong, J. Y. (n.d.). *Vehicle System Dynamics: International Journal of Vehicle Mechanics and Mobility* A Comparison of Various Computer Simulation Models for Predicting the Directional Responses of Articulated Vehicles. December 2014, 37–41. https://doi.org/10.1080/00423118708968885
[66] He, Y., Ren, J. A comparative study of car-trailer dynamics models. SAE Int. J. Passenger. Cars – Mech. Syst. 6(1): 2013.
[67] Islam, M.M., He, Y., Zhu, S., Wang, Q. A comparative study of multi-trailer articulated heavy-vehicle models. Proc IMechE Part D: J Automobile Engineering. 2014; 229(9): 1200-1228.
[68] El-Gindy, M. (1995). An Overview of Performance Measures for Heavy Commercial Vehicle in North America. *International Journal of Heavy Vehicle Design*, *16*(4), 441–463.
[69] He Y, Elmaraghy H, Elmaraghy W. A design analysis approach for improving the stability of dynamic systems with application to the design of car-trailer systems. J Vib Control. 2005;11(12):1487–1509.
[70] He, Y. Design of rail vehicles with passive and active suspensions using multidisciplinary optimization, multibody dynamics, and genetic algorithms. PhD Thesis, Department of Mechanical Engineering, University of Waterloo, Canada, 2003.
[71] He, Y., McPhee, J. Optimization of the lateral stability of rail vehicles. Vehicle System Dynamics, 2002; 57(10):1545-1571.
[72] Dugoff, H, Fancher, PS, Segal, L. Tire performance characteristics affecting vehicle response to steering and braking control inputs. Final Report, Contract CST-460, Office of Vehicle Systems Research, US National Bureau of Standards, 1969.
[73] Rajamani, R. Vehicle Dynamics and Control. 2nd ed. New York: Springer, 2012.
[74] Yu, Z. Theory of Automobiles, 5th ed. Publishing House of the Mechanical Industry, Beijing, China. 2011.
[75] Wong, J. Theory of ground vehicles, 4th ed. John Wiley & sons, Inc., 2008.
[76] Zhu, S, He, Y. A driver-adaptive stability control strategy for sport utility vehicles. Veh Syst Dyn. 2017; 55(8):1206-1240.
[77] Paden, B, Cáp, M, Yong, SZ, et al. A survey of motion planning and control techniques for self-driving urban vehicles. IEEE Transactions on intelligent vehicles. 2016; 1(1): 33-55.
[78] Liu, C, Zhan, W, Tomizuka, M. Speed profile planning in dynamic environments via temporal optimization. in Proc. Intell. Vehicles Symp. (IV), 2017, pp. 154–159.
[79] Gu, T, Dolan, JM, Lee, JW. Runtime-bounded tunable motion planning for autonomous driving. in IEEE Intelligent Vehicles Symposium (IV), 2016, pp. 1301–1306.
[80] International Organization for Standardization. Road vehicles – heavy commercial vehicle combinations and articulated buses – lateral stability test methods. ISO-14791:2000(E). Geneva: International Organization for Standardization; 2000.
[81] Ervin, RD, MacAdam, CC. The dynamic response of multiply-articulated truck combinations to steering input. SAE paper 820973; 1982.
[82] Fancher PS, Winkler CB. A methodology for measuring rearward amplification. Proceedings of the 3rd International Symposium on Heavy Vehicle Weights and Dimensions; 1992; Cambridge, UK.
[83] Shiller, Z, Sundar, S. Emergency lane-change maneuvers of autonomous vehicles. ASME Journal of Dynamic Systems, Measurement and Control. 1998; 120(1):37-44.

[84] Yang, G, Xu, H, Wang, Z, Tian, Z. Truck acceleration behavior study and acceleration lane length recommendations for metered on-ramps. International Journal of Transportation Science and Technology. 2016; 5: 93-102.
[85] Yamashita, AS, Alexandre, PM, Zanin, AC, Odloak, D. Reference trajectory tuning of model predictive control. Control Engineering Practice. 2016; 50:1-11.
[86] Osman, HM. Optimizing model based predictive control for combustion boiler process at high model uncertainty. Chemical and Biochemical Engineering Quarterly. 2017; 31(3): 313-324.
[87] Nebeluk, R, Ławryńczuk, M. Tuning of multivariable model predictive control for industrial tasks. Algorithms. 2021; 14(10): 1-15.
[88] He, Y, Islam, MM. An automated design method for active trailer steering systems of articulated heavy vehicles. ASME J Mech Des. 2012;134(4):041002 (15 pages).
[89] Kharrazi S, Lidberg M, Fredriksson J. A generic controller for improving lateral performance of heavy vehicle combinations. Proc Inst Mech Eng D, J Automob Eng. 2013;227(5):619–642.
[90] Roebuck R,Odhams A, Tagesson K, et al. Implementation of trailer steering control on a multiunit vehicle at high speeds. ASME J Dyn Syst Meas Control. 2014;136(2):021016 (14 pages).
[91] Salhi, H., & Bouani, F. (2019). Practical study of derivative-free observer-based nonlinear adaptive predictive control. In New Trends in Observer-Based Control: An Introduction to Design Approaches and Engineering Applications. Elsevier Inc. https://doi.org/10.1016/B978-0-12-817038-0.00007-X.
[92] Canadian Task Force on Vehicle Weights and Dimensions Policy. (2019). Heavy Truck Weight and Dimension Limits for Interprovincial Operations in Canada. December 2016. https://comt.ca/english/programs/trucking/MOU 2019.pdf

Appendix

A1. System matrices of 3 DOF tractor/semi-trailer model

$$\mathbf{M}=\begin{bmatrix} 1 & 0 & 0 & 0 \\ 0 & \text{m1}+\text{m2} & -\text{m2}*\text{d} & -\text{m2}*\text{e} \\ 0 & \text{m1}*\text{d} & \text{Izz} & 0 \\ 0 & \text{m1}*\text{e} & 0 & \text{Izz\_tlr} \end{bmatrix}$$

$$\boldsymbol{D} = \left(\frac{1}{Vx}\right)\begin{bmatrix} 0 & 0 & Vx & -Vx \\ \text{Vx}*(3*\text{ct}) & \text{cf}+\text{cr}+3*\text{ct} & -(\text{m1}+\text{m2})*(\text{Vx\^{}2})+\text{a}*\text{cf}-\text{b}*\text{cr}-3*\text{d}*\text{ct} & -(\text{e}+\text{h})*\text{ct}-\text{ct}*(5*\text{h}+2*\text{e}) \\ 0 & \text{a}*\text{cf}-\text{b}*\text{cr}+2*\text{d}*\text{cf} & -\text{m1}*\text{d}*(\text{Vx\^{}2})+(\text{a\^{}2})*\text{cf}+(\text{b\^{}2})*\text{cr}+\text{d}*\text{cf}*(\text{a}-\text{b}) & 0 \\ -\text{h}*\text{Vx}*(6*\text{ct}) & 2*\text{e}*\text{cf}-6*\text{ct}*\text{h} & \text{a}*\text{e}*\text{cf}-\text{b}*\text{e}*\text{cf}-(\text{m1}*\text{e}*\text{Vx}*\text{Vx})+6*\text{ct}*\text{d}*\text{h} & \text{ct}*\text{h}*(6*\text{e}+14*\text{h}) \end{bmatrix}$$

$$\boldsymbol{E} = \begin{bmatrix} 0 \\ -cf \\ -a*cf-d*cf \\ e*(-cf) \end{bmatrix}$$

$$\text{A} = inv(\boldsymbol{M})*\mathbf{D}$$

$$\text{B} = inv(\boldsymbol{M})*\mathbf{E}$$

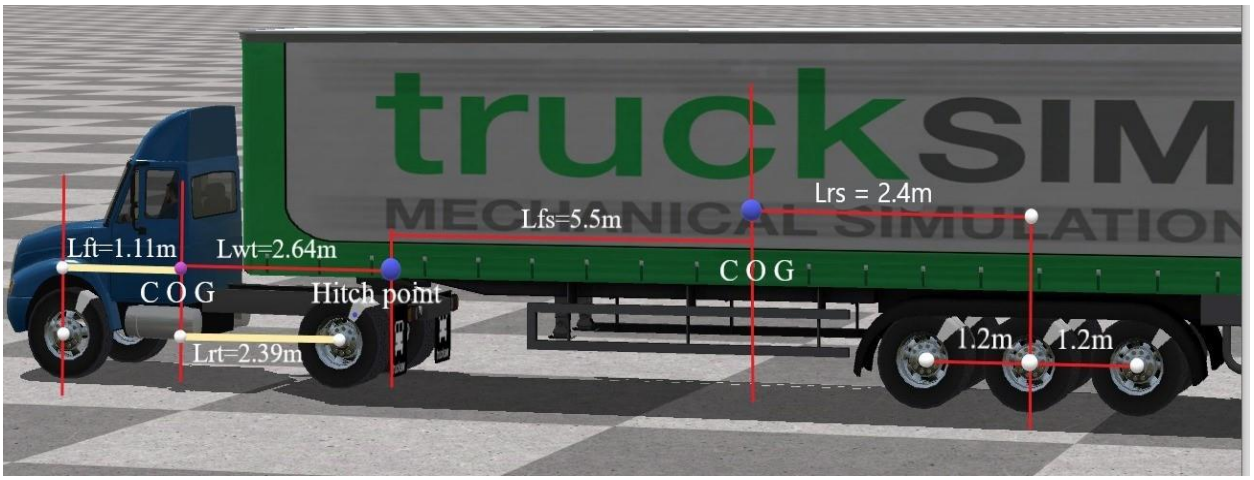

Figure A1. Single rear axle tractor semi-trailer

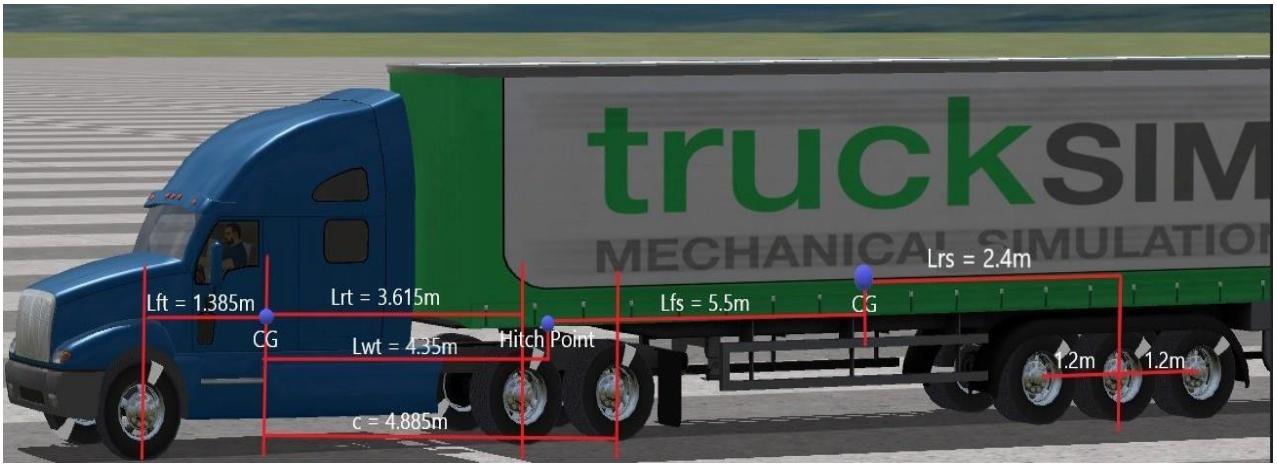

Figure A2. Double rear axle tractor semi-trailer

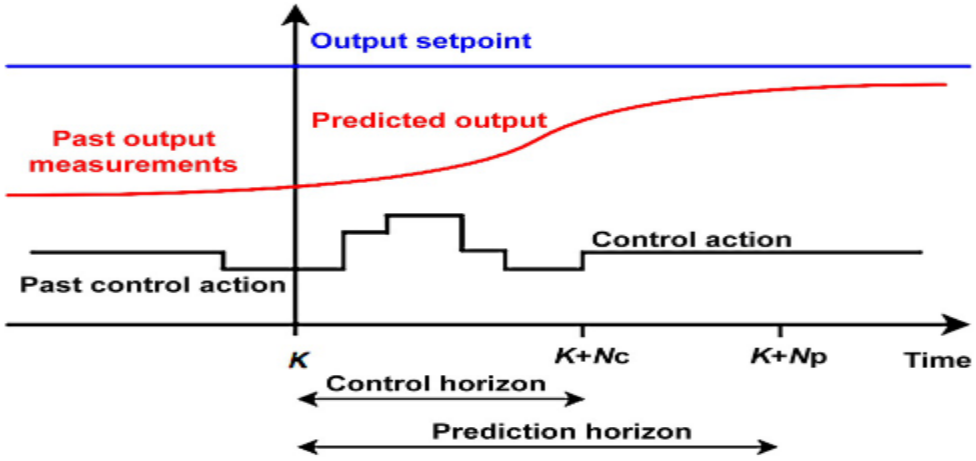

Figure A3. Model Predictive Control Approach [91]

Table A1. Dimensions of tractor semi-trailer

Dimensions	Single Rear Axle Tractor Semi-trailer	Double Rear Axle Tractor Semi-trailer
L_{ft} = a	1.11 m	1.385 m
$L_{rt} = b$	2.39 m	4.25 m
$L_{wt} = d$	2.64 m	4.35 m
$L_{fs} = e$	5.5 m	5.5 m
$L_{rs} = 2h$	2.4 m	2.4 m
$m_t = m1$	5496 kg	7878 kg
$m_s = m2$	7807 kg	7807 kg